PETROGENESIS OF OFF-AXIS LAVAS ERUPTED ALONG THE 8˚20’ N SEAMOUNT CHAIN, EAST PACIFIC RISE

by

Molly Kassandra Anderson

A thesis

submitted in partial fulfillment

of the requirements for the degree of

Master of Science in Geoscience

Boise State University

May 2019

BOISE STATE UNIVERSITY GRADUATE COLLEGE

DEFENSE COMMITTEE AND FINAL READING APPROVALS

of the thesis submitted by

Molly Kassandra Anderson

Thesis Title: Petrogenesis of Off-Axis Lavas Erupted Along the 8°20’ N Seamount Chain, East Pacific Rise

Date of Final Oral Examination: 22 March 2019

The following individuals read and discussed the thesis submitted by student Molly Kassandra Anderson and they evaluated her presentation and response to questions during the final oral examination. They found that the student passed the final oral examination.

Dorsey V. Wanless, Ph.D.	Chair, Supervisory Committee
Mark Schmitz, Ph.D.	Member, Supervisory Committee
Brittany D. Brand, Ph.D.	Member, Supervisory Committee

The final reading approval of the thesis was granted by Dorsey V. Wanless, Ph.D., Chair of the Supervisory Committee. The thesis was approved by the Graduate College.

DEDICATION

To Melinda Hibbard, Sylvia Fine, Sally Neil, and LuAnn Newton for making all the difference and reminding me that well-behaved women seldom make history (Laurel Thatcher Ulrich).

ACKNOWLEDGEMENTS

Foremost, I would like to thank my advisor Dr. Dorsey Wanless for her guidance and support throughout this project. She provided every possible opportunity for me to explore my passion and learn; for that I am forever grateful. I also thank my committee members Dr. Mark Schmitz and Dr. Brittany Brand for their time, advice, and encouragement. I would like to give special thanks to Dr. Michael Perfit for teaching me how to be an aquanaut and for sharing his enthusiasm and expertise for this project. I thank Dr. Dan Fornari and Dr. Patricia Gregg for making this research possible through their extraordinary efforts. I thank the officers and crew of R/V Atlantis and HOV Alvin, without whom this project would be impossible. I also thank Dr. George Kamenov at University of Florida, Katie Bermudez at University of Florida, and Dr. Marion Lytle at Boise State University for laboratory assistance and training. I give special thanks to Darin Schwartz and Dr. Robin Trayler for consulting on petrologic modelling, programming, and data management. I would also like to thank my husband Michael for his endless support and encouragement, and my family for always asking why I am still in school but backing me anyways. This work was supported by Burnham Research Funds from the Geosciences Department at Boise State University.

ABSTRACT

Lavas erupted at off-axis seamounts provide a window into mantle heterogeneity and melting systematics that are not easily observed on-axis at fast spreading mid-ocean ridges (MORs). This is because axial melts are efficiently mixed and homogenized within shallow axial magma chambers prior to eruption. To understand the deeper magmatic processes contributing to oceanic crustal formation, we examine the compositions of lavas erupted along a chain of off-axis seamounts, adjacent to the East Pacific Rise (EPR). Essential questions include: (1) What is the range of compositional variability erupted off-axis and how does that compare to lavas erupted on-axis? (2) Is there a systematic spatial or morphological distribution of compositional variations off-axis? (3) What petrologic processes form the basalts erupted off-axis?

To investigate off-axis magmatism, we systematically mapped the 8˚20’ N seamount chain in November of 2016 on R/V *Atlantis* using shipboard EM122 multibeam system and AUV *Sentry*. This ~200 km-long chain of off-axis seamounts and volcanic ridges is oriented perpendicular to the ridge axis, west of the EPR and north of the Siqueiros Fracture Zone. The high-resolution shipboard and AUV-based multibeam and sidescan sonar maps are combined with geochemical analyses of ~300 basalts, collected using HOV *Alvin* and dredging, to evaluate the magmatic plumbing system feeding these off-axis eruptions. Major and trace element contents and radiogenic isotope ratios are used to assess extents of fractional crystallization, magma mixing, melting systematics, and mantle source variability.

A complex distribution of highly variable lava compositions is observed along the seamount chain, reflecting a mantle and magmatic plumbing system that produce heterogeneity on small spatial scales. Major and trace element concentrations as well as radiogenic isotopes reveal a continuum of depleted, normal, and enriched basalt compositions across the seamount chain and within individual seamounts. For example, MgO contents vary from 10.25 to 4.56 wt. % across the seamount chain and by as much as 3.61 wt. % from features sampled at an individual seamount. $(La/Sm)_N$ contents span the entire range of known values for basalts from the northern EPR (0.45—2.76), as do radiogenic isotope ratios (i.e., ƐNd = 6.26—11.18). In some cases, isotope ratios are correlated with trace element ratios – while others are not – indicating complex relationships exist between mantle sources, melting, and mixing processes on both regional and local scales off-axis. We combine the geochemical results and bathymetric maps with petrologic models to evaluate extents and depths of fractional crystallization, source variability, source mixing, and mantle melting in the off-axis environment.

TABLE OF CONTENTS

LIST OF TABLES

LIST OF FIGURES

LIST OF ABBREVIATIONS

AUV	Autonomous underwater vehicle
DDMM	Depleted depleted mid-ocean ridge mantle
DMORB	Depleted mid-ocean ridge basalt
DMM	Depleted mid-ocean ridge mantle
EPR	East Pacific Rise
EMM	Enriched mid-ocean ridge mantle
EMORB	Enriched mid-ocean ridge basalt
HOV	Human-operated vehicle
MORB	Mid-ocean ridge basalt
NMORB	Normal mid-ocean ridge basalt

PETROGENESIS OF OFF-AXIS LAVAS ERUPTED ALONG THE 8˚20’ N SEAMOUNT CHAIN, EAST PACIFIC RISE

Introduction

At mid-ocean ridges (MORs), decompression melting occurs in the underlying mantle as tectonic plates diverge. The onset of melting beneath MORs is estimated to occur at ~60 km depth and the base of the melting regime is ~100 km wide (Batiza, Niu, & Zayac, 1990; Langmuir, Klein, & Plank, 1992; Phipps-Morgan, 1987; Plank & Langmuir, 1992). While the depth to the base of the melting region is constant, the top of the melting region deepens away from the ridge axis due to increasing lithospheric thickness, resulting in a triangular melting region centered beneath the ridge axis (Langmuir et al., 1992; Plank & Langmuir, 1992). Thus, the highest extents of mantle melting occur directly beneath the ridge axis where the triangle is tallest, with progressively lower extents of melting with distance from the ridge axis (Langmuir et al., 1992; O’Hara, 1985; Plank & Langmuir, 1992).

The partial melts formed in the mantle buoyantly rise, focus beneath the ridge axis (Phipps-Morgan, 1987; Spiegelman & McKenzie, 1987), and ascend into the crust, where they eventually solidify or erupt to form the oceanic crust (Langmuir et al., 1992; Perfit et al., 1994; Plank & Langmuir, 1992). At magmatically robust fast-spreading MORs there is a nearly steady state magma chamber or axial melt lens (Batiza et al., 1996; Perfit & Chadwick, 1998) that forms at the base of the sheeted dikes (~1-2 km below the seafloor;

Detrick et al., 1987). These melt lenses are located directly below the ridge axis and promote efficient mixing and homogenization of mantle melts prior to eruption on the seafloor (Rubin & Sinton, 2007; Sinton & Detrick, 1992). Mixing of melts formed from the entire melting regime results in the eruption of a relatively limited compositional range (Batiza & Niu, 1992; Perfit et al., 1994; Stracke & Bourdon, 2009), called normal mid-ocean ridge basalts (NMORB). However, enriched mid-ocean ridge basalts (EMORB) are also erupted on-axis at fast-spreading centers (Batiza & Niu, 1992; Waters et al., 2011), suggesting that some magmas may bypass the axial magma chamber and erupt on the seafloor. The formation of EMORB lavas is attributed to a compositionally heterogeneous mantle source (Waters et al., 2011) or variations in the extent of melting of the same depleted upper mantle that forms NMORB (Batiza et al., 1990).

Off-axis volcanic features, such as ridge flanks and seamounts, provide an alternative view into melting systematics and compositional heterogeneities in the upper mantle compared to on-axis lavas due to the absence of steady state magma chambers. Previous studies have shown that lavas erupted away from the ridge axis are extremely heterogeneous in composition compared to lavas erupted on-axis (Allan & Batiza, 1987; Batiza et al., 1990; Rodey Batiza, Smith, & Niu, 1989; Brandl et al., 2012; Fornari, Perfit, Allan, Batiza, et al., 1988; Fornari, Perfit, Allan, & Batiza, 1988; Niu & Batiza, 1997b, 1997a; Niu, Regelous, Wendt, Batiza, & O'Hara, 2002; Shimizu et al., 2016; Zindler, Staudigel, & Batiza, 1984). These studies suggest that ridge flank and seamount lavas can by-pass the axial magma chamber, decreasing the extent of mixing and homogenization prior to eruption (Batiza & Niu, 1992; Fornari et al., 1988a; Perfit & Chadwick, 1998). Compositional variations in off-axis lavas are observed on remarkably small scales

(Brandl et al., 2012; Fornari et al., 1988b; Niu & Batiza, 1997a; Zindler et al., 1984), some less than 5 km apart (Fornari et al., 1988b) and as close to the ridge axis as ~4 km (Niu & Batiza, 1997b). Radiogenic isotope ratios in off-axis lavas suggest that the upper mantle feeding the MOR magmatic system may be more heterogeneous than is commonly observed on-axis (Zindler et al., 1984). However, the disparate sampling off-axis thus far has been limited to single seamounts, abyssal hills, or short seamount chains, leaving the spatial distribution of heterogeneity in the near-ridge upper mantle ambiguous (Batiza et al., 1990; Brandl et al., 2012; Niu & Batiza, 1997a, 1997b; Zindler et al., 1984).

To further assess the spatial distribution of compositional heterogeneity in the upper mantle and to determine the magmatic processes responsible for the formation of off-axis seamounts, we investigate a chain of seamounts adjacent to the EPR (Figure 1). The nearly perpendicular alignment of the 8°20’ N seamount chain with the EPR axis provides a unique opportunity to investigate mantle source variability and melting systematics on a transect away from the ridge axis, from the center of the melting triangle to well beyond its edge. Further, in this off-axis setting magmas are not influenced by the nearly steady state on-axis magma chamber, providing a window into deeper mantle processes near MORs. To investigate these seamounts, we systematically mapped and sampled the entire 8°20’ N seamount chain using ship and AUV based multibeam, the HOV *Alvin*, and dredging. Approximately 300 basalt samples were collected from the 200 km-long seamount chain west of the fast-spreading EPR. We use major and trace element contents and radiogenic isotope ratios of the seamount lavas to investigate the petrogenesis of the seamounts. We then use forward models to evaluate mantle

heterogeneity, melting systematics, and extents of fractional crystallization to create a model that can account for the heterogeneous basalt compositions erupted along the seamount chain.

Geologic and Tectonic Setting of the 8°20’ N Seamounts

The 8°20’ N seamount chain, named by its approximate latitude, is an east-west trending, nearly linear, ~200 km-long group of volcanic constructions located west of the northern EPR and Siqueiros ridge-transform intersection (Figure 1). It is situated ~20 km north of the Siqueiros fracture zone (Scheirer & Macdonald, 1995); the inactive remnant of the Siqueiros transform fault and region of structural weakness (Behn, Lin, & Zuber, 2002). The Siqueiros transform contains 4 intra-transform spreading centers thought to represent changes in the Pacific-Cocos plate direction of separation during the last several million years (Gregg, Behn, Lin, & Grove, 2009). The 8°20'N chain consists of numerous volcanic seamounts, cones, and ridges formed on oceanic crust that was originally produced at the spreading center (Carbotte & Macdonald, 1992). Previous magnetic studies of the region indicate that the seamounts may have formed near or off-axis (Carbotte & Macdonald, 1992), and thus may provide a window into mantle conditions away from the ridge axis.

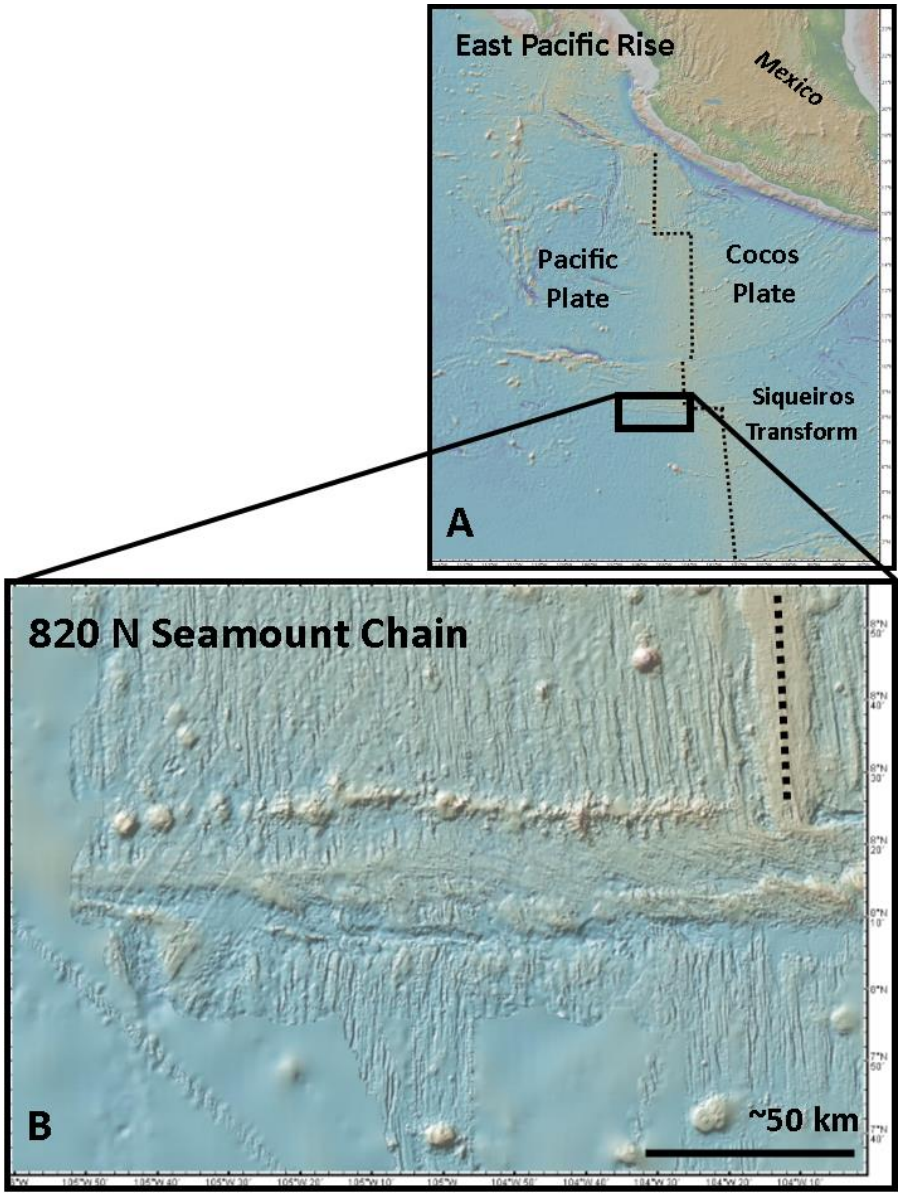

Figure 1. A) Bathymetric map showing the location of the study site (black box) in relation to the East Pacific Rise (black dashed line). B) Bathymetric map of the 8˚20' N seamount chain, oriented E-W perpendicular to the East Pacific Rise (dashed line). Maps created in GeoMapApp 3.6.8.

OASIS Cruise

In November 2016, the AT37-05 OASIS cruise sampled, mapped, and collected potential field data (gravity and magnetics) across the 8°20’ N seamount chain on R/V *Atlantis.* Bathymetric surveys across the entire study site were conducted using shipboard EM122 multibeam system. Magnetic anomalies were measured using SeaSPY Overhauser Magnetometer System, and gravity data were measured using a BGM-3 sea gravimeter. Shipboard EM122 multibeam (~75 m grid resolution) was collected over the entire study area, and AUV *Sentry* near-bottom high-resolution multibeam (~1 m) was focused on seamounts coincident with sample collection. As a result, one-meter resolution bathymetric maps are available for many dive sites, but not the entire study area. A total of 16 HOV (human-operated vehicle) *Alvin* dives and 19 dredges were conducted along the seamount chain, resulting in ~300 basalt samples for geochemical analysis (Table A.1, Figure 2). A follow-up cruise to the 8°20’ N seamount chain occurred in December of 2018 and included four additional *Alvin* dives. Results from the more recent cruise are not reported here.

Morphologically, the 8°20’ N seamount chain is composed of a complex array of volcanic constructs that include several east-west trending, nearly continuous ridges (give ~longitude), smaller cones, ridge parallel features and individual volcanic seamounts (Figure 2). The volcanic feature sampled nearest to axis is NEPR seamount (~ 22 km away), and the farthest examined from axis at ~ 209 km is Liona seamount, which is offset to the north of the main 8°20'N chain (Figure 2). Note each named volcanic sampling region may be composed of multiple features/morphologies (Table A.1). Volcanic constructions along the chain are divided into four morphologic categories

based on EM122 bathymetric maps and high-resolution *Sentry* maps, which are described in section 5.

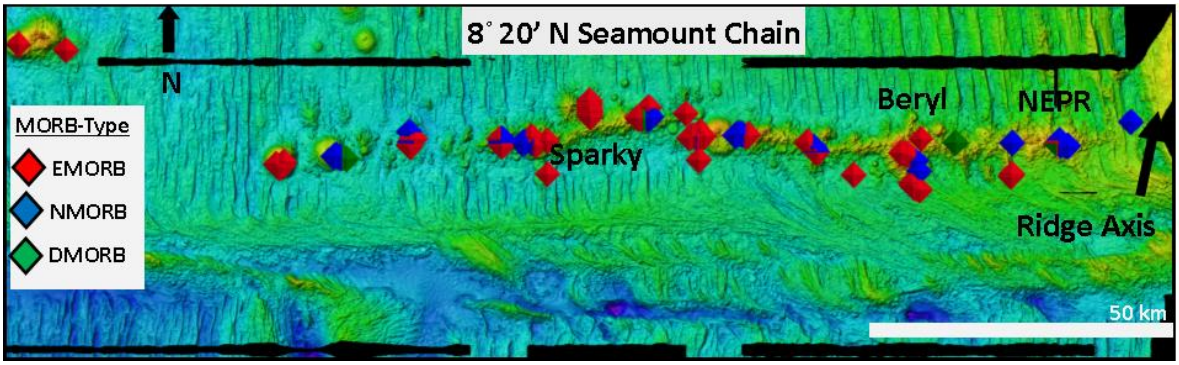

Figure 2. Bathymetric map of the ~200 km-long 8˚20' N seamount chain collected during November 2016 on the R/V Atlantis OASIS AT37-05 cruise. Seamount names and the locations of the ~300 basalt samples (colored diamonds) are shown. Red-colored diamonds represent enriched mid-ocean ridge basalt samples, blue-colored diamonds represent normal mid-ocean ridge basalt samples, and green-colored diamonds represent depleted mid-ocean ridge basalt samples. Map created in Fledermaus.

Methods

Major Elements

Basaltic glass chips were hand-picked for geochemical analyses. When present, phenocryst and alteration-free basaltic glass was selected from each sample. Three to five glass chips were handpicked from each sample using a binocular microscope and were mounted in 1-inch epoxy disks for geochemical analysis. The mounts were polished in 6, 3, and 1 µm diamond grits, and then hand-polished using 1 µm alumina grit.

Major element concentrations of 281 sample glasses were determined using the Cameca SX5-FE microprobe at University of Florida and a JEOL 8800 electron microprobe at USGS Denver. The accelerating voltage was 15 kV, beam current was 20 nA, and beam diameter was 10 µm. Count times varied for different elements. At University of Florida and USGS, Na was analyzed first for 10 seconds because of its

volatile nature. Mg, Si, Al, Fe, Mn, and Ca were also analyzed for 10 seconds each on all 281 samples. Ti, P, K, and Cl were analyzed for 20 seconds. Ni, Cr, and S were analyzed for 10 seconds on a minority of sample analyses but were often below detection limits and unmeasured on subsequent samples. Ten spots were measured on each glass and averaged. Secondary basalt standard 2392 (Perfit et al., 2012) was run approximately every 10-15 samples to account for any instrument drift. Measured standard values are provided in Table A.4. A set of 52 samples was analyzed at both labs for interlab comparison, which – based on measured standards JDF (at UF) and 2392, A99, and USNM (at USGS) – resulted in relative % corrections < 4% of SiO2, Na2O and CaO. The remaining standard major elements measured within one standard deviation and required no correction. Duplicate analyses are presented in Table A.5.

Trace Elements

Using the same epoxy mounts, trace element concentrations were determined on 148 samples via a Laser Ablation ThermoElectron X-Series II Quadrupole Inductively Coupled Plasma Mass Spectrometer (LA-ICP-MS) at Boise State University. The repeat rate was 10 Hz and dwell time 30 seconds using ~0.278 mJ of energy. Each glass sample was ablated 5 times (3 on one chip and 2 on another where multiple chips were available for a given sample) using 80-110 μm rounded spots and averaged. Standards used included KL2, ML3B, StHls, T1, GOR132, ATHO, BHVO, BCR, and BIR, with BHVO, BCR, and BIR run every 5 samples.

Radiogenic Isotopes

Radiogenic isotopes were collected on 19 geochemically and spatially diverse basalts at the University of Florida. Approximately 50 mg of fresh, phenocryst-free glass was hand-picked using a binocular microscope. Due to alteration and manganese coating, glass chips were cleaned using a combination of leaching methods (Goss et al., 2010; Sims et al., 2002; Waters et al., 2011). Glass chips were sonicated in DI water for 20 minutes and rinsed. Then the glasses were put in capped Teflon and leached in 35% H_2O_2 for 15 minutes on a hot plate at 130˚ C. The samples were rinsed three times in DI, then in capped Teflon leached in 2 mL of 6 M HCL for either 30 or 60 minutes (depending on the amount of remaining manganese coating) at 130˚ C. The samples were rinsed in DI then sonicated for 15 minutes in DI before rinsing three times in DI water. Samples were then dried in an oven at 50˚ C overnight.

Clean glasses were digested in 3 mL HNO_3 + 1.5 mL HF, and after evaporated drying, dissolved in 6 N HCl and subsequently evaporate dried. The dried residue was dissolved and separated for Pb, Sr, and Nd using column chemistry, following methods described in Goss et al. (2010): Pb was separated through 100 μL Teflon columns in HBr eluent then washed 3x in 1 mL 1 N HBr, then collected in 1 mL 3N HNO_3. Sr and Nd were collected subsequently using 1 N HBr and purified for analysis. Biorad AG50W resin columns were used to separate Sr from REE, and Nd was separated from REE through 100 mL columns of HDEHP-coated resin. Pb, Sr, and Nd isotopes were then measured at the University of Florida using a Nu-Plasma multicollector (MC) ICP-MS, also using methods described in Goss et al. (2010).

Geochemical Results

Mid-Ocean Ridge Basalt Types

To assess geochemical heterogeneity along the 8°20’ N seamount chain, we measured major and trace element contents, and radiogenic isotope ratios of lavas from the entire seamount chain. Major element contents and uncertainties analyzed basalt glasses are reported in Table A.1. Trace element contents and uncertainties are reported in Table A.2. Radiogenic isotope (Sr, Nd, and Pb) ratios and errors are reported in Table A.3.

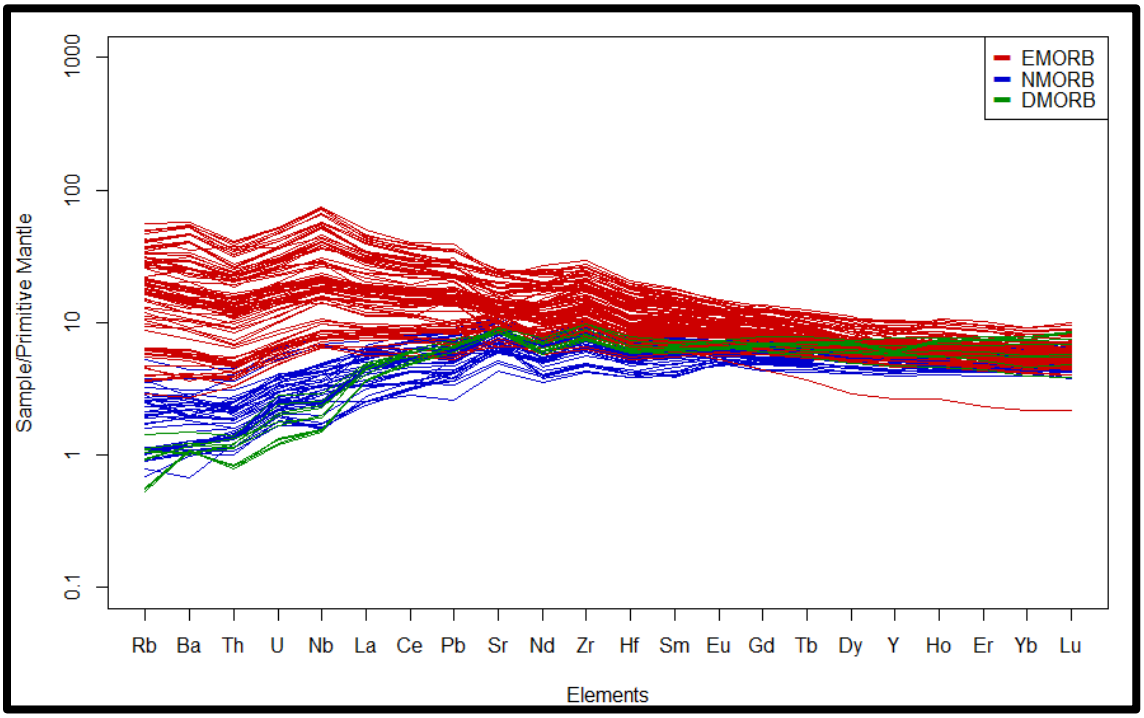

Figure 3. Primitive mantle-normalized trace element diagram of the 8˚20’ N seamount lavas (normalized to McDonough & Sun (1995) primitive mantle). Samples are divided into MORB type (EMORB red; NMORB blue; DMORB green) as described in the text. Note the relative slopes of the most incompatible trace elements (from Rb to Sr) for each MORB-type.

The seamount lavas are extremely heterogeneous, forming a compositional continuum from remarkably depleted to enriched basalts (Figure 3). To evaluate the processes involved in producing this range of compositions we classify each basalt as a

Depleted MORB (DMORB), NMORB, or EMORB (Table A.1). We define these MORB-type geochemical groups primarily based on their Th/La ratio (Shimizu et al., 2016), as well as Nb/La, La/Sm_N, and K/Ti ratios (i.e., Waters et al., 2011; Figure 4). DMORB are typically less than 0.035 Th/La, 0.60 La/Sm_N, and 8 K/Ti, whereas EMORB are greater than 0.068 Th/La and greater than 11 K/Ti. NMORB, most like the compositions found on axis, fall between these values. Since the data form a continuum rather than distinct geochemical groups, these parameters are used in tandem with one another (Figure 4). Using this classification scheme, there are 176 EMORB, 86 NMORB, and only 19 DMORB lavas. Below, we describe the geochemical affinities of each MORB type.

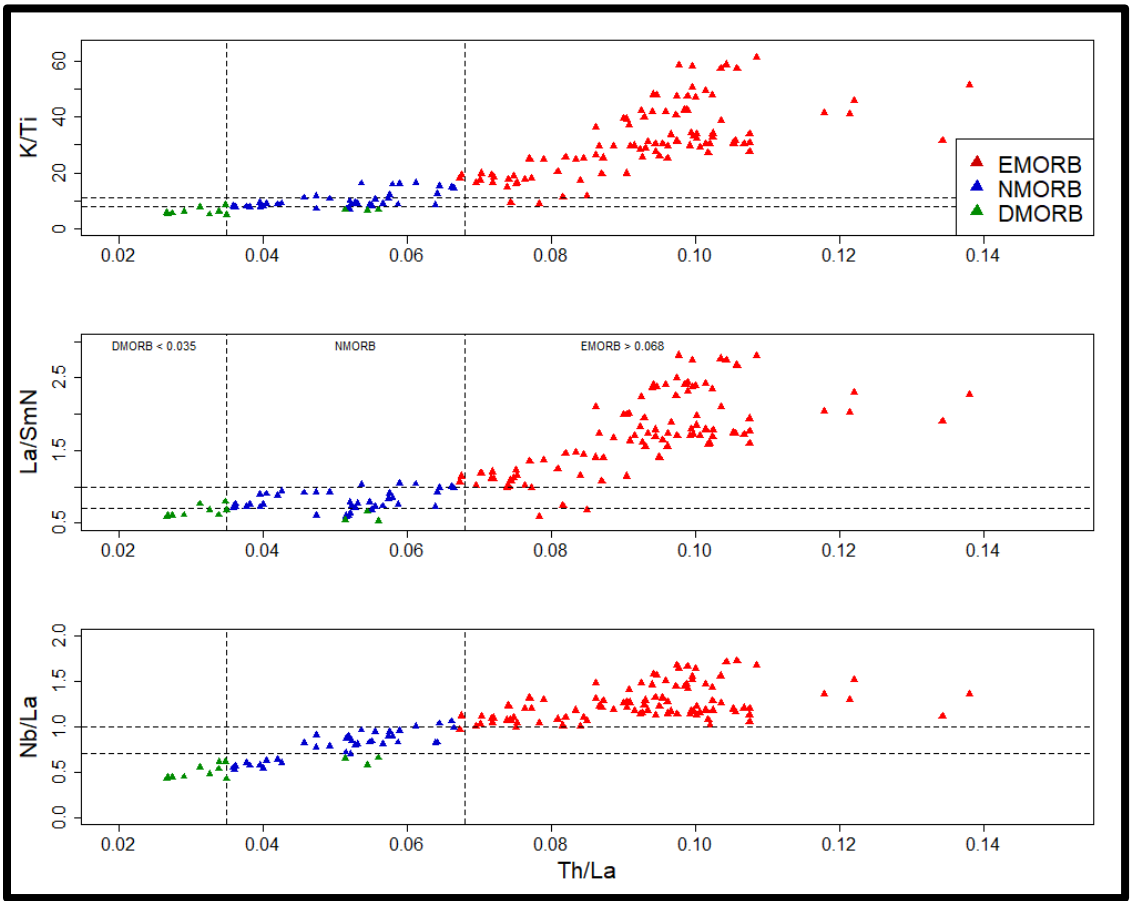

Figure 4. Major and trace element ratios used to determine MORB-type (enriched, normal, and depleted) classification system for the 8˚20' N seamount lavas. Categories are determined by examining how enriched or depleted the trace element ratios (or K/Ti) are relative to on-axis "typical" or normal MORB (Shimizu et al., 2016; Waters et al., 2011). Dashed lines are boundaries for each MORB-type and are described in the text.

Enriched MORB

The majority of the seamount lavas are EMORB, which have enriched trace element contents and ratios compared to NMORB lavas. EMORB lavas are characterized by high K/Ti ($100*(K_2O/TiO_2)$) ratios (16.5 – 61.3) and the lowest MgO contents (although they range from 4.6 – 8.8 wt %). Ratios of LREEs to MREEs in EMORB lavas are high (i.e., La/SmN ranges from 0.7 – 2.8), as are MREE to HREE ratios (i.e., Sm/YbN ~ 0.9 – 3.1). Highly incompatible element ratios of elements with similar

distribution coefficients (i.e., Nb/La ~ 0.9 – 1.8) are also more enriched than NMORB and DMORB lavas. Additionally, the EMORB are consistently more enriched in $^{87}Sr/^{86}Sr$ ratios (0.702630 – 0.702743) and Pb-series ratios (i.e., $^{206}Pb/^{204}Pb$ 18.173 – 18.781, and are more depleted in $^{143}Nd/^{144}Nd$ ratios (0.513043 – 0.513119).

Normal MORB

The second most abundant lava composition erupted at the seamounts is NMORB, which closely resemble compositions typical of on-axis MOR lavas. The NMORB are characterized by moderate K/Ti ratios (6.7 – 16.4) and high MgO contents (7.1 – 10.6 wt %). Ratios of LREEs to MREEs are lower than those of EMORB (i.e., La/SmN ~ 0.5 - 1), and ratios of MREEs to HREEs are lower than EMORB, but closely resemble DMORB (i.e., Sm/YbN ~ 0.9 – 1.5). Highly incompatible element ratios with similar distribution coefficients are more depleted (i.e., Nb/La ~ 0.5 - 1) than EMORB as well as DMORB. The NMORB are also consistently more depleted than EMORB but more enriched than DMORB in $^{87}Sr/^{86}Sr$ (0.702693 – 0.703198) and Pb-series ratios (i.e., $^{206}Pb/^{204}Pb$ are 18.53636 – 18.71381), and are more enriched than EMORB but more depleted than DMORB in $^{143}Nd/^{144}Nd$ ratios (0.512959 – 0.513104).

Depleted MORB

The least abundant lava composition erupted on the seamounts is DMORB, which are characterized by the depletion of highly incompatible elements. They are the most mafic (MgO content 8.2 – 9.8 wt %) lavas and have the lowest K/Ti ratios (< 9). DMORB LREE to MREE ratios are lower than NMORB (i.e., La/SmN 0.5 – 0.8), but the MREE to HREE ratios are greater than those of NMORB (i.e., Sm/YbN ranges from 0.7 – 1.7) and overlap the more enriched EMORB heavy rare earth elements. DMORB highly

incompatible element ratios with similar distribution coefficients are most depleted (i.e., Nb/La ~ 0.4 – 0.7). The DMORB are also consistently more depleted than EMORB and NMORB in $^{87}Sr/^{86}Sr$ (0.702333 – 0.702667) and Pb-series ratios (i.e., $^{206}Pb/^{204}Pb$ 17.91149 – 18.5356), and are more enriched in $^{143}Nd/^{144}Nd$ ratios (0.513058 – 0.513211).

Volcanic Morphologies

Bathymetric mapping of the seamount chain indicates that it is not simply comprised of numerous individual seamount edifices, but is instead a morphologically complex chain of volcanic constructs. Mapping in 2016 revealed ~30 volcanic edifices including individual seamounts, small cones, and volcanic ridges composed N-S trending rift zones and nearly linear ridges that are oriented E-W, approximately parallel to the Siqueiros transform fault (Figure 1). While detailed morphologic analyses are not included in this study, it is important to provide a general description in order to compare lava chemistry to volcanic features. The seamount names, sample locations, associated volcanic morphology, and chemical MORB-types are provided in Table A.1.

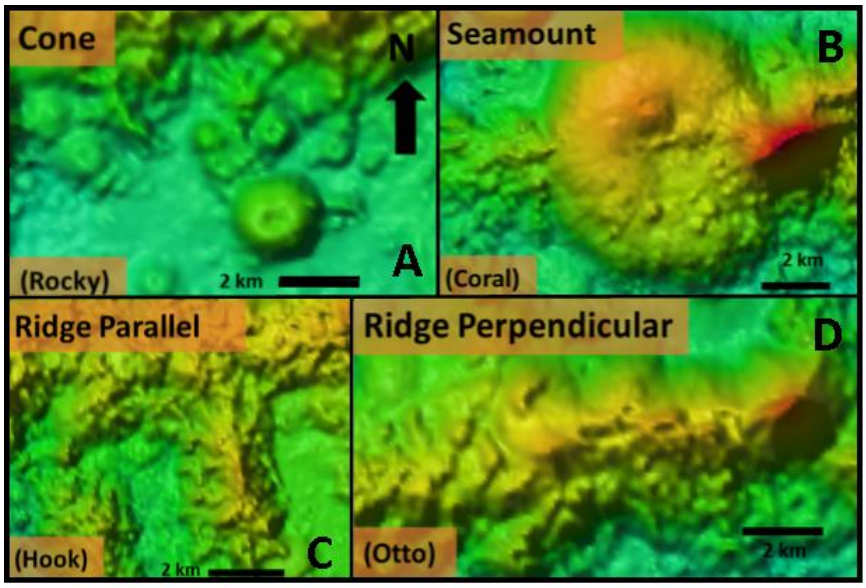

Figure 5. Bathymetric maps highlighting different volcanic morphologies observed along the 8˚20' N seamount chain. (A) Cone morphology (south of Rocky ridge), (B) Seamount morphology (Coral seamount), (C) Ridge parallel ridge (Hook ridge), and (D) Ridge perpendicular ridge (Otto ridge). Scale bars (2 km) show relative sizes of each feature and emphasize that cones are smaller than seamounts, and ridge parallel ridges are thinner than ridge perpendicular ridges. Note: cones are generally located off the chain, and ridge parallel ridges are either offset or extend outward from the chain. Seamounts and ridge perpendicular ridges are along the chain.

Each volcanic construct along the chain is classified as either a (1) seamount, (2) cone, (3) ridge parallel ridge, or (4) ridge perpendicular ridge depending on the morphologic affinities (Figure 5). A seamount is defined here as a distinctly rounded volcanic feature (> 4 km in diameter) that stands at least 500 m above the surrounding seafloor (Figure 5b). These are most apparent on the western end of the chain, most distal to the EPR axis. Seamounts include Liona, Max, and Avery seamounts. However, less obvious examples of seamount morphologies include NEPR and Wayne. While these two seamounts are more elongate, their overall shapes are comparable to the larger, rounded seamounts. By contrast, volcanic cones are smaller features, usually < 2 km in diameter. They are typically offset from the chain or distinct from larger rounded features

(seamounts) and are not linear (Figure 5). These are located near the base of the seamount chain (within a few km north or south of the main, primary edifices) and some contain small depressions in their centers. The ridge perpendicular (RPerp) morphology describes volcanic features that are elongated perpendicular to the EPR axis and form the bulk of the seamount chain (Figure 5). These ridges crosscut the underlying abyssal hill fabric, are nearly linear in the East-West direction, and are clearly comprised of multiple volcanic eruptions. Interspersed within the E-W trending volcanic ridges are several larger seamounts that have N-S trending rift zones or ridges. These ridge parallel (RPar) features are elongate in the direction of the abyssal hill faults (i.e., Sparky) and can bend or hook eastward towards the Siqueiros transform fault, mimicking the underlying seafloor fabric (i.e., Beryl; Figure 2).

DISCUSSION

Compositional Variability in the Off-Axis 8˚20’ N Seamount Chain

While lavas erupted on-axis at fast-spreading MORs are typically limited in composition due to efficient homogenization of magmas in the shallow axial melt lens (Rubin & Sinton, 2007; Sinton & Detrick, 1992), lavas erupted at off-axis seamounts can provide a window into mantle compositions obscured on-axis (Batiza et al., 1990; Batiza et al., 1989; Brandl et al., 2012; Fornari et al., 1988a; Niu et al., 2002; Niu & Batiza, 1997b, 1997a; Shimizu et al., 2016; Zindler et al., 1984). Here, we compare major and trace element contents and radiogenic isotope ratios in lavas erupted along the 8°20' N chain with adjacent on-axis EPR lavas and other nearby seamounts to assess the variability of the 8°20'N lavas compared to other regional datasets.

The 8°20’ N seamount lava compositions are extremely variable compared to lavas erupted on-axis along the adjacent EPR segment (8 - 10° N; Figure 6 - 8). While the on-axis lavas have relatively limited major and trace element ratios (5 – 9 K/Ti ratios, 0.6 – 0.7 La/SmN ratios, and 0.03 – 0.05 Th/La ratios), the seamount lavas have compositions that range from 4.9 – 61.3 K/Ti, 0.53 – 2.81 La/SmN, and 0.027 – 0.138 Th/La (Figure 7). The compositional heterogeneity preserved in off-axis lavas suggests that the magmas producing the seamounts likely by-pass homogenization in the axial magma chamber (Batiza & Niu, 1992; Perfit & Chadwick, 1998), and thus provide a window into the deeper magmatic system.

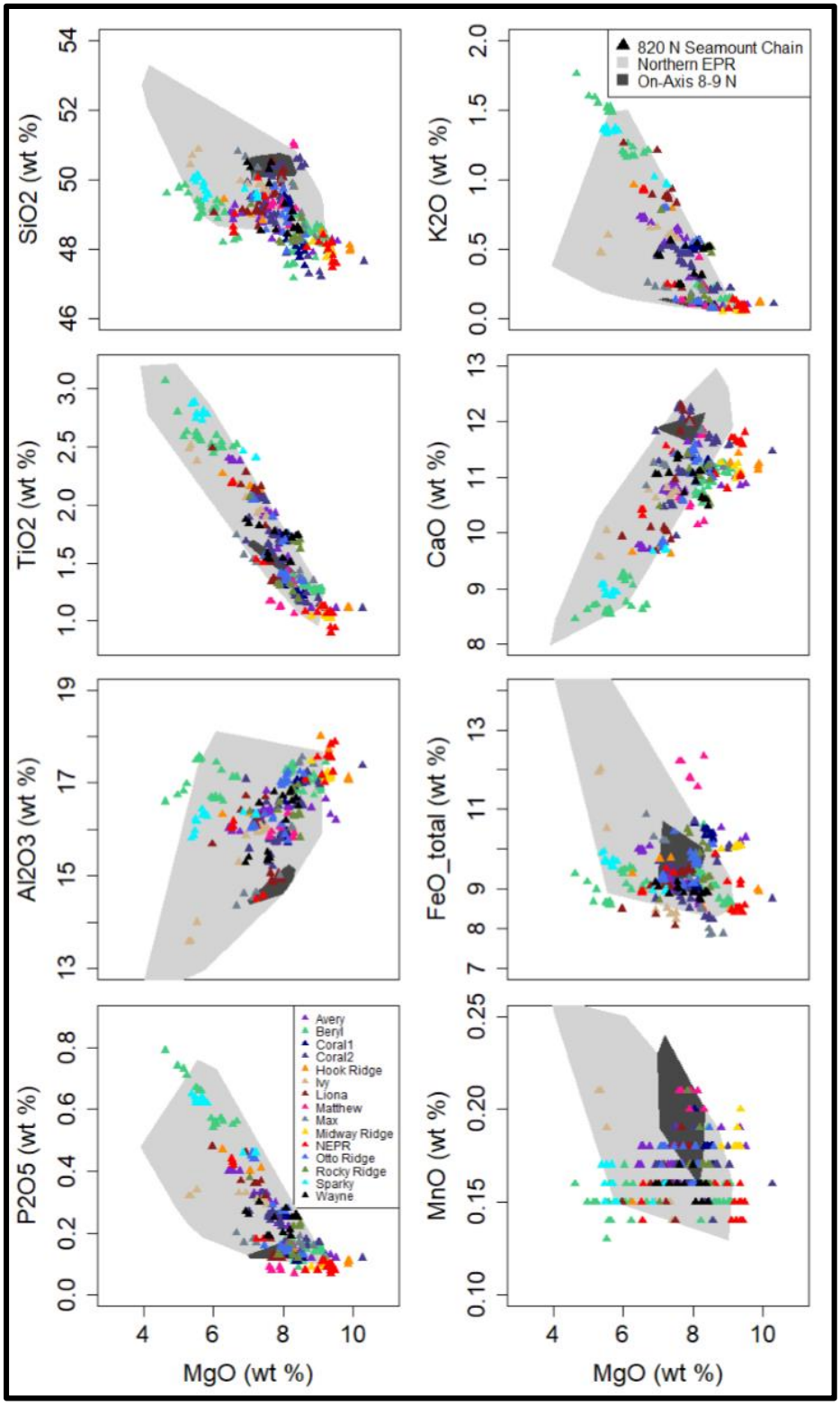

Figure 6. Major element bivariate diagrams of the 8˚20 N seamount lavas. Local on-axis data from the 8—10˚ N EPR ridge segment (dark grey region), and data from the entire northern EPR region including off-axis seamounts (light grey region) are shown for comparison.

The seamount lava compositions are also compared with a northern EPR dataset (which includes samples from on-axis, near-axis on the ridge, and off-axis locations between 8 – 11° N) to evaluate heterogeneity compared to other off-axis lavas. The 8°20’ N seamount lavas span the entire range of major and trace element compositions as well as radiogenic isotope ratios (Figures 6 – 8) of the northern EPR lavas. The similarity of the seamount compositions with the northern EPR dataset provides additional evidence that the off-axis lavas are tapping a different magmatic system compared to on-axis lavas.

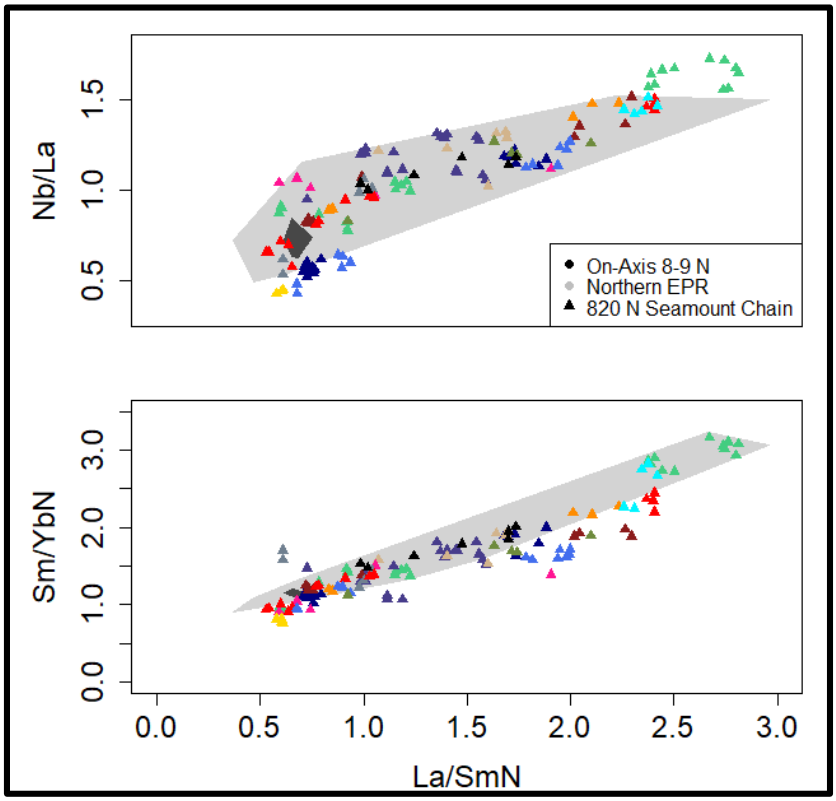

Figure 7. Trace element ratios of the 8˚20 N seamount lavas. Local on-axis data from the 8-10˚ N EPR ridge segment (dark grey region) and data from the entire northern EPR region including off-axis seamounts (light grey region) are shown for comparison. Note how the seamount compositions spread well beyond the on-axis EPR data and span the entire range of trace element ratios of the northern EPR region. La/SmN and Sm/YbN are normalized to McDonough & Sun (1995) primitive mantle.

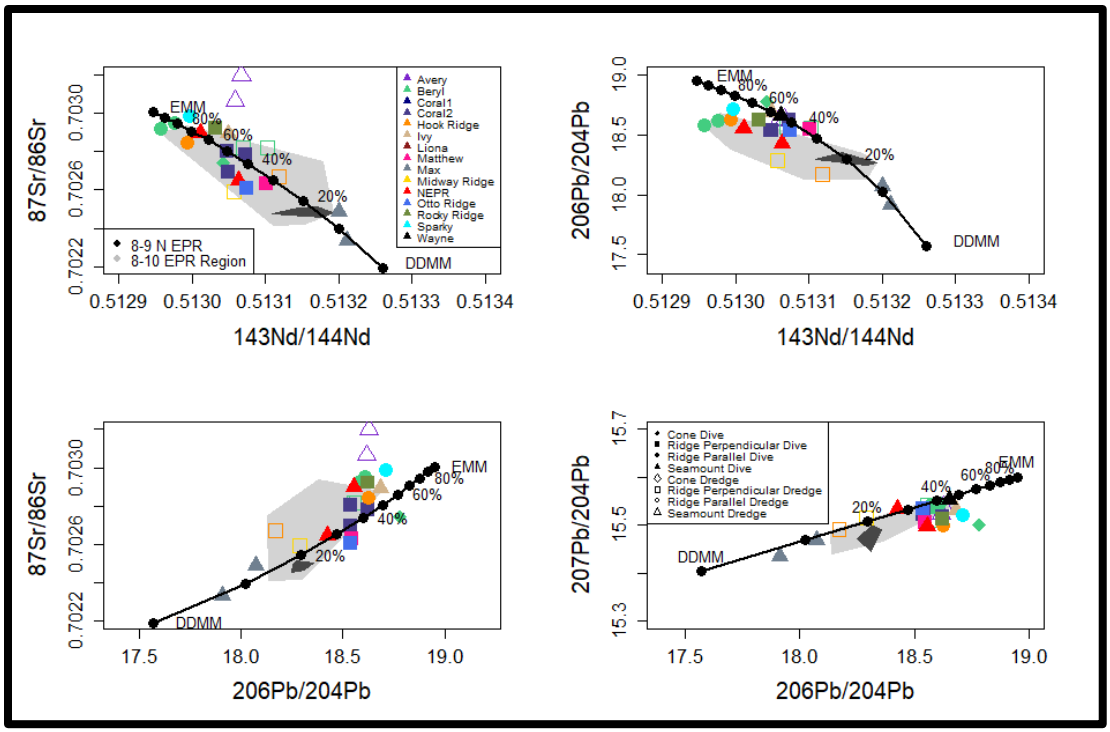

Figure 8. Radiogenic isotope (Pb, Sr, and Nd) ratios of the 8˚20 N seamount lavas compared with on-axis data (dark grey region) and the northern EPR (light grey region). Error bars are smaller than the symbols used and thus are not shown. Mid-ocean ridge mantle reservoirs EMM (Enriched MORB Mantle from Donnelly et al., 2004) and DDMM (Depleted Depleted MORB Mantle from Workman & Hart, 2005) are shown as mantle end-members for the seamount compositions. Binary mixing models (black line) between EMM and DDMM are shown with dots indicating 10% increments.

The spatial distribution of the MORB-types is examined along-chain and with height on the seamount edifice (represented by depth below sea level) to determine if there are systematic variations chemistry that may be related to specific magmatic processes. Increasing lithospheric thickness with distance from the ridge axis truncates the melting column at greater depths. This results in lower extents of melting and therefore more enriched melts at the wings of the melting triangle compared to the center (Langmuir et al., 1992). Therefore, variations in extents of melting may produce a systematic change in lava composition with distance from the ridge axis. However, there is no obvious systematic variation in lava chemistry along the ~200 km chain of

seamounts (Figure 2, 9, 10).

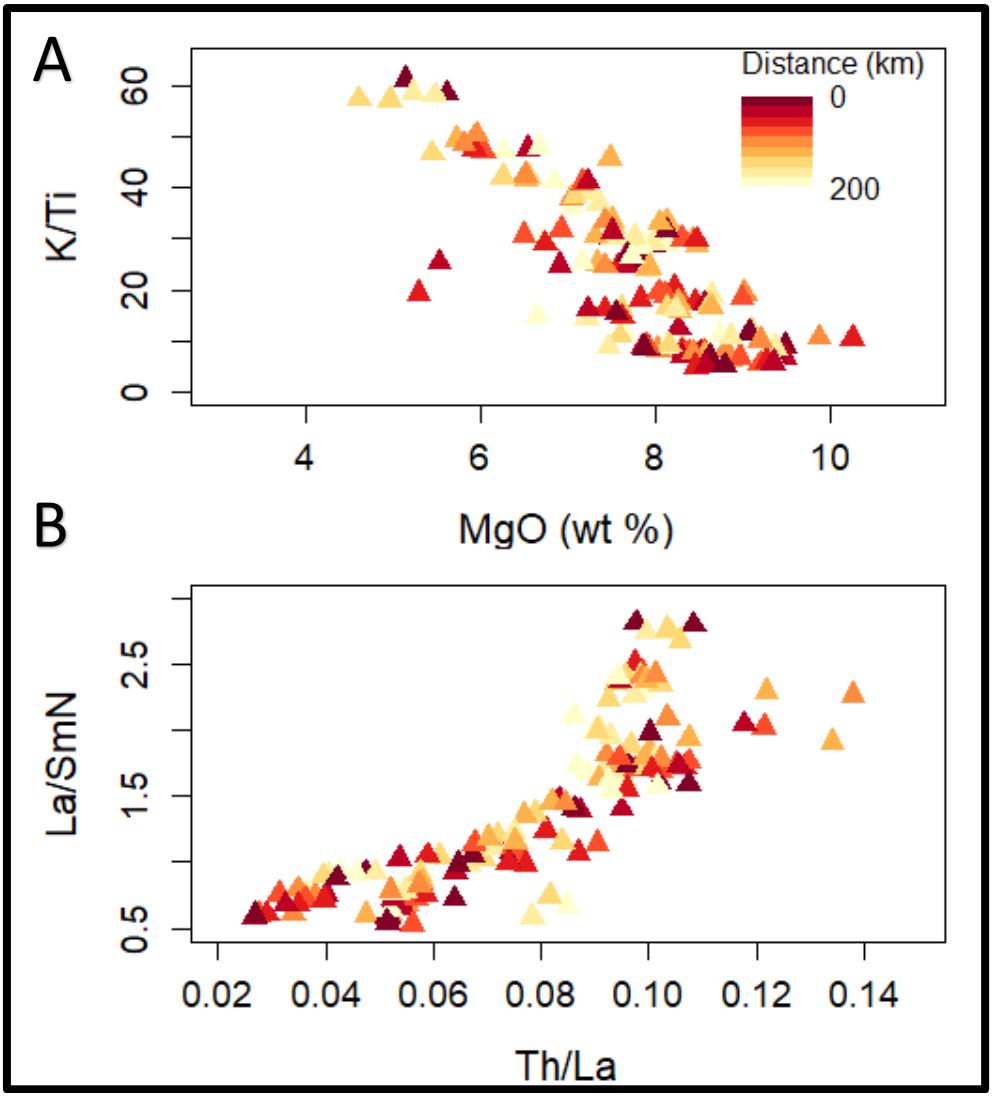

Figure 9. Seamount lava chemistry with distance from axis (color gradient from darker shades closest to axis and lighter shades farther from axis) for (A) MgO (wt%) vs K/Ti ratios, and (B) Th/La vs La/SmN ratios. In general, there is no systematic variation in chemistry with distance from the ridge axis.

Alternatively, there may be systematic variations with height on the volcanic edifices, indicating that the magma compositions are changing over time. If the seamounts are progressively forming as they move away from the ridge axis and are built from vertical ascent of magmas from the melting triangle, then the base of the seamounts may be more depleted than the tops. However, there is no obvious systematic variation in

lava chemistry with height on each seamount (Figure 11; Supplementary Figures 1, 2). In fact, EMORB, NMORB, and DMORB lavas are found at almost all longitudes along the chain (Figures 2, 9, 10), suggesting that systematic variations in melting alone cannot account for the compositional heterogeneity observed along the seamount chain.

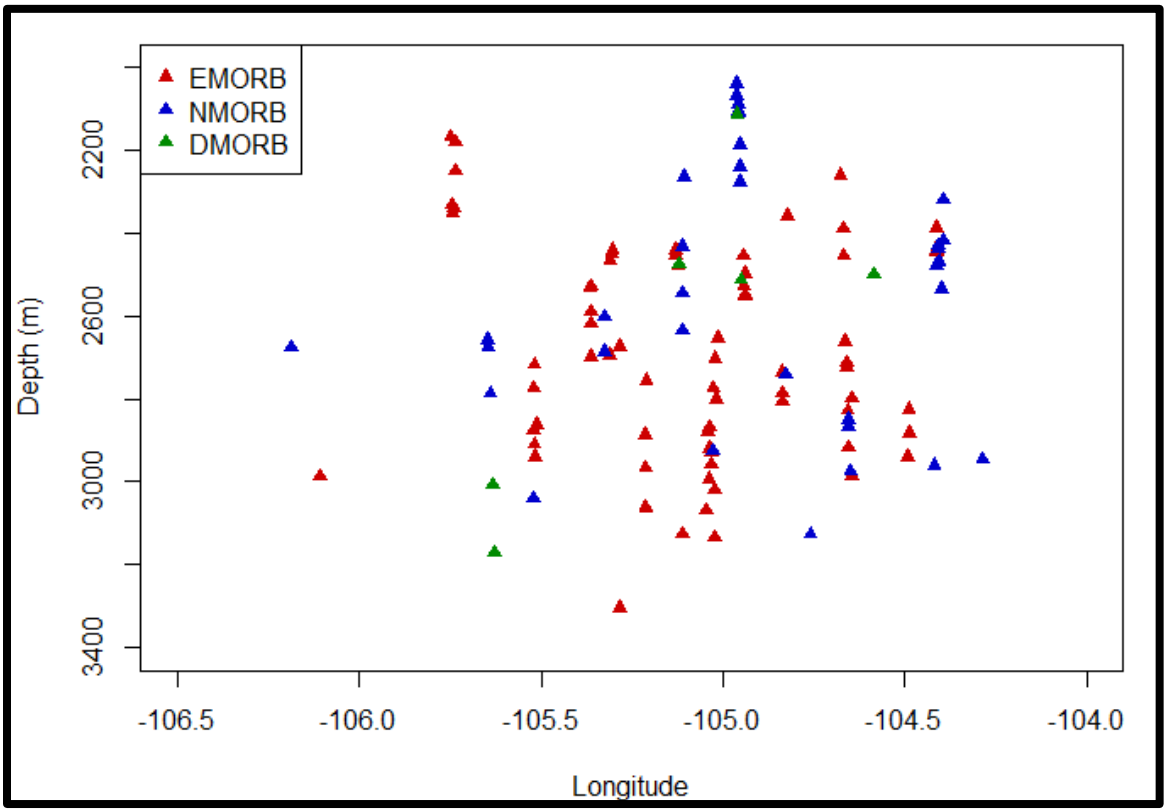

Figure 10. Spatial distribution of chemistry with distance from axis and depth along the seamount chain. Y-axis is reversed (meters below sea level). In general, there is no systematic variation in MORB type with depth or distance from the ridge axis.

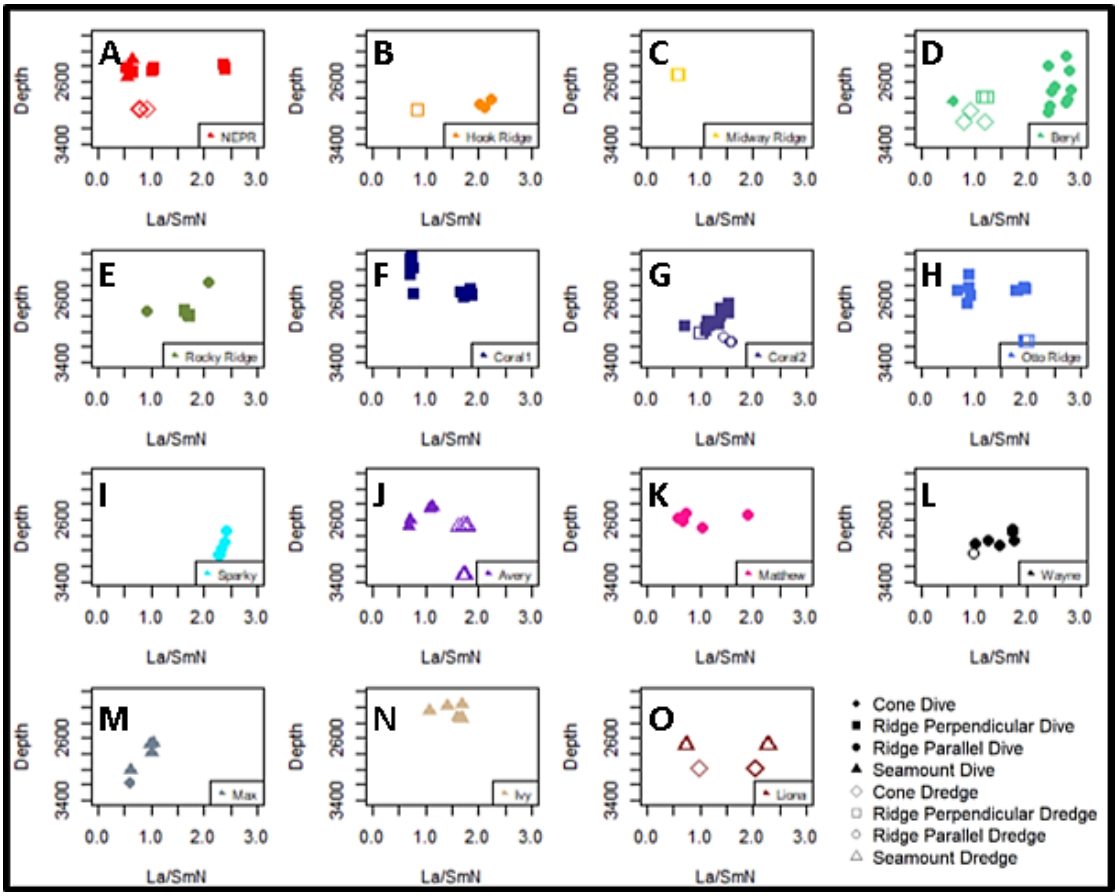

Figure 11. La/SmN of the 8˚20' N lavas versus depth below sea level (m) for each seamount, starting from closest to axis (A. NEPR) through farthest from axis (O. Liona). Shapes indicate volcanic morphology types. Open symbols are from dredges and closed symbols are from Alvin dives. In general, there is no systematic difference in MORB-type with depth. More examples of this are provided in supplementary material.

Despite the lack of clear systematic changes observed in compositions with distance and depth along the chain, there are some differences in composition with volcanic morphology (Cone, Seamount, Ridge Parallel, and Ridge Perpendicular) (Figure 12). For example, cones (small round features located off the main chain) are primarily composed of DMORB and NMORB lavas (Figure 12), and the ridge-parallel features (linear features oriented parallel to the abyssal hill fabric) primarily erupt EMORB. By contrast, lavas collected from the larger primary E-W trending volcanic edifices within

the chain (seamounts and ridge perpendicular constructions) span the entire range of compositions without any clear preferential lava composition.

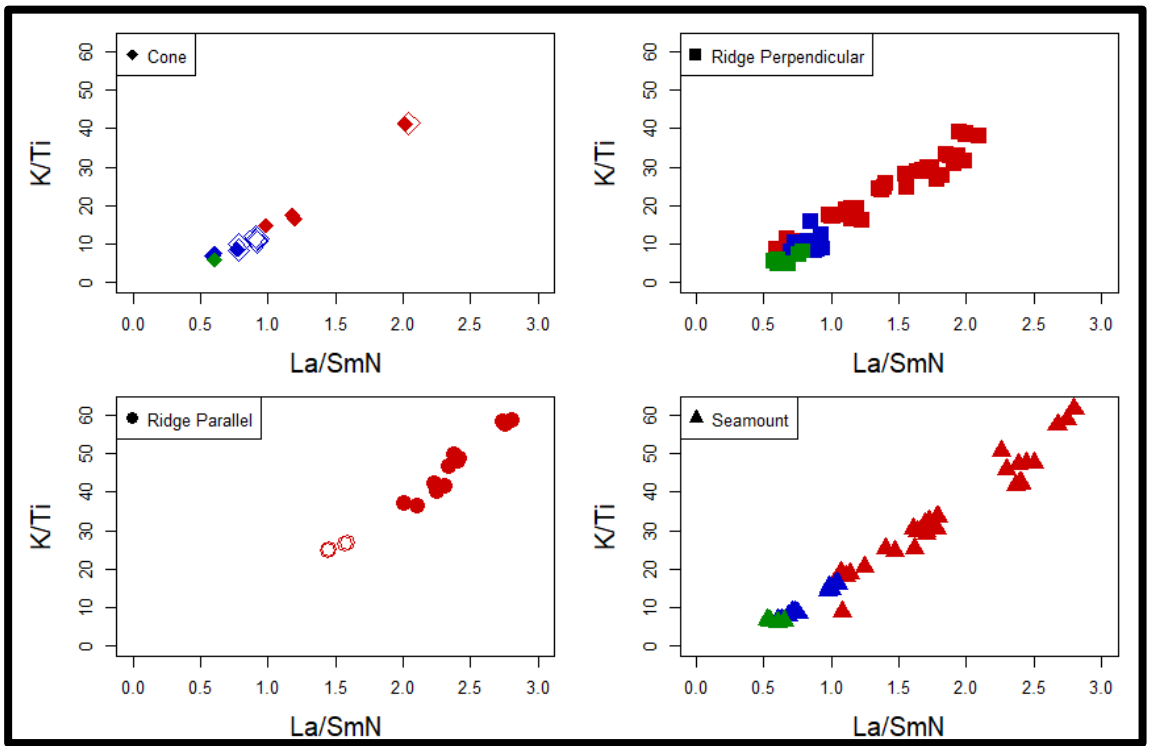

Figure 12. La/SmN against K/Ti ratios for each volcano morphology type. Shapes are morphology types. Open symbols are from dredges and closed symbols are from Alvin dives. Cones are primarily depleted in major and trace element ratios, whereas ridge parallel features are exclusively enriched. Ridge perpendicular features and seamounts span the entire range of compositions.

Some seamounts erupt a limited compositional range (i.e., Figure 13C), while others erupted a wide range of compositions (i.e., Figure 13A). This distribution indicates that each seamount has undergone a unique series of petrologic processes. Next, I discuss how petrologic models are used to evaluate the processes involved in the formation of the 8°20'N Seamounts.

Modeling Geochemical Variability Along the Seamount Chain

Numerical models are used to constrain the roles of fractional crystallization, mantle melting, and source heterogeneity in the petrogenesis of lavas along the 8°20'N

off-axis seamount chain. The processes that are involved in the formation of lavas erupted along the entire seamount chain are evaluated using specific examples from three volcanic edifices (NEPR, Beryl, and Sparky). These three seamounts span almost the entire length of the chain (NEPR ~22 km, Beryl ~50 km, and Sparky ~ 120 km from axis), the different volcano morphologies (NEPR is a seamount, Beryl is a ridge-parallel ridge with some cones surrounding it, and Sparky is a ridge-parallel ridge), and the entire range of lava compositions represented in this study.

Fractional Crystallization Models

As magmas cool they will undergo variable extents of crystallization, resulting in a change the composition of the liquid magma. This process is often responsible for small-scale heterogeneity in erupted lavas on-axis (O'Hara, 1965, 1977) and on individual seamounts (e.g., Allan & Batiza, 1987). To assess whether the variability in lava compositions erupted along the chain and at individual seamounts results from fractional crystallization of mafic magmas liquid lines of descent are calculated using Rhyolite-MELTs (Ghiorso & Gualda, 2015; Gualda, Ghiorso, Lemons, & Carley, 2012). Modeling conditions include a parent composition of the most mafic lavas from each seamount, water contents of 0.1 – 1 wt %, pressures of 0.5 – 3 kbar, and an oxygen fugacity of QFM.

Not surprisingly, petrologic models indicate that the full range of lava compositions erupted along the 200 km long seamount chain cannot be explained by fractional crystallization of a single parent magma (Figure 13). In particular, the range of K/Ti ratios observed suggests that multiple parent magmas are involved in the formation of the seamount lavas. Furthermore, multiple parent magmas are required to explain each

MORB type (EMORB, NMORB, and DMORB) (Figure 13), suggesting that each seamount requires multiple parent magmas.

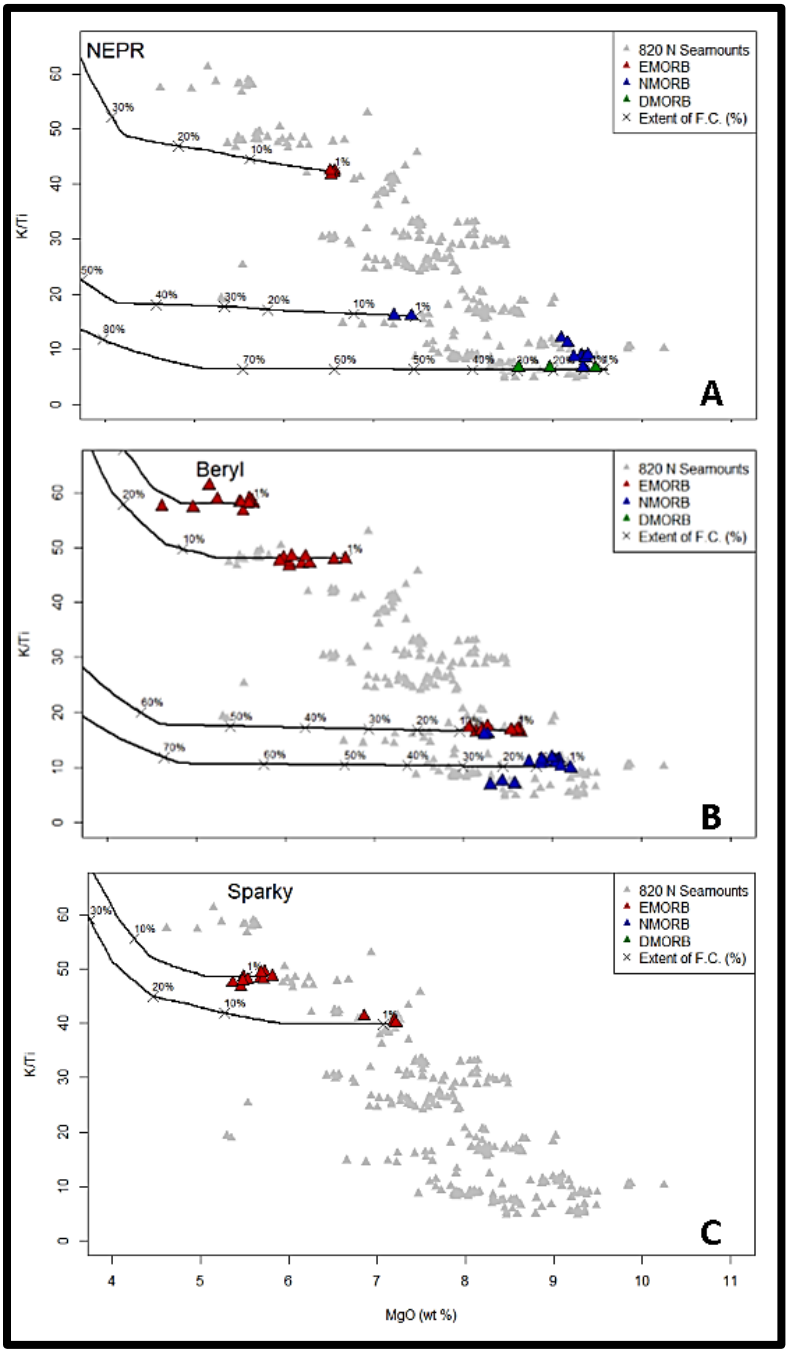

Figure 13. K/Ti ratios versus MgO contents for three seamounts: (A) NEPR, (B) Beryl, and (C) Sparky. Grey symbols show the compositions of all 8˚20' N seamount lavas. Colored symbols indicate compositions of lavas (by MORB type) erupted at

each seamount. Several fractional crystallization trends for each seamount are shown as black lines, with 10% increments shown as Xs. Multiple parent magmas are required to account for the range of K/Ti ratios observed at each seamount. Modeling parameters are provided in the text.

General trends consistent with MORB type magmas provide further insight into fractional crystallization along the chain. DMORB lavas have the most mafic parents and require the most crystallization (up to 30%) to explain the range of major element contents. By contrast, NMORB lavas require moderate extents of crystallization (< 20%) from the most mafic parent, while the EMORB are much more restricted in major element contents and can be explained by <5% crystallization (Figure 13). These results are consistent with previous fractional crystallization modeling showing that NMORB are around 20% crystallized while EMORB are crystallized to around 10% (Niu, Waggoner, Sinton, & Mahoney, 1996)

Multiple parent magmas are also required to account for the range of lavas erupted at individual seamounts. For example, Beryl seamount, which has the most variable major element contents, requires at least four parent magmas (one NMORB and three EMORB) to account for the compositional variability (Figure 13B). The NMORB lavas erupted at Beryl require at least 20% crystallization of sample OS19_J. However, based on K/Ti ratios, the EMORB lavas require <10% crystallization of three different parent magmas: OS9_C, 4860_4, and 4860_10.

Multiple parent magmas are also required to account for the range of major element contents at the most homogeneous seamounts. For example, the variability in K/Ti ratios requires at least two parents and crystallization of <5% (Figure 13C) to explain the erupted compositions at Sparky. Combined, these observations from each seamount suggest that the 8˚20’ N seamount chain formed from multiple volcanic events

and may require variations in mantle source and extents of melting in addition to fractional crystallization to explain the heterogeneity in major element concentrations.

Mantle Source Components

To determine if mantle source variability can account for the heterogeneous lava compositions, we measured radiogenic isotope ratios (Pb, Sr, and Nd). Radiogenic isotope ratios, unlike major and trace elements, are unchanged by mantle melting and crystallization, and thus more reliably reflect the source composition in the mantle. The radiogenic isotope ratios in the seamount lavas are highly variable, suggesting that the mantle source feeding the seamounts is heterogeneous (Figure 14). To further investigate mantle heterogeneity, we compare the seamount lava compositions to two end-member mantle components, the Enriched MORB Mantle (EMM) from Donnelly et al. (2004), and the Depleted Depleted MORB Mantle (DDMM) from Workman & Hart (2005)).

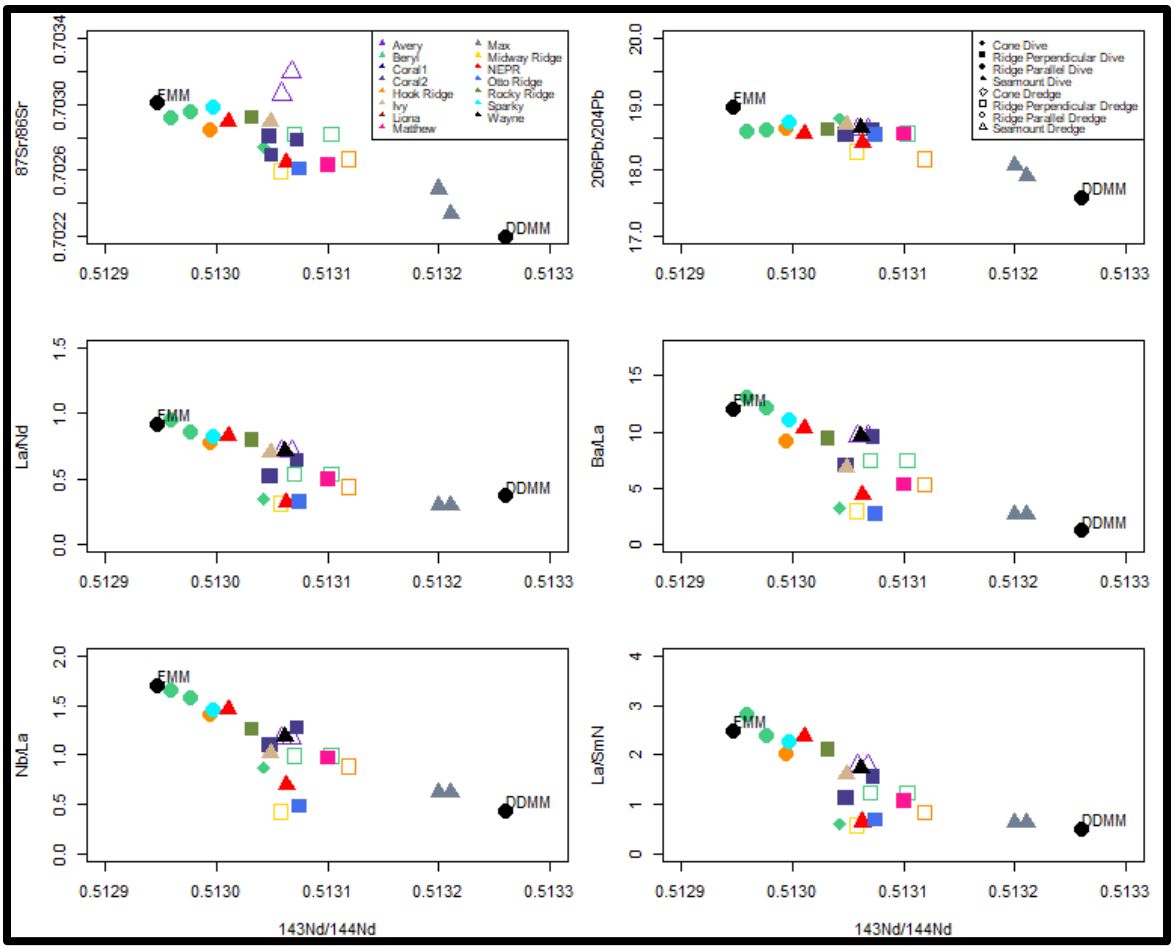

Figure 14. Radiogenic isotope ratios versus trace element ratios used for constraining mantle source component (black dots) trace element concentrations. These radiogenic isotopes are compared with trace element ratios containing the same denominator. These relationships form a linear representation of binary mixing among the seamounts between EMM and DDMM, and provide constraints for trace element concentrations of the source components forming the 8˚20' N seamount lavas. The trace element ratios for the mantle source components have been adjusted to best fit the end-members of the seamount lava compositions (Table A.6).

The EMM component is representative of a reservoir composed of enriched material unrelated to a mantle plume or the depleted upper mantle tapped by MORs (Donnelly et al., 2004). The addition of an enriched component in the upper mantle without the presence of a nearby plume can be attributed to subducted and recycled oceanic crust, which through time is mixed into the depleted upper mantle (Niu & Batiza, 1997b; Shimizu et al., 2016). This results in a volumetrically small, but perhaps

ubiquitous EMM component distributed throughout the upper mantle, which may be obscured in on-axis MORB due to efficient mixing in the axial magma chamber.

The DDMM component is representative of the most depleted 'end-member' of the depleted upper mantle, which is calculated as 2 sigma more depleted than the average DMM feeding on-axis MOR eruptions (Workman & Hart, 2005). I also investigated the average DMM (Workman & Hart, 2005), but found that it cannot explain the most depleted lavas erupted along the chain, so we use the depleted end member of the depleted MORB mantle instead.

To determine the mantle sources contributing to the range of compositions observed along the 8°20'N seamount chain, we compare these mantle end-members to the seamount lavas (Figure 8 & 14). EMORB lavas erupted at ridge-parallel features, such as Sparky and Beryl seamounts, have radiogenic isotope ratios similar to EMM, while Max Seamount and the ridge perpendicular portion of Hook Ridge most closely reflect the DDMM end-member (Figure 8). All the other seamounts have lava compositions that mostly lie between these two end-member components in radiogenic isotope space (Figure 8). There are several samples that deviate slightly from the binary mixing (Figure 8), indicating a third component may be present. Since the seamount data form a nearly linear continuum between the DDMM and EMM mantle components, binary mixing models of these sources are assumed for explaining heterogeneity among the seamounts. While binary mixing of DDMM and EMM mantle components can account for the radiogenic isotope variability of the seamounts, combining trace element ratios with radiogenic isotope ratios indicates that simple binary mixing between the end-members cannot explain the full range of trace element compositions (Figure 15). If source

variability controlled the geochemical variability, then trace element ratios should change systematically with the radiogenic isotope ratios. While in some cases, trace elements change mostly systematically with radiogenic isotope ratios (Nd isotopes and La/SmN of EMORB and NMORB but not DMORB; Figure 15), this trend is inconsistent across trace element ratios (Pb isotope ratios do not correlate with trace elements La/SmN or Gd/Yb). In fact, MORB-types are impacted to different degrees by trace element ratios and radiogenic isotope variability. For example, EMORB (red triangles in Figure 15) are constrained in Pb isotope variability but vary widely in La/SmN concentrations. On the contrary, NMORB and DMORB vary widely in Pb isotope variability and are constrained in La/SmN concentrations. This indicates that source variability and melting processes influence the MORB-types differently. Thus, we consider if variations in melting of a compositionally heterogeneous mantle source can account for the range of compositions erupted along the seamount chain by modelling each MORB-type group.

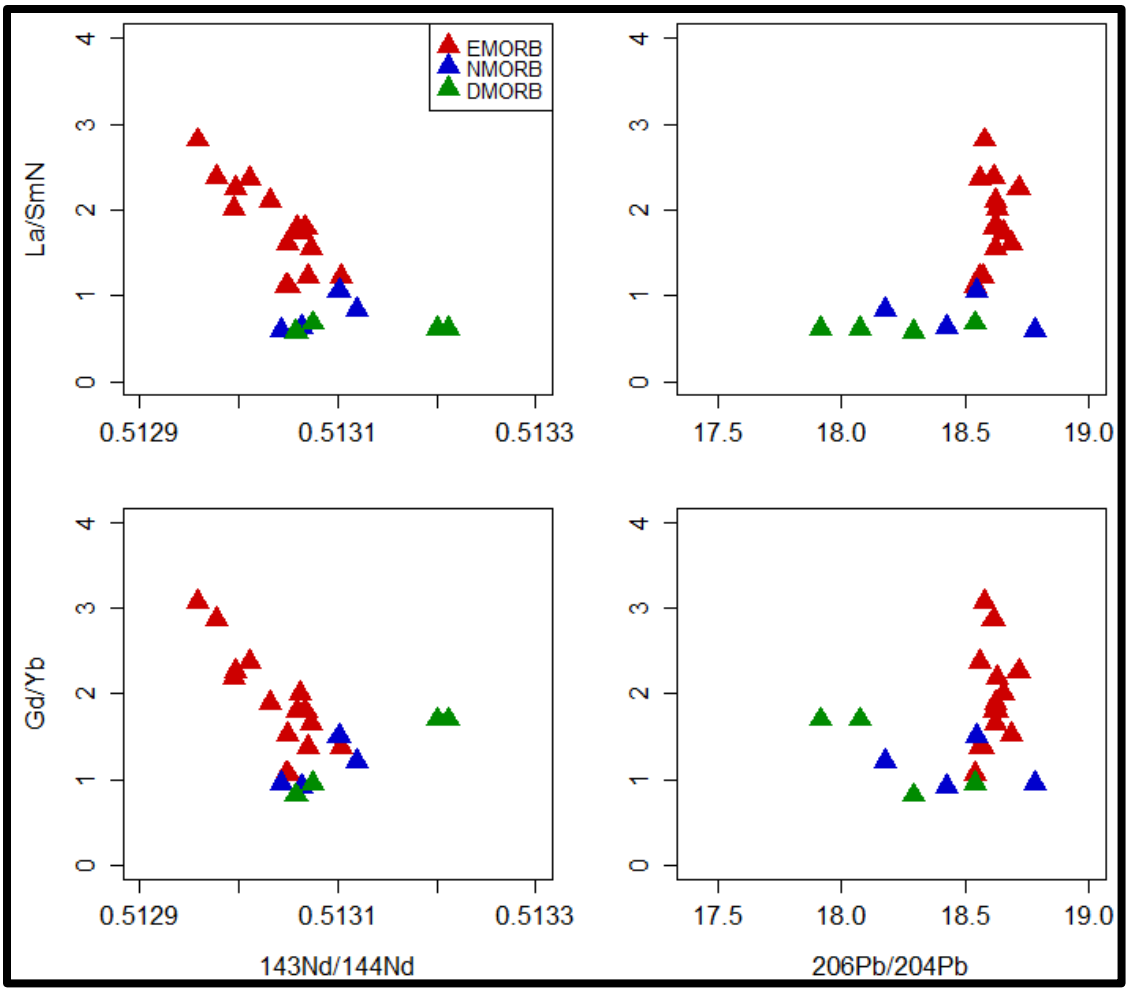

Figure 15. Radiogenic isotope ratios and trace element ratios demonstrate how correlated the MORB-types are in some instances, but are not correlated in others. Nd isotope ratios correlate well with trace element ratios of EMORB, but do not correlate well with NMORB or DMORB. Similarly, Pb isotope ratios do not correlate well with NMORB or DMORB, but also don't correlate well for EMORB.

Melting and Source Variability Constraints on Geochemical Heterogeneity

Trace element ratios in the seamount lavas cannot be explained by simple binary mixing of two mantle components or melting of a single mantle source alone (Figure 15). The radiogenic isotopes clearly indicate the presence of two (and perhaps three) mantle components, suggesting that the seamount lavas formed through a combination of source heterogeneity and variations in the extent of melting. To differentiate between the signatures of mantle melting and source heterogeneity, trace element ratios (La/SmN and

Nb/La) are used in conjunction with isotope ratios because their relative concentrations behave somewhat predictably during melting (Hofmann, 1997). La/SmN ratios are used to evaluate degrees of mantle melting due to their distinct partition coefficients during melting (higher ratios indicate lower extents of melting). By contrast, Nb and La have similar partition coefficients during melting, but can vary with source; thus, variations in Nb/La ratios can be used as a proxy for heterogeneity in the mantle (Hofmann, 1997). To validate the use of these ratios, radiogenic isotope ratios are compared with Nb/La ratios. In general, the two datasets are correlated (Figure 16), indicating Nb/La can be used as an approximate proxy for mantle source heterogeneity in the absence of isotope analyses.

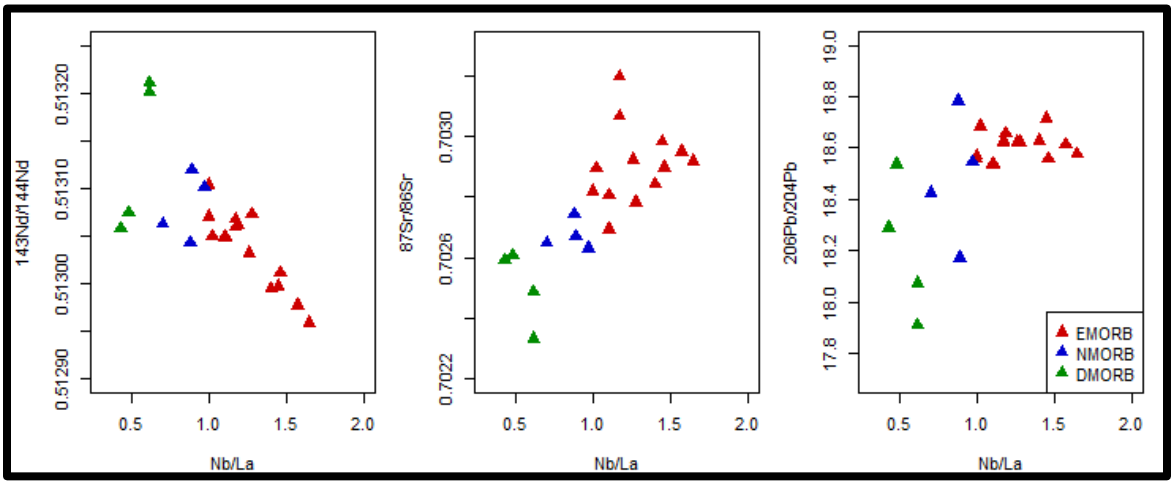

Figure 16. Nb/La as a source proxy showing the comparison between a trace element ratio of highly incompatible trace elements with similar incompatibilities and radiogenic isotopes. Note the consistent correlation between this trace element ratio and radiogenic isotopes for the MORB-types.

To model melting of a heterogeneous mantle source, we first determined the starting compositions of the end-member mantle components in terms of trace elements. The trace element contents in mantle end-members may be variable and are difficult to constrain because they are highly influenced by mantle melting. To estimate trace element contents in both end-members at 8°20’ N (EMM and DDMM), we compare

radiogenic isotope ratios (Pb, Sr, and Nd) with trace element ratios sharing common denominators (i.e., La/Nd vs 143Nd/144Nd ratios). Based on this comparison (Figure 14), trace element contents for the end-member components in the petrologic models were adjusted slightly from reported EMM and DDMM to more closely match local end-members of the seamount lavas (Supplementary Table A.6). The estimated trace element concentrations for each component are mixed in 10% increments to produce a suite of parent compositions (Figure 17), which are subsequently melted using alphaMELTs (Smith & Asimow, 2005). Water contents for starting compositions, based on H_2O/Ce ratios, were 100 ppm for DDMM (Workman & Hart, 2005) and 400 ppm for EMM, and concentrations of mixtures in between. Melting models were run using isentropic, polybaric melting starting at 30 – 40 kbar and at 1300 – 1400 ˚C; however, the best-fit models were consistently 1400˚ C and 40 kbar (Figure 17).

Assuming two-component mantle mixing, the entire range of seamount lava compositions can be explained by 1 – 15% melting of a heterogeneous mantle composed of mixtures of DDMM and EMM (Figure 17). In general, the DMORB lavas are produced by ~5 - 15% melting of predominantly DMM (containing up to 5% EMM; Figure 16). NMORB are formed from 5 – 15% melting of a slightly more enriched mantle slightly than DMORB (~ 5 – 15% EMM). EMORB, however, span a much wider range of melting extents and source variability, ranging from <1% melting of a 10% EMM mantle to >15% melting of a 100% EMM mantle. This confirms previous assertions that the MORB-types are influenced by each process to different degrees (Figure 15), where EMORB vary greatly by melting and DMORB vary by source composition. Whether the mantle is mixed prior to, during, or after melting remains

ambiguous in these models. However, these results suggest that the full range of lava compositions erupted along the seamount chain, including major and trace element contents and radiogenic isotope ratios, are explained by various extents of melting and fractional crystallization of a heterogeneous mantle.

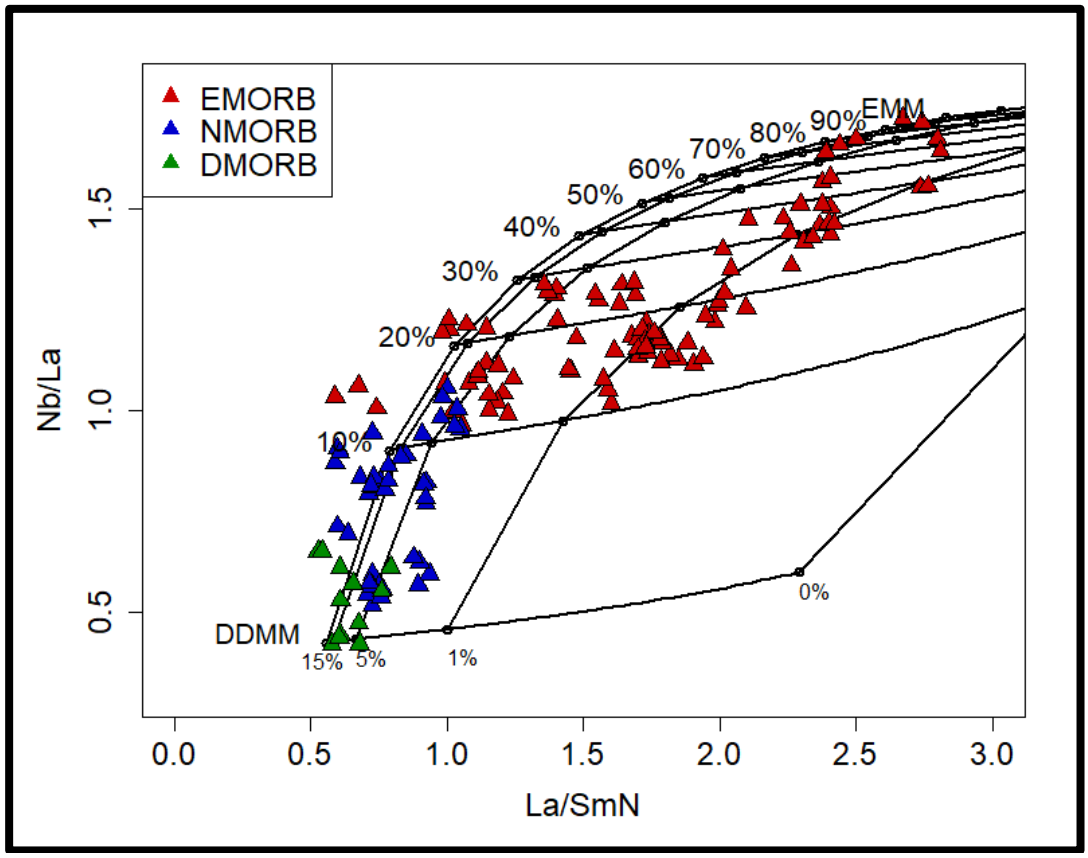

Figure 17. La/SmN and Nb/La of the seamount lavas for each MORB-type. Models for melting change along the x-axis (La/SmN variability) and models for source mixing between a depleted MORB mantle and an enriched MORB mantle change along the y-axis (Nb/La variability). Note that Nb/La changes very little with melting. The grid demonstrates melting and source conditions that could form each lava sample by mixing the mantle sources and melting or melting and then mixing the mantle.

Melting Systematics and Mantle Source Along Chain

The proximity of the seamount chain to the EPR axis and its nearly perpendicular nature allows for a detailed investigation into changes in mantle source and melting

systematics with distance from the ridge axis. Relatively simple models for melting beneath MORs invoke a triangular melting region (Langmuir et al., 1992), centered directly beneath the ridge axis, where higher extents of melting occur at the center of the triangle and lower extents of melting occur at the edge of the melting column (Figure 18). This model for mantle melting predicts that more enriched melts will form in the wings of the melting triangle, farthest from the ridge axis. If the seamount chain is simply formed from the vertical ascent of magmas created in the melting triangle directly below each seamount, we would expect to see a systematic change in the melting extents along the chain (Figure 18). This is not observed, however, for the seamount chain both large-scale (across the length of the chain; Figure 9) and small-scale (at each seamount; Figure 11). If the seamounts form from melts of different sources (Figure 18), we would expect to see a correlation between radiogenic isotope ratios and trace element ratios, indicating a source control on heterogeneity. While in some cases the radiogenic isotopes and trace element ratios correlate well, in other cases they do not (Figure 15). This suggests that a combination of melting and mixing of a heterogeneous mantle is required to account for the range of compositions erupted at the off-axis seamount chain.

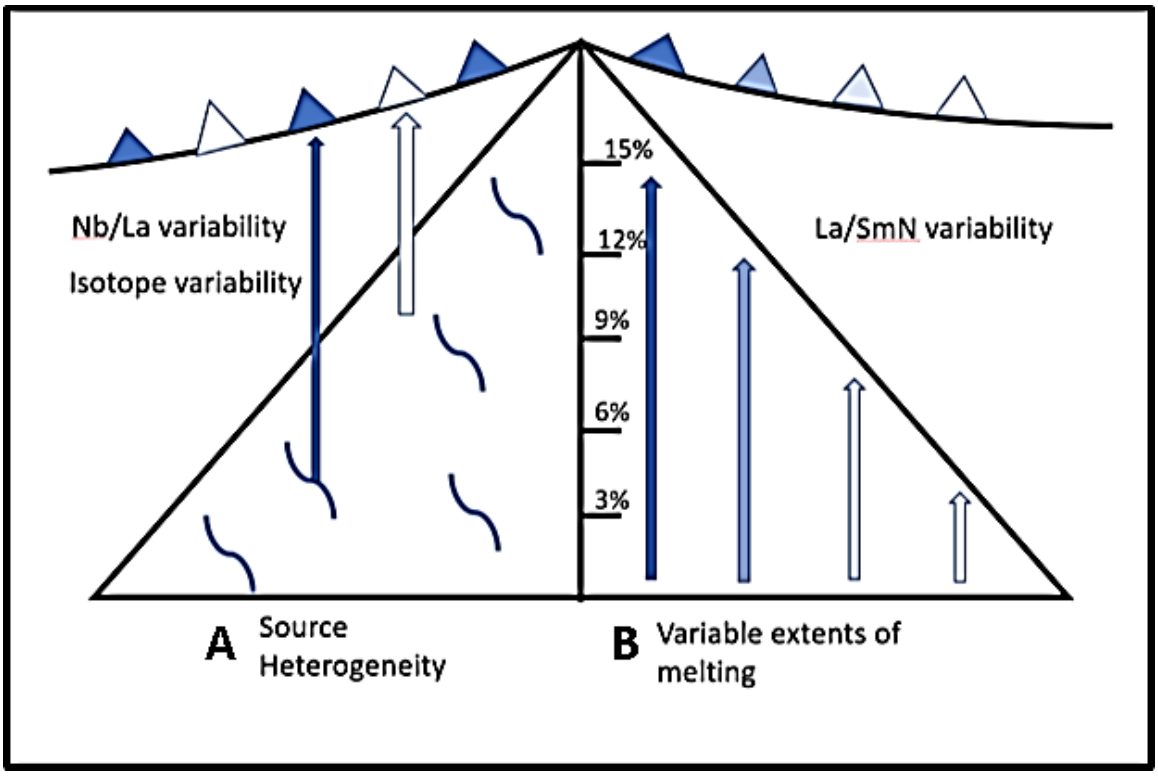

Figure 18. Models for mantle melting and source heterogeneity with changing trace element contents. Triangles represent the seamounts formed on the oceanic crust. The arrows represent various melts formed in the mantle beneath the mid-ocean ridge (top point of the large black triangle), and reflect the conditions of the mantle in which they were produced (melting triangle; large black triangle). Two models for compositional variability are proposed: (A) The source heterogeneity model invokes randomly dispersed enriched portions of mantle (blue squiggly lines) that have been entrained into the ambient depleted upper mantle (open space). Eruptions of melts (the blue and white arrows) from a system controlled solely by source heterogeneity would asystematically distribute variable trace element ratios Nb/La as well as radiogenic isotopes. Additionally, for a source control on heterogeneity, the trace element ratios and radiogenic isotopes should correlate. Alternatively, (B) Melt variability model invokes the more systematic eruption of more depleted lavas from higher extents of melting (darker blue arrows toward the center of the triangle) and more enriched lavas from lower extents of melting (lighter arrows toward the edge of the melt triangle). For melt variability controls on heterogeneity, trace element ratios should vary systematically, while the radiogenic isotopes should remain constant.

Notably, most individual seamounts span a wide range of compositions, suggesting that melting systematics and mantle sources are variable on remarkably small spatial scales. This observation is even true for NEPR seamount (Figure 19), which is the

closest seamount to the EPR axis and thus may be the most influenced by the MOR magmatic system. Based on petrologic modeling, both mantle sources are required to explain the lavas erupted at NEPR seamount, one to account for the DMORB lavas (< 5% EMM and ~15% melting) and a second mantle source to explain the EMORB (~30% EMM). Even more remarkable is the proximity of these two lava compositions; the DMORB were erupted within ~600 m of the most enriched EMORB (Figure 19). This suggests that both mantle components are present and can be preserved very near to the ridge axis and that they must exist over small spatial scales.

Lavas erupted along the ridge-parallel features are consistently more enriched than the depleted cone samples (Figure 12). Beryl Seamount has elongate ridge parallel rifts and numerous cone features, which allows us to evaluate the petrogenesis of spatially related volcanic features. The cone is the most depleted lava from this seamount, followed by the NMORB on the ridge-perpendicular features, and then the most enriched on the ridge-parallel portions of Beryl (Figure 20). The isotopes vary greatly between the different morphologies on Beryl, suggesting that each feature may form from a different magmatic event.

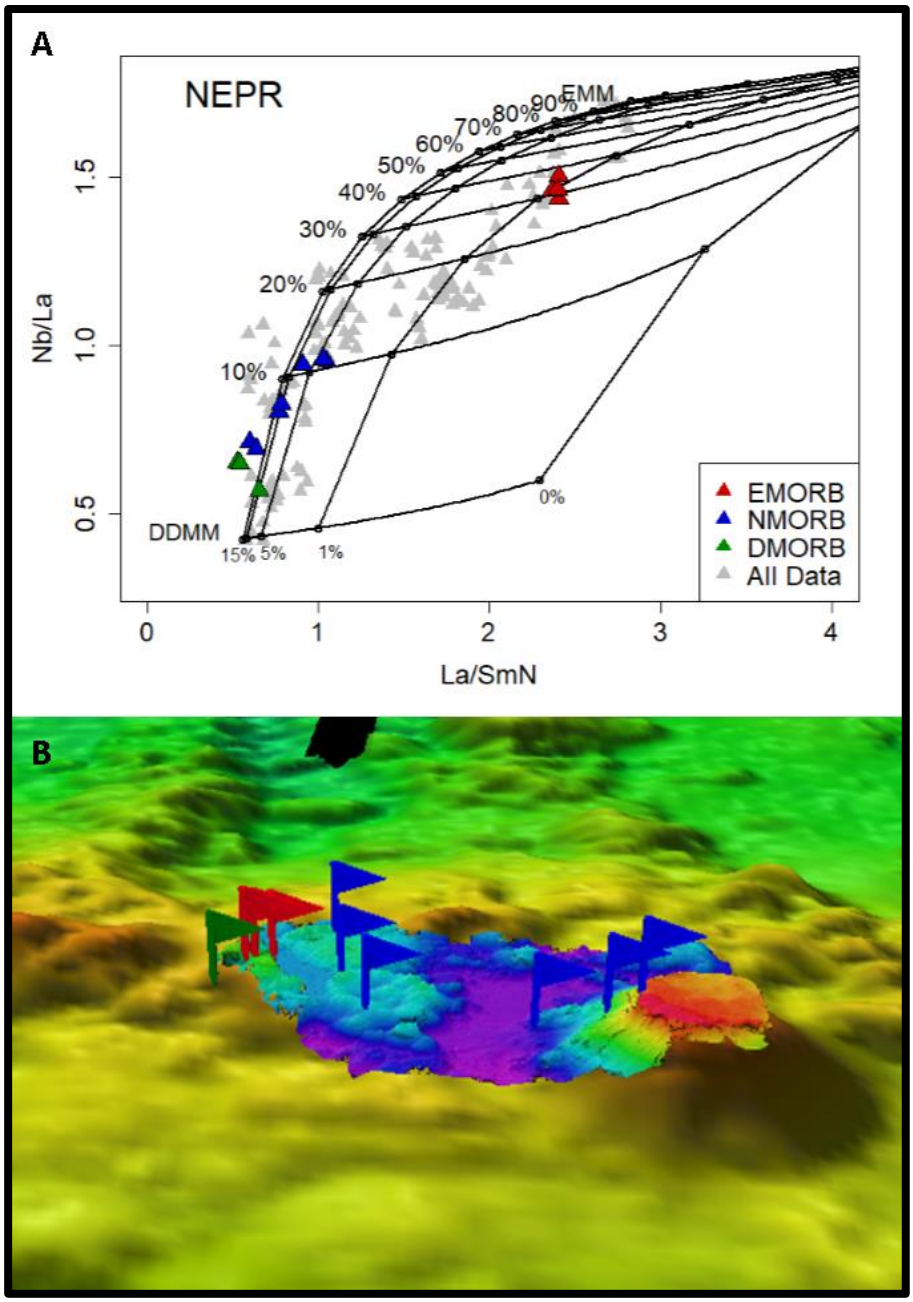

Figure 19. (A) La/SmN and Nb/La of the seamount lavas for each MORB-type on NEPR seamount. Grey symbols represent the whole 8˚20' N seamount dataset. Colored triangles represent samples from NEPR seamount. Models for melting change along the x-axis (La/SmN variability) and models for source mixing between a depleted MORB mantle and an enriched MORB mantle change along the y-axis (Nb/La variability). The grid demonstrates melting and source conditions that could form each lava sample by mixing the mantle sources and melting or melting and then mixing the mantle. (B) High-resolution Sentry map overlay of EM122 bathymetric map of NEPR seamount with sample locations (colored flags) and lava types (red EMORB, blue NMORB, green DMORB).

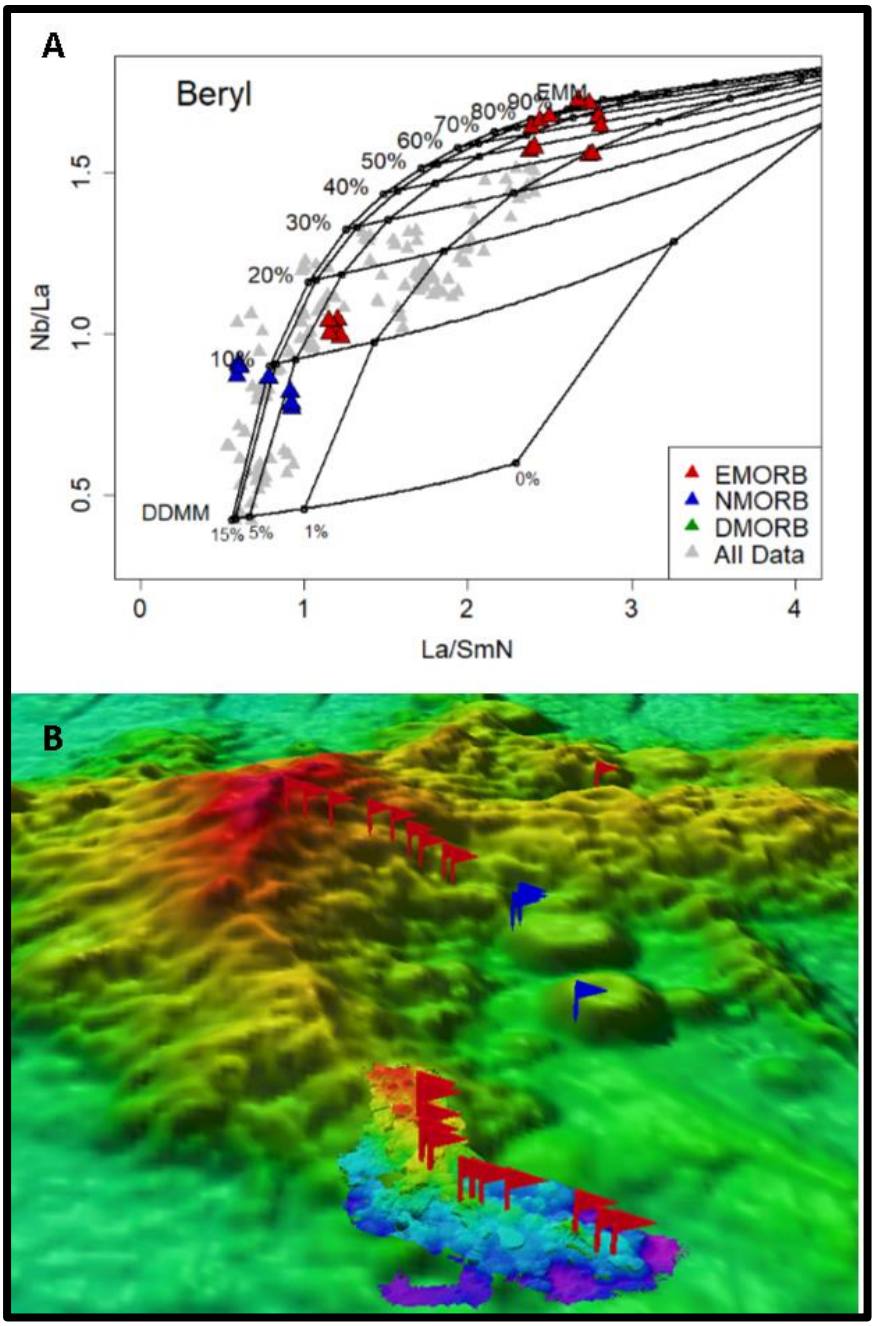

Figure 20. (A) La/SmN and Nb/La of the seamount lavas for each MORB-type on Beryl seamount. Grey symbols represent the whole 8˚20' N seamount dataset. Colored triangles represent samples from Beryl seamount. Models for melting change along the x-axis (La/SmN variability) and models for source mixing between a depleted MORB mantle and an enriched MORB mantle change along the y-axis (Nb/La variability). The grid demonstrates melting and source conditions that could form each lava sample by mixing the mantle sources and melting or melting and then mixing the mantle. (B) High-resolution Sentry map overlay of EM122 bathymetric map of Beryl seamount with sample locations (colored flags) and lava types (red EMORB, blue NMORB, green DMORB).

Combined, these observations suggest that the seamount lavas are not formed by systematically tapping different portions of the MOR melting triangle. They also suggest that there is no systematic variability in the proportion of either end-member mantle component with distance from the ridge axis. Instead, they suggest that the 8°20'N seamount chain formed from variable extents of melting of a heterogeneous mantle (Figure 21).

Concluding Model for Petrogenesis of the 8˚20 N Seamounts

On-axis MOR studies have dominated research on geochemical processes in the near-MOR environment. However, studies on-axis at fast-spreading ridges are limited by the efficient mixing and homogenization of magmas across the entire melting region prior to eruption, and therefore samples collected on-axis may be less representative of heterogeneity in the mantle. Off-axis seamounts are investigated to more accurately assess mantle systematics and mantle heterogeneity because the lavas erupted at seamounts may bypass homogenization in the axial magma chamber.

The location and orientation of the 8˚20’N seamount chain provides an opportunity to investigate mantle heterogeneity and melting systematics near the ridge system. The asystematic distribution of seamount heterogeneity requires a combination of a heterogeneous mantle source melting to variable extents over short length scales (Figure 21). Seamount lava compositions span from extremely depleted DMORB to highly enriched EMORB, sometimes within a single seamount; this variability ranges well beyond the compositions found on-axis. This preservation of extreme heterogeneity suggests that the seamount lavas by-pass the on-axis magma chamber and associated plumbing system (Figure 21). Because of their proximity to the EPR, it is likely that the

EMM and DDMM mantle components are present within the on-axis MOR lavas, but their end-member signatures are overprinted in the on-axis magma chamber. The continuum of data in major and trace element contents and radiogenic isotope ratios supports the possibility of extensive incomplete mixing of enriched and depleted mantle, which on-axis likely mix to a greater extent and thus mask the compositional heterogeneity.

While asystematic distribution of compositions indicates that heterogeneity needs to be assessed on a seamount-by-seamount basis, some trends emerge between MORB-type lava compositions across the chain that may be of consequence to near-ridge mantle processes. For example, small cones decorating the outer edges of the seamount chain are primarily DMORB, and the N-S trending ridge parallel features extending north and south from the chain are distinctly EMORB. These correlations could have implications for tectonic influences on volcanism (such as rifting of the crust away from the ridge axis), but are not explored further in this paper.

Petrologic models indicate that the seamounts are formed by a combination of fractional crystallization and variable extents of melting of a heterogeneous mantle. Fractional crystallization accounts for some variability within each seamount, but multiple parent magmas are necessary to explain the range of compositions. Further, variability in trace element contents and radiogenic isotope ratios within individual seamounts requires that the source heterogeneity and extents of melting vary on a small scale (Figure 21). Comparisons between radiogenic isotope ratios and trace element ratios with the same denominator indicate binary mixing between EMM and DDMM must be contributing to the seamount heterogeneity, but cannot form the full extent of trace

element ratios. Here, two mantle components are assumed, but there is compelling evidence for a third component in radiogenic isotope ratios (Figure 8 & 14). To explain the full range of trace element ratio variability, lavas must be formed by melting a heterogeneous mantle to variable extents. Magnitudes of mantle melting and source heterogeneity are constrained by melting of a variably mixed DDMM or EMM mantle up to 15%. In general, the DMORB are formed from higher extents of melting (5 – 15%) than the EMORB (some <1%). The order in which mixing and melting occur, however, remain ambiguous and require further exploration.

The seamounts are more depleted and enriched than on-axis samples but overlap the more homogeneous on-axis sample compositions. This observation indicates that, while seamounts are sampling the same mantle that ultimately melts and focuses and homogenizes on-axis, the seamount lavas are transported through a different plumbing system (Figure 21). Because the heterogeneity exists near the axis (< 22 km), and on small-scales across the seamount chain, a mantle heterogeneity model requires that mantle systematics vary on small scales even approaching the ridge axis.

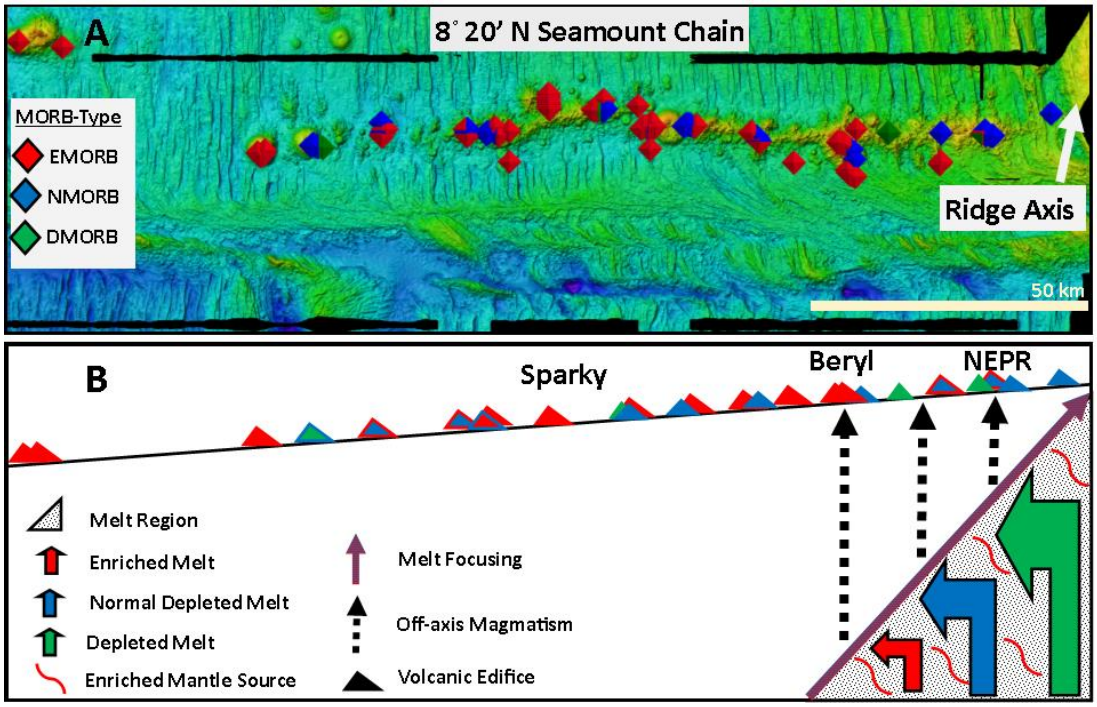

Figure 21. Model for 820 N seamount chain petrogenesis. (A) Bathymetric map of the ~200 km-long 8˚20' N seamount chain. Seamount names and the locations of the ~300 basalt samples (colored diamonds) are shown. Red-colored diamonds represent enriched mid-ocean ridge basalt samples, blue-colored diamonds represent normal mid-ocean ridge basalt samples, and green-colored diamonds represent depleted mid-ocean ridge basalt samples. Map created in Fledermaus. (B) Model for the generation of heterogeneous seamount lavas invoking melting of a heterogeneous mantle to various degrees in the melting region (dotted grey triangle) and erupting off-axis, effectively by-passing on-axis homogenization. Colored arrows indicate different compositions of the mantle due to variable degrees of melting and the direction of mantle flow, and the mixed color arrow is the direction of melt focusing toward the ridge axis. Red squiggly lines represent heterogeneities present in the mantle due to source variability. Dashed arrows demonstrate where magmas are pulled from prior to eruption on the surface forming the long chain of volcanic edifices (triangles) with time as the oceanic crust moves away from the axis.

REFERENCES

Allan, J. F., & Batiza, R. (1987). Petrology and chemistry of lavas from seamounts flanking the East Pacific Rise axis, 21 N: Implications concerning the mantle source composition for both seamount and adjacent EPR lavas. *American Geophysical Union*, 255–282.

Batiza, R., & Niu, Y. (1992). Petrology and Magma Chamber Processes at the East Pacific Rise ~9°30'N. *Journal of Geophysical Research*, *97*(B5), 6779–6797. https://doi.org/http://dx.doi.org/10.1037/xge0000076

Batiza, R., Niu, Y., Karsten, J. L., Boger, W., Potts, E., Norby, L., & Butler, R. (1996). Steady and Non-Steady State Magma Chambers Below the East Pacific Rise, *23*(3), 221–224.

Batiza, R., Niu, Y., & Zayac, W. C. (1990). Chemistry of seamounts near the East Pacific Rise: Implications for the geometry of subaxial mantle flow. *Geology*, *18*(11), 1122–1125. https://doi.org/10.1130/0091-7613(1990)018<1122:COSNTE>2.3.CO;2

Batiza, R., Smith, T. L., & Niu, Y. (1989). Geological and petrologic evolution of seamounts near the EPR based on submersible and camera study. *Marine Geophysical Researches*, *11*(3), 169–236. https://doi.org/10.1007/BF00340203

Behn, M. D., Lin, J., & Zuber, M. T. (2002). Evidence for weak oceanic transform faults. *Geophysical Research Letters*, *29*(24), 1–4. https://doi.org/10.1029/2002GL015612

Brandl, P. A., Beier, C., Regelous, M., Abouchami, W., Haase, K. M., Garbe-Schonberg, D., & Galer, S. J. G. (2012). Volcanism on the flanks of the East Pacific Rise: Quantitative constraints on mantle heterogeneity and melting processes. *Chemical Geology*, *298–299*, 41–56. https://doi.org/10.1016/j.chemgeo.2011.12.015

Carbotte, S., & Macdonald, K. (1992). East Pacific Rise 8°–10°30′N: Evolution of ridge segments and discontinuities from SeaMARC II and three-dimensional magnetic studies. *Journal of Geophysical Research*, *97*(B5), 6959. https://doi.org/10.1029/91JB03065

Detrick, R. S., Buhl, P., Vera, E., Mutter, J., Orcutt, J., Madsen, J., & Brocher, T. (1987). Multi-channel seismic imaging of a crustal magma chamber along the East Pacific Rise. *Nature*, *326*(6108), 35–41. https://doi.org/10.1038/326035a0

Donnelly, K. E., Goldstein, S. L., Langmuir, C. H., & Spiegelman, M. (2004). Origin of enriched ocean ridge basalts and implications for mantle dynamics. *Earth and Planetary Science Letters*, *226*(3–4), 347–366. https://doi.org/10.1016/j.epsl.2004.07.019

Fornari, D. J., Perfit, M. R., Allan, J. F., & Batiza, R. (1988b). Small-scale heterogeneities in depleted mantle sources: near-ridge seamount lava geochemistry and implications for mid-ocean-ridge magmatic processes. *Nature*, *331*, 511–513. https://doi.org/10.1038/332141a0

Fornari, D. J., Perfit, M. R., Allan, J. F., Batiza, R., Haymon, R., Barone, A., … Luckman, M. A. (1988a). Geochemical and structural studies of the Lamont seamounts: seamounts as indicators of mantle processes. *Earth and Planetary Science Letters*, *89*(1), 63–83. https://doi.org/10.1016/0012-821X(88)90033-7

Ghiorso, M. S., & Gualda, G. A. R. (2015). An H2O--CO2 mixed fluid saturation model compatible with rhyolite-MELTS. *Contributions to Mineralogy and Petrology*, *169*. https://doi.org/10.1007/s00410-015-1141-8

Goss, A. R., Perfit, M. R., Ridley, W. I., Rubin, K. H., Kamenov, G. D., Soule, S. A., … Fornari, D. J. (2010). Geochemistry of lavas from the 2005-2006 eruption at the East Pacific Rise, 9°46'N-9°56N: Implications for ridge crest plumbing and decadal changes in magma chamber compositions. *Geochemistry, Geophysics, Geosystems*, *11*(5), 1–35. https://doi.org/10.1029/2009GC002977

Gregg, P. M., Behn, M. D., Lin, J., & Grove, T. L. (2009). Melt generation, crystallization, and extraction beneath segmented oceanic transform faults.

Journal of Geophysical Research: Solid Earth, *114*(11). https://doi.org/10.1029/2008JB006100

Gualda, G. A. R., Ghiorso, M. S., Lemons, R. V., & Carley, T. L. (2012). Rhyolite-MELTS: A Modified Calibration of MELTS Optimized for Silica-rich, Fluid-bearing Magmatic Systems. *Journal of Petrology*, *53*(5), 875–890. https://doi.org/10.1093/petrology/egr080

Hofmann, A. W. (1997). Mantle geochemistry: the message from oceanic volcanism. *Nature*, *385*, 219–229.

Langmuir, C., Klein, E., & Plank, T. (1992). Petrological Systematics of Mid-Ocean Ridge Basalts: Constraints on Melt Generation Beneath Ocean Ridges. *American Geophysical Union*, *71*, 183–279.

Niu, Y., & Batiza, R. (1997a). Extreme mantle source heterogeneities beneath the northern East Pacific Rise: trace element evidence from near-ridge seamounts. *International Geological Congress, 30th, Proceedings*, *v. 15*(March), 109–120.

Niu, Y., & Batiza, R. (1997b). Trace element evidence from seamounts for recycled oceanic crust in the Eastern Pacific mantle. *Earth and Planetary Science Letters*, *148*(3), 471–483. https://doi.org/10.1016/S0012-821X(97)00048-4

Niu, Y., Regelous, M., Wendt, I. J., Batiza, R., & O'Hara, M. J. (2002). Geochemistry of near-EPR seamounts: Importance of source vs. process and the origin of enriched mantle component. *Earth and Planetary Science Letters*, *199*(3–4), 327–345. https://doi.org/10.1016/S0012-821X(02)00591-5

Niu, Y., Waggoner, D. G., Sinton, J. M., & Mahoney, J. (1996). Mantle source heterogeneity and melting processes beneath seafloor spreading centers: The East Pacific Rise, 18 - 19 S. *Journal of Geophysical Research*, *101*(B12), 27,711-27,733.

O'Hara, M. J. (1965). Primary magmas and the origin of basalts. *Scottish Journal of Geology*, *1*(1), 19–40.

O'Hara, M. J. (1977). Geochemical evolution during fractional crystallisation of a periodically refilled magma chamber. *Nature*, *266*, 503–507.

O'Hara, M. J. (1985). Importance of the "shape" of the melting regime during partial melting of the mantle. *Nature, 314*, 58–62.

Perfit, M., & Chadwick, W. (1998). Magmatism at Mid-Ocean Ridges: Constraints from Volcanological and Geochemical investigations. *Geophysical Monograph Series*, *106*(January), 59–115. https://doi.org/10.1029/GM106p0059.Cited

Perfit, M. R., Fornari, D. J., Smith, M. C., Bender, J. F., Langmuir, C. H., & Haymon, R. M. (1994). Small-scale spatial and temporal variations in mid-ocean ridge crest magmatic processes. *Geology*, *22*(4), 375–379.

Perfit, M., Wanless, V. D., Ridley, W. I., Klein, E., Smith, M., Goss, A., … Fornari, D. (2012). Lava Geochemistry as a Probe into Crustal Formation at the East Pacific Rise. *Oceanography*, *25*(1), 89–93. https://doi.org/10.5670/oceanog.2012.06

Phipps-Morgan, J. (1987). Melt migration beneath mid-ocean spreading centers. *Geophysical Research Letters*, *14*(12), 1238–1241.

Plank, T., & Langmuir, C. H. (1992). Effects of the Melting Regime on the Composition of the Oceanic Crust. *Journal of Geophysical Research*, *97*(B13), 19749–19770.

Rubin, K. H., & Sinton, J. M. (2007). Inferences on mid-ocean ridge thermal and magmatic structure from MORB compositions. *Earth and Planetary Science Letters*, *260*(1–2), 257–276. https://doi.org/10.1016/j.epsl.2007.05.035

Scheirer, D. S., & Macdonald, K. C. (1995). Near-axis seamounts on the flanks of the East Pacific Rise, 8°N to 17°N. *Journal of Geophysical Research*, *100*(B2), 2239–2259. https://doi.org/10.1029/94JB02769

Shimizu, K., Saal, A. E., Myers, C. E., Nagle, A. N., Hauri, E. H., Forsyth, D. W., … Niu, Y. (2016). Two-component mantle melting-mixing model for the generation of mid-ocean ridge basalts: Implications for the volatile content of the Pacific upper mantle. *Geochimica et Cosmochimica Acta*, *176*, 44–80. https://doi.org/10.1016/j.gca.2015.10.033

Sims, K. W. ., Goldstein, S. ., Blichert-toft, J., Perfit, M. ., Kelemen, P., Fornari, D. ., … Bender, J. (2002). Chemical and isotopic constraints on the generation and

transport of magma beneath the East Pacific Rise. *Geochimica et Cosmochimica Acta*, *66*(19), 3481–3504. https://doi.org/10.1016/S0016-7037(02)00909-2

Sinton, J. M., & Detrick, R. S. (1992). Mid-ocean ridge magma chambers. *Journal of Geophysical Research*, *97*(B1), 197–213. https://doi.org/10.1029/91JB02508

Smith, P. M., & Asimow, P. D. (2005). Adiabat-1ph: A new public front-end to the MELTS, pMELTS, and pHMELTS models. *Geochemistry, Geophysics, Geosystems*, *6*(1). https://doi.org/10.1029/2004GC000816

Spiegelman, M., & McKenzie, D. (1987). Simple 2-D models for melt extraction at mid-ocean ridges and island arcs. *Earth and Planetary Science Letters*, *83*(1–4), 137–152. https://doi.org/10.1016/0012-821X(87)90057-4

Stracke, A., & Bourdon, B. (2009). The importance of melt extraction for tracing mantle heterogeneity. *Geochimica et Cosmochimica Acta*, *73*(1), 218–238. https://doi.org/10.1016/j.gca.2008.10.015

Waters, C. L., Sims, K. W. W., Perfit, M. R., Blichert-Toft, J., & Blusztajn, J. (2011). Perspective on the genesis of E-MORB from chemical and isotopic heterogeneity at 9-10°n East Pacific Rise. *Journal of Petrology*, *52*(3), 565–602. https://doi.org/10.1093/petrology/egq091

Workman, R. K., & Hart, S. R. (2005). Major and trace element composition of the depleted MORB mantle (DMM). *Earth and Planetary Science Letters*, *231*(1–2), 53–72. https://doi.org/10.1016/j.epsl.2004.12.005

Zindler, A., Staudigel, H., & Batiza, R. (1984). Isotope and trace element geochemistry of young Pacific seamounts: implications for the scale of upper mantle heterogeneity. *Earth and Planetary Science Letters*, *70*(2), 175–195. https://doi.org/10.1016/0012-821X(84)90004-9

APPENDIX A

Geochemical Data

Table A.1 Major Element Concentrations of the 8˚20' N seamount lavas measured on microprobes at UF and USGS. Major element concentrations are in wt. %

Sample	Seamount	Lava Type	Morphology	Lab	Latitude	Longitude	Depth	SiO_2	TiO_2	Al_2O_3	FeO	MnO	MgO	CaO	Na_2O	K_2O	P_2O_5	K_2O/TiO_2
OS11_A	NEPR	NMORB	Cone	USGS	8.44457	-104.28612	2947	48.17	1.06	17.57	8.53	0.15	9.33	11.62	2.62	0.09	0.1	8.93
OS11_B	NEPR	NMORB	Cone	USGS	8.44457	-104.28612	2947	48.21	1.07	17.56	8.51	0.15	9.33	11.63	2.65	0.09	0.1	8.85
OS11_C	NEPR	NMORB	Cone	USGS	8.44457	-104.28612	2947	47.81	1.07	17.54	8.47	0.15	9.37	11.65	2.61	0.09	0.1	8.47
OS11_D	NEPR	NMORB	Cone	USGS	8.44457	-104.28612	2947	48.4	1.13	17.17	8.47	0.14	9.1	11.7	2.64	0.14	0.11	12.09
OS11_E	NEPR	NMORB	Cone	USGS	8.44457	-104.28612	2947	48	1.06	17.57	8.52	0.14	9.24	11.65	2.64	0.09	0.09	8.63
OS11_F	NEPR	NMORB	Cone	USGS	8.44457	-104.28612	2947	48.14	1.13	17	8.4	0.15	9.17	11.7	2.68	0.13	0.11	11.16
OS11_G	NEPR	NMORB	Cone	USGS	8.44457	-104.28612	2947	47.61	1.06	17.23	8.4	0.14	9.4	11.58	2.69	0.1	0.09	9.07
4854_13	NEPR	NMORB	Seamount	UF	8.40394	-104.39374	2319	47.62	0.95	17.83	9.11	0.16	9.34	11.01	2.44	0.06	0.08	6.74
4854_11	NEPR	NMORB	Seamount	UF	8.40406	-104.39519	2418	47.46	0.9	17.83	9.2	0.14	9.35	11.04	2.45	0.06	0.07	6.86
4854_9	NEPR	DMORB	Seamount	UF	8.40452	-104.39838	2535	48.04	1.08	17.08	9.87	0.16	8.62	11.05	2.55	0.07	0.08	6.67
4854_8	NEPR	NMORB	Seamount	UF	8.40502	-104.40617	2469	50.04	1.53	14.49	9.51	0.16	7.23	11.55	2.88	0.25	0.18	16.17
4854_7	NEPR	NMORB	Seamount	UF	8.40854	-104.40762	2436	49.5	1.5	14.57	9.41	0.18	7.42	11.44	2.8	0.24	0.18	16.11
4854_6	NEPR	DMORB	Seamount	UF	8.41381	-104.40842	2430	48.2	1.07	17.55	9.17	0.16	8.97	10.79	2.56	0.07	0.08	6.75
4854_5	NEPR	EMORB	Seamount	UF	8.41049	-104.41119	2434	48.63	2.18	16.05	8.95	0.15	6.51	10.41	3.11	0.93	0.44	42.44
4854_4	NEPR	EMORB	Seamount	UF	8.40945	-104.41191	2388	48.46	2.19	16.02	8.91	0.15	6.52	10.4	3.19	0.92	0.44	41.73
4854_3	NEPR	EMORB	Seamount	UF	8.40924	-104.41232	2440	48.47	2.2	16.06	8.89	0.14	6.55	10.31	3.19	0.92	0.43	41.94
4854_2	NEPR	EMORB	Seamount	UF	8.40922	-104.41234	2444	49.01	2.2	16.18	8.95	0.16	6.56	10.42	3.16	0.93	0.42	42.39
4854_1	NEPR	DMORB	Seamount	UF	8.40810	-104.41376	2478	47.57	0.94	17.88	8.58	0.15	9.48	11.8	2.34	0.06	0.08	6.61
OS12_B	Hook Ridge	NMORB	RPerp	USGS	8.44354	-104.42000	2961	49.79	1.31	16	8.53	NaN	8.28	11.82	2.72	0.21	0.15	15.84
OS12_D	Hook Ridge	NMORB	RPerp	USGS	8.44354	-104.42000	2961	47.95	1.11	17.12	8.97	NaN	9.86	11.16	2.51	0.12	0.11	10.55
OS12_E	Hook Ridge	NMORB	RPerp	USGS	8.44354	-104.42000	2961	48.11	1.12	17.07	8.99	NaN	9.84	11.21	2.55	0.11	0.1	10.17
OS12_F	Hook Ridge	NMORB	RPerp	USGS	8.44354	-104.42000	2961	48.01	1.11	17.05	8.92	NaN	9.87	11.24	2.52	0.12	0.11	10.61
OS12_G	Hook Ridge	NMORB	RPerp	USGS	8.44354	-104.42000	2961	48.52	1.12	18	8.48	NaN	9.05	11.25	2.71	0.13	0.1	11.41
OS12_H	Hook Ridge	NMORB	RPerp	USGS	8.44354	-104.42000	2961	48.06	1.07	17.72	8.43	NaN	9.3	11.43	2.55	0.1	0.1	9.23
OS12_I	Hook Ridge	NMORB	RPerp	USGS	8.44354	-104.42000	2961	47.96	1.11	17.1	9	NaN	9.84	11.12	2.46	0.12	0.11	10.51
4855_2	Hook Ridge	EMORB	RPar	UF	8.35626	-104.48912	2883	48.83	2.13	16.06	9.78	0.16	7.35	9.62	3.25	0.79	0.41	36.98
4855_3	Hook Ridge	EMORB	RPar	UF	8.35736	-104.48959	2825	49.42	2.27	16.32	9.38	0.15	6.25	9.65	3.42	0.96	0.47	42.08
4855_1	Hook Ridge	EMORB	RPar	UF	8.35280	-104.49137	2940	48.99	2.16	16.34	9.76	0.16	7.05	9.75	3.26	0.78	0.4	36.21
OS13_A	Midway Ridge	DMORB	RPerp	UF	8.41004	-104.58592	2500	48	1.04	17.25	10.06	0.19	9.27	11.05	2.51	0.05	0.09	4.91
OS13_B	Midway Ridge	DMORB	RPerp	UF	8.41004	-104.58592	2500	47.92	1.04	17.1	10.1	0.2	9.35	11.1	2.54	0.05	0.09	5.18
OS13_C	Midway Ridge	DMORB	RPerp	UF	8.41004	-104.58592	2500	48	1.04	17.12	10.07	0.18	9.2	10.97	2.51	0.06	0.09	5.43
OS13_D	Midway Ridge	DMORB	RPerp	UF	8.41004	-104.58592	2500	47.93	1.02	17.07	10.09	0.19	9.27	11	2.51	0.06	0.1	5.98
OS13_E	Midway Ridge	DMORB	RPerp	UF	8.41004	-104.58592	2500	47.92	1.02	17.16	10.07	0.18	9.35	11.04	2.54	0.06	0.09	5.67
OS13_F	Midway Ridge	DMORB	RPerp	UF	8.41004	-104.58592	2500	47.75	1.05	17.04	10.03	0.18	9.18	11.19	2.52	0.06	0.09	5.46
OS13_G	Midway Ridge	DMORB	RPerp	UF	8.41004	-104.58592	2500	47.94	1.05	17.13	10.08	0.18	9.28	11.24	2.5	0.05	0.09	5.17
OS13_H	Midway Ridge	DMORB	RPerp	UF	8.41004	-104.58592	2500	48.21	1.04	17.46	10	0.18	8.79	11.26	2.56	0.05	0.09	5.07
OS9_A	Beryl	NMORB	RPerp	USGS	8.41618	-104.64545	2800	48.34	1.32	17.25	9.03	0.16	8.23	11.17	2.79	0.21	0.14	16.04
OS9_B	Beryl	EMORB	RPerp	USGS	8.41618	-104.64545	2800	48.44	1.33	17.07	9.07	0.16	8.62	11.16	2.8	0.23	0.16	17.04
OS9_C	Beryl	EMORB	RPerp	USGS	8.41618	-104.64545	2800	48.6	1.31	17.18	9.07	0.15	8.64	11.08	2.78	0.22	0.15	16.48
OS9_E	Beryl	EMORB	RPerp	USGS	8.41618	-104.64545	2800	48.73	1.32	17.2	9.08	0.16	8.6	11.14	2.79	0.22	0.16	16.51
OS9_F	Beryl	EMORB	RPerp	USGS	8.41618	-104.64545	2800	48.17	1.31	17.15	9.08	0.15	8.6	11.12	2.77	0.22	0.16	16.88
OS9_H	Beryl	EMORB	RPerp	USGS	8.41618	-104.64545	2800	48.15	1.3	17.04	9.07	0.14	8.53	11.08	2.77	0.22	0.15	16.87
4860_1	Beryl	EMORB	RPar	USGS	8.32989	-104.64724	2987	48.26	2.5	17.12	9.06	0.14	6.54	8.63	3.85	1.19	0.55	47.78
4860_2	Beryl	EMORB	RPar	USGS	8.33009	-104.64830	2926	48.89	2.6	17.44	9.12	0.16	6.07	8.76	3.95	1.26	0.55	48.45
OS18_A	Beryl	NMORB	Cone	USGS	8.36108	-104.64903	2976	48.14	1.27	16.84	8.69	0.15	9.07	11.14	2.83	0.15	0.14	11.54
OS18_B	Beryl	NMORB	Cone	USGS	8.36108	-104.64903	2976	48.35	1.26	16.9	8.67	0.16	9.05	11.14	2.85	0.14	0.15	11.23
OS18_C	Beryl	NMORB	Cone	USGS	8.36108	-104.64903	2976	48.63	1.25	17	8.67	0.15	9.02	11.17	2.84	0.14	0.15	11.23
OS18_D	Beryl	NMORB	Cone	USGS	8.36108	-104.64903	2976	48.46	1.28	17.06	8.75	0.15	8.73	11.22	2.91	0.14	0.16	11.03
OS18_E	Beryl	NMORB	Cone	USGS	8.36108	-104.64903	2976	48.42	1.27	16.9	8.62	0.16	9.04	11.18	2.81	0.14	0.15	10.88
OS18_F	Beryl	NMORB	Cone	USGS	8.36108	-104.64903	2976	48.69	1.27	17.08	8.67	0.16	8.91	11.22	2.83	0.14	0.16	10.86
OS18_G	Beryl	NMORB	Cone	USGS	8.36108	-104.64903	2976	48.54	1.27	17.18	8.62	0.15	8.86	11.25	2.85	0.14	0.16	10.68
OS18_H	Beryl	NMORB	Cone	USGS	8.36108	-104.64903	2976	48.54	1.28	17.06	8.65	0.15	9.09	11.14	2.84	0.13	0.15	10.21
OS18_I	Beryl	NMORB	Cone	USGS	8.36108	-104.64903	2976	48.16	1.27	17.02	8.75	0.15	8.99	11.07	2.81	0.15	0.16	11.83
OS18_J	Beryl	NMORB	Cone	USGS	8.36108	-104.64903	2976	47.76	1.24	16.74	8.58	0.15	8.87	11.08	2.88	0.14	0.14	11.50
4860_3	Beryl	EMORB	RPar	USGS	8.33130	-104.64971	2885	48.2	2.54	17.27	8.98	0.14	6.22	8.67	3.88	1.23	0.57	48.38
4853_2	Beryl	NMORB	Cone	UF	8.37874	-104.65410	2850	48.79	1.17	16.8	10.38	0.18	8.57	10.9	2.49	0.08	0.11	7.03
4853_3	Beryl	NMORB	Cone	UF	8.38015	-104.65417	2867	48.99	1.17	16.83	10.39	0.19	8.43	10.83	2.52	0.09	0.09	7.53
4860_4	Beryl	EMORB	RPar	USGS	8.33361	-104.65425	2918	48.33	2.52	17.12	9.17	0.15	6.67	8.7	3.83	1.21	0.56	47.98
4853_1	Beryl	NMORB	Cone	UF	8.37812	-104.65480	NaN	48.97	1.23	16.6	10.61	0.18	8.3	10.92	2.53	0.09	0.11	6.90
4860_5	Beryl	EMORB	RPar	USGS	8.33401	-104.65602	2915	48.92	2.62	17.5	8.65	0.13	5.52	8.57	4.14	1.48	0.67	56.64
4860_6	Beryl	EMORB	RPar	USGS	8.33418	-104.65665	2866	48.89	2.59	17.49	8.67	0.15	5.48	8.55	4.13	1.51	0.67	58.19
4860_7	Beryl	EMORB	RPar	USGS	8.33406	-104.65743	2827	49.6	3.07	16.59	9.38	0.16	4.61	8.46	4.29	1.76	0.79	57.45
4860_8	Beryl	EMORB	RPar	USGS	8.33674	-104.65968	2849	49.4	2.62	17.49	8.67	0.15	5.5	8.59	4.17	1.52	0.67	58.15
4860_10	Beryl	EMORB	RPar	USGS	8.33896	-104.66028	2760	49.04	2.55	17.53	8.59	0.14	5.64	8.53	4.1	1.48	0.66	57.97
4860_9	Beryl	EMORB	RPar	USGS	8.33736	-104.66034	2784	49.02	2.58	17.51	8.59	0.14	5.59	8.54	4.14	1.5	0.66	57.98
4860_11	Beryl	EMORB	RPar	USGS	8.34121	-104.66043	2727	49.24	2.57	17.48	8.62	0.14	5.57	8.55	4.15	1.48	0.66	57.82
4860_13	Beryl	EMORB	RPar	USGS	8.34243	-104.66090	2721	49.35	2.58	17.56	8.66	0.15	5.59	8.62	4.15	1.52	0.66	58.89
4860_12	Beryl	EMORB	RPar	USGS	8.34198	-104.66093	2713	49.21	2.57	17.52	8.69	0.16	5.62	8.61	4.16	1.5	0.66	58.55

Sample	Seamount	Lava Type	Morphology	Lab	Latitude	Longitude	Depth	SiO_2	TiO_2	Al_2O_3	FeO	MnO	MgO	CaO	Na_2O	K_2O	P_2O_5	K_2O/TiO_2
4853_7	Beryl	EMORB	Seamount	UF	8.38627	-104.66113	2724	49.2	2.48	16.65	9.49	0.17	6.03	9.26	3.64	1.18	0.55	47.40
4853_8	Beryl	EMORB	Seamount	UF	8.38682	-104.66210	2717	49.15	2.45	16.65	9.4	0.15	5.98	9.27	3.65	1.18	0.54	48.10
4853_9	Beryl	EMORB	Seamount	UF	8.38824	-104.66456	2662	49.14	2.52	16.69	9.46	0.15	5.93	9.2	3.63	1.2	0.57	47.50
4853_10	Beryl	EMORB	Seamount	UF	8.38918	-104.66588	2556	49.31	2.5	16.68	9.55	0.15	6.18	9.21	3.68	1.17	0.57	47.04
4853_11	Beryl	EMORB	Seamount	UF	8.39055	-104.66775	2454	49.83	2.59	16.82	8.68	0.15	5.14	8.69	3.98	1.59	0.73	61.31
4853_12	Beryl	EMORB	Seamount	UF	8.39083	-104.67015	2390	49.06	2.49	16.6	9.5	0.16	6.27	9.06	3.61	1.17	0.56	47.07
4853_13	Beryl	EMORB	Seamount	UF	8.39168	-104.67431	2317	49.39	2.5	16.72	9.48	0.15	6.04	9.14	3.54	1.16	0.56	46.65
4853_14	Beryl	EMORB	Seamount	UF	8.39218	-104.67704	2261	49.6	2.63	16.98	8.99	0.15	5.23	8.71	3.94	1.55	0.71	58.69
4853_15	Beryl	EMORB	Seamount	UF	8.39246	-104.67900	NaN	49.77	2.8	16.74	9.17	0.15	4.96	8.62	3.96	1.6	0.74	57.28
OS19_A	Beryl	EMORB	Cone	USGS	8.35568	-104.76002	3127	47.91	1.42	17.29	9.42	0.16	8.14	10.7	2.88	0.23	0.17	16.51
OS19_B	Beryl	EMORB	Cone	USGS	8.35568	-104.76002	3127	47.91	1.41	17.28	9.52	0.16	8.07	10.73	2.94	0.24	0.17	17.27
OS19_C	Beryl	EMORB	Cone	USGS	8.35568	-104.76002	3127	47.17	1.38	17.32	9.29	0.17	8.25	10.54	2.91	0.23	0.18	16.56
OS19_D	Beryl	EMORB	Cone	USGS	8.35568	-104.76002	3127	47.56	1.38	17.37	9.37	0.14	8.21	10.67	2.94	0.24	0.17	17.09
OS19_E	Beryl	NMORB	Cone	USGS	8.35568	-104.76002	3127	47.57	1.39	17.37	9.29	0.15	8.27	10.64	2.93	0.22	0.17	16.12
OS19_F	Beryl	EMORB	Cone	USGS	8.35568	-104.76002	3127	47.95	1.37	17.41	9.38	0.16	8.27	10.74	2.84	0.24	0.17	17.42
OS19_G	Beryl	EMORB	Cone	USGS	8.35568	-104.76002	3127	47.53	1.39	17.14	9.51	0.18	8.06	10.66	2.97	0.24	0.18	17.21
OS19_H	Beryl	EMORB	Cone	USGS	8.35568	-104.76002	3127	48.18	1.37	17.2	9.4	0.17	8.2	10.88	2.95	0.23	0.17	16.67
OS19_J	Beryl	NMORB	Cone	USGS	8.35568	-104.76002	3127	48.31	1.07	17.44	8.43	0.14	9.2	11.64	2.59	0.11	0.12	9.93
4856_12	Rocky Ridge	EMORB	RPerp	UF	8.39234	-104.82328	2358	49.28	2.07	16.38	8.72	0.15	7.03	10.47	3.36	0.78	0.38	37.90
4856_10	Rocky Ridge	NMORB	RPerp	UF	8.39485	-104.82337	2382	48.31	1.19	16.96	10.01	0.16	8.41	11.21	2.9	0.13	0.12	10.52
4856_9	Rocky Ridge	EMORB	RPerp	UF	8.39763	-104.82547	2493	48.29	1.32	16.82	9.89	0.19	8.19	11.01	3.06	0.24	0.17	18.48
4856_8	Rocky Ridge	NMORB	RPerp	UF	8.40071	-104.82687	2608	48.17	1.3	16.59	10.38	0.17	7.89	11.14	2.96	0.16	0.13	12.44
4856_7	Rocky Ridge	NMORB	RPerp	UF	8.40184	-104.82808	2683	48.22	1.32	16.41	10.5	0.21	7.83	11.42	2.97	0.13	0.13	10.09
4856_6	Rocky Ridge	NMORB	RPerp	UF	8.40298	-104.82863	2741	48.21	1.25	16.88	10.16	0.16	8.27	11.12	2.92	0.16	0.13	12.45
4856_5	Rocky Ridge	EMORB	RPerp	UF	8.40640	-104.83624	2783	48.58	1.67	16.33	9.29	0.17	8.43	10.59	2.96	0.5	0.22	29.97
4856_3	Rocky Ridge	EMORB	RPerp	UF	8.40746	-104.83776	2807	48.33	1.68	16.28	9.26	0.17	8.31	10.59	2.99	0.5	0.22	29.89
4856_4	Rocky Ridge	EMORB	RPerp	UF	8.40688	-104.83776	2787	48.5	1.7	16.31	9.31	0.17	8.47	10.51	2.99	0.51	0.22	29.78
4856_2	Rocky Ridge	EMORB	RPerp	UF	8.40905	-104.83815	2798	48.32	1.7	16.3	9.22	0.17	8.26	10.66	2.97	0.51	0.22	29.94
4856_1	Rocky Ridge	EMORB	RPerp	UF	8.41148	-104.83915	2736	48.88	1.62	15.82	9.04	0.16	8.48	10.96	2.75	0.47	0.23	28.90
4852_2	Coral1	EMORB	RPerp	UF	8.42316	-104.93982	2549	49.54	1.71	15.84	8.98	0.16	7.98	11.08	2.82	0.49	0.26	28.86
4852_1	Coral1	EMORB	RPerp	UF	8.42317	-104.93983	2551	49.41	1.76	15.71	9.08	0.16	8.13	11.08	2.8	0.51	0.25	28.82
4852_3	Coral1	EMORB	RPerp	UF	8.42317	-104.93995	2499	49.43	1.76	15.85	9.09	0.17	7.88	11.12	2.85	0.51	0.26	29.04
4852_4	Coral1	EMORB	RPerp	UF	8.42297	-104.94033	2498	49.43	1.73	15.82	9.1	0.17	7.98	11.05	2.85	0.51	0.25	29.14
4852_5	Coral1	EMORB	RPerp	UF	8.42199	-104.94199	2529	49.32	1.71	15.96	9.01	0.17	8.1	11.04	2.81	0.56	0.25	33.02
4852_6	Coral1	EMORB	RPerp	UF	8.42065	-104.94347	2455	49.3	1.68	15.87	9.05	0.17	8.14	11.05	2.82	0.56	0.25	33.19
4852_7	Coral1	DMORB	RPerp	UF	8.42440	-104.95079	2512	48.26	1.3	16.58	10.64	0.2	8.03	11.33	2.94	0.11	0.13	8.19
4852_8	Coral1	NMORB	RPerp	UF	8.42543	-104.95387	2277	48.2	1.24	16.98	10.34	0.18	8.34	11.18	2.87	0.09	0.11	7.29
4852_9	Coral1	NMORB	RPerp	UF	8.42562	-104.95413	2240	47.52	1.22	17.05	10.28	0.17	8.56	11.11	2.87	0.09	0.12	7.47
4852_10	Coral1	NMORB	RPerp	UF	8.42551	-104.95480	2186	47.77	1.23	17.03	10.47	0.18	8.41	11.31	2.91	0.09	0.11	7.51
4852_11	Coral1	NMORB	RPerp	UF	8.42542	-104.95726	2108	47.95	1.24	17.02	10.4	0.18	8.57	11.11	2.83	0.1	0.12	7.68
4852_12	Coral1	NMORB	RPerp	UF	8.42485	-104.95871	2088	48.11	1.21	17.02	10.23	0.17	8.57	11.09	2.87	0.09	0.13	7.39
4852_13	Coral1	NMORB	RPerp	UF	8.42415	-104.95950	2104	48.1	1.22	16.98	10.33	0.18	8.54	11.07	2.89	0.09	0.12	7.55
4852_14	Coral1	DMORB	RPerp	UF	8.42347	-104.96069	2113	47.9	1.26	17.07	10.5	0.18	8.39	11.16	2.83	0.09	0.12	7.48
4852_15	Coral1	NMORB	RPerp	UF	8.42315	-104.96196	2068	48.07	1.27	16.91	10.52	0.18	8.31	11.11	2.9	0.1	0.13	7.91
4852_16	Coral1	NMORB	RPerp	UF	8.42242	-104.96254	2039	48.04	1.2	17.04	10.39	0.18	8.51	11.1	2.85	0.09	0.12	7.66
4859_16	Coral2	EMORB	RPerp	UF	8.42146	-105.01521	2654	49.5	1.66	16.59	9.03	0.16	7.85	11.45	2.86	0.47	0.26	28.25
4859_15	Coral2	EMORB	RPerp	UF	8.42115	-105.01670	2700	49.38	1.7	16.49	9	0.16	7.85	11.37	2.78	0.46	0.25	26.86
4859_14	Coral2	EMORB	RPerp	UF	8.42110	-105.01793	2753	49.92	1.69	17.08	8.75	0.17	6.93	11.82	2.92	0.45	0.27	26.68
4859_13	Coral2	EMORB	RPerp	UF	8.42127	-105.02011	2801	50.41	1.51	15.79	8.52	0.16	7.88	12.03	2.69	0.39	0.24	25.69
4859_12	Coral2	EMORB	RPerp	UF	8.42079	-105.02145	2703	50.37	1.58	15.2	8.68	0.17	7.68	12.06	2.68	0.39	0.25	24.84
OS17_A	Coral2	EMORB	RPerp	UF	8.42976	-105.02181	3021	50.35	1.19	16.61	8.32	0.15	8.45	11.76	2.55	0.21	0.13	17.34
OS17_B	Coral2	EMORB	RPerp	UF	8.42976	-105.02181	3021	50.62	1.18	16.59	8.29	0.15	8.43	11.68	2.51	0.2	0.13	16.88
OS17_C	Coral2	EMORB	RPerp	UF	8.42976	-105.02181	3021	50.57	1.21	16.5	8.29	0.15	8.33	11.75	2.58	0.21	0.14	17.15
OS17_E	Coral2	EMORB	RPerp	UF	8.42976	-105.02181	3021	50.39	1.16	16.62	8.24	0.15	8.46	11.74	2.53	0.2	0.14	17.53
OS17_F	Coral2	EMORB	RPerp	UF	8.42976	-105.02181	3021	50.42	1.16	16.51	8.22	0.14	8.57	11.6	2.5	0.2	0.13	17.27
OS7_A	Coral2	EMORB	RPar	UF	8.38070	-105.02490	3134	49.48	1.89	15.58	9.7	0.17	7.02	11.28	2.73	0.5	0.27	26.21
OS7_B	Coral2	EMORB	RPar	UF	8.38070	-105.02490	3134	48.97	1.74	15.77	9.44	0.17	7.68	11.09	2.7	0.47	0.27	26.83
OS7_C	Coral2	EMORB	RPar	UF	8.38070	-105.02490	3134	48.79	1.77	15.78	9.42	0.18	7.6	11.07	2.62	0.46	0.26	26.11
OS7_D	Coral2	EMORB	RPar	UF	8.38070	-105.02490	3134	48.85	1.77	15.8	9.41	0.17	7.61	11.09	2.66	0.47	0.26	26.35
OS7_E	Coral2	EMORB	RPar	UF	8.38070	-105.02490	3134	48.93	1.77	15.8	9.4	0.16	7.58	11.14	2.67	0.47	0.26	26.38
OS7_F	Coral2	EMORB	RPar	UF	8.38070	-105.02490	3134	49.02	1.77	15.71	9.53	0.16	7.79	11.06	2.66	0.47	0.26	26.39
OS7_G	Coral2	EMORB	RPar	UF	8.38070	-105.02490	3134	48.74	1.73	15.74	9.46	0.16	7.73	11.06	2.65	0.46	0.25	26.50
4859_11	Coral2	EMORB	RPerp	UF	8.42017	-105.02491	2770	50.14	1.65	15.28	8.93	0.17	7.55	12.22	2.76	0.41	0.25	25.17
4859_10	Coral2	EMORB	RPerp	UF	8.42022	-105.02577	2774	50.18	1.67	15.39	8.89	0.16	7.57	12.26	2.77	0.41	0.26	24.58
4859_9	Coral2	EMORB	RPerp	UF	8.42046	-105.02779	2832	50.08	1.62	15.45	8.79	0.17	7.63	12.31	2.75	0.41	0.24	25.15
4859_8	Coral2	NMORB	RPerp	UF	8.42073	-105.02934	2926	47.65	1.11	17.38	8.75	0.16	10.25	11.46	2.68	0.11	0.12	10.27
4859_6	Coral2	EMORB	RPerp	UF	8.42119	-105.03156	2960	47.34	1.2	17.03	10.01	0.18	8.99	11.56	2.58	0.22	0.17	18.38
4859_7	Coral2	EMORB	RPerp	UF	8.42083	-105.03192	2931	47.29	1.15	17.23	9.68	0.17	8.68	11.64	2.61	0.22	0.16	18.82
4859_5	Coral2	EMORB	RPerp	UF	8.42144	-105.03297	2931	47.2	1.14	16.97	10.1	0.17	9.02	11.58	2.55	0.22	0.17	19.34
4859_4	Coral2	EMORB	RPerp	UF	8.42215	-105.03639	2869	49.36	1.51	15.92	8.76	0.17	7.93	12.24	2.71	0.37	0.22	24.48
4859_3	Coral2	EMORB	RPerp	UF	8.42105	-105.03780	2920	49.45	1.52	15.82	8.75	0.16	7.91	12.17	2.76	0.37	0.23	24.15
4859_2	Coral2	EMORB	RPerp	UF	8.41969	-105.03938	2993	47.79	1.24	17	9.86	0.17	8.64	11.69	2.66	0.23	0.18	18.84
4859_1	Coral2	EMORB	RPerp	UF	8.41788	-105.04138	2882	47.88	1.52	15.95	10.71	0.19	8.04	11.04	2.91	0.3	0.17	19.39
OS16_A	Coral2	EMORB	RPar	UF	8.45955	-105.04702	3070	49.08	2.08	16.08	9.46	0.16	7.38	10.54	3.1	0.52	0.31	24.96
OS16_B	Coral2	EMORB	RPar	UF	8.45955	-105.04702	3070	49.16	2.05	16.07	9.61	0.18	7.34	10.57	3.2	0.52	0.32	25.16
OS16_C	Coral2	EMORB	RPar	UF	8.45955	-105.04702	3070	49.29	2.07	16.1	9.57	0.16	7.4	10.48	3.2	0.52	0.33	24.91
OS16_D	Coral2	EMORB	RPar	UF	8.45955	-105.04702	3070	49.56	2.09	16.18	9.43	0.16	7.16	10.46	3.21	0.52	0.32	25.04
OS16_E	Coral2	EMORB	RPar	UF	8.45955	-105.04702	3070	50.24	2.03	16.58	9.32	0.17	7.51	9.94	2.5	0.49	0.32	24.07
OS16_F	Coral2	EMORB	RPar	UF	8.45955	-105.04702	3070	49.59	2.08	16.12	9.53	0.19	7.43	10.47	3.19	0.51	0.33	24.64

Sample	Seamount	Lava Type	Morphology	Lab	Latitude	Longitude	Depth	SiO_2	TiO_2	Al_2O_3	FeO	MnO	MgO	CaO	Na_2O	K_2O	P_2O_5	K_2O/TiO_2
4857_18	Otto Ridge	NMORB	RPerp	UF	8.45384	-105.10629	2265	48.25	1.34	17.03	9.63	0.17	8.16	11.34	3.08	0.12	0.15	9.06
4857_17	Otto Ridge	NMORB	RPerp	UF	8.45340	-105.10760	2321	48.47	1.4	16.93	9.78	0.17	7.95	11.41	3.16	0.12	0.15	8.87
4857_16	Otto Ridge	NMORB	RPerp	UF	8.45276	-105.10940	2405	48.75	1.37	17.05	9.67	0.16	8.05	11.47	3.13	0.12	0.14	9.05
4857_15	Otto Ridge	NMORB	RPerp	UF	8.45258	-105.11015	2432	48.54	1.56	16.32	10.43	0.18	7.46	11.41	3.27	0.14	0.16	8.77
OS14_A	Otto Ridge	EMORB	RPerp	UF	8.47033	-105.11047	3127	49.54	2.05	16.09	9.29	0.18	7.13	9.76	3.24	0.79	0.44	38.64
OS14_B	Otto Ridge	EMORB	RPerp	UF	8.47033	-105.11047	3127	49.48	2.04	16.07	9.24	0.18	7.2	9.81	3.27	0.8	0.44	39.09
OS14_C	Otto Ridge	EMORB	RPerp	UF	8.47033	-105.11047	3127	49.54	2.05	16.05	9.21	0.16	7.12	9.86	3.23	0.8	0.44	38.88
OS14_D	Otto Ridge	EMORB	RPerp	UF	8.47033	-105.11047	3127	49.43	2.06	16.01	9.24	0.18	7.08	9.8	3.26	0.79	0.45	38.48
OS14_E	Otto Ridge	EMORB	RPerp	UF	8.47033	-105.11047	3127	49.58	2.04	16.08	9.32	0.17	7.09	9.72	3.24	0.79	0.46	38.71
OS14_F	Otto Ridge	EMORB	RPerp	UF	8.47033	-105.11047	3127	49.46	2.07	16.03	9.36	0.18	7.13	9.74	3.29	0.79	0.45	38.28
4857_14	Otto Ridge	NMORB	RPerp	UF	8.45182	-105.11126	2481	47.95	1.35	16.98	9.6	0.16	8.05	11.58	3.04	0.12	0.14	9.21
4857_13	Otto Ridge	NMORB	RPerp	UF	8.45154	-105.11178	2526	48.97	1.37	17.18	9.85	0.17	8.1	10.9	3.21	0.13	0.16	9.22
4857_12	Otto Ridge	NMORB	RPerp	UF	8.45142	-105.11197	2546	48.98	1.37	17.25	9.74	0.17	8.13	11.02	3.22	0.12	0.16	8.86
4857_11	Otto Ridge	NMORB	RPerp	UF	8.45107	-105.11260	2590	48.9	1.41	17.04	9.88	0.18	8.06	10.9	3.21	0.12	0.14	8.63
4857_9	Otto Ridge	NMORB	RPerp	UF	8.45080	-105.11301	2636	48.97	1.41	17.01	9.92	0.17	7.92	11.04	3.27	0.12	0.16	8.49
4857_7	Otto Ridge	DMORB	RPerp	UF	8.45073	-105.12000	2476	48.35	1.35	17.24	10.13	0.19	8.46	11.08	3.02	0.07	0.13	4.88
4857_8	Otto Ridge	DMORB	RPerp	UF	8.45073	-105.12000	2476	48.42	1.34	17.19	10.11	0.18	8.58	10.99	3.03	0.07	0.13	5.01
4857_4	Otto Ridge	EMORB	RPerp	UF	8.45013	-105.12316	2480	49.8	1.89	16.27	9.04	0.18	7.7	10.57	3.13	0.52	0.29	27.65
4857_5	Otto Ridge	EMORB	RPerp	UF	8.45014	-105.12317	2480	49.8	1.9	16.21	9.14	0.17	7.69	10.6	3.17	0.51	0.29	26.89
4857_3	Otto Ridge	EMORB	RPerp	UF	8.45179	-105.12717	2420	49.74	1.68	16.1	9.13	0.16	7.94	11.47	2.83	0.55	0.27	32.97
4857_2	Otto Ridge	EMORB	RPerp	UF	8.45191	-105.12983	2440	49.15	1.7	15.88	9.13	0.18	8.05	11.27	2.73	0.56	0.27	33.07
4857_1	Otto Ridge	EMORB	RPerp	UF	8.45190	-105.13016	2456	49.01	1.76	15.75	9.23	0.17	8.13	11.3	2.69	0.56	0.28	31.58
4858_14	Sparky	EMORB	RPar	UF	8.45340	-105.21088	2588	50.09	2.79	16.17	9.68	0.17	5.53	8.88	3.82	1.34	0.62	47.93
4858_13	Sparky	EMORB	RPar	UF	8.45524	-105.21096	2601	50.1	2.75	16.23	9.7	0.15	5.48	8.9	3.81	1.33	0.63	48.40
4858_10	Sparky	EMORB	RPar	UF	8.46212	-105.21109	2657	49.8	2.78	16.43	9.56	0.17	5.67	8.91	3.82	1.34	0.64	48.20
4858_9	Sparky	EMORB	RPar	UF	8.46514	-105.21138	2756	49.56	2.78	16.29	9.69	0.15	5.81	8.93	3.86	1.35	0.62	48.56
4858_11	Sparky	EMORB	RPar	UF	8.45798	-105.21188	2670	49.44	2.81	16.35	9.75	0.16	5.71	8.95	3.89	1.35	0.63	48.06
4858_2	Sparky	EMORB	RPar	UF	8.47714	-105.21192	3087	49.59	2.4	16.31	8.92	0.16	7.19	9.69	3.44	0.97	0.46	40.39
4858_8	Sparky	EMORB	RPar	UF	8.46788	-105.21208	2890	49.89	2.73	16.31	9.62	0.16	5.68	8.87	3.86	1.34	0.63	49.21
4858_3	Sparky	EMORB	RPar	UF	8.47623	-105.21215	3062	49.45	2.41	16.33	8.99	0.16	7.21	9.7	3.41	0.96	0.46	39.98
4858_1	Sparky	EMORB	RPar	UF	8.48148	-105.21217	3066	49.74	2.46	16.36	8.96	0.15	6.85	9.66	3.43	1.02	0.46	41.29
4858_12	Sparky	EMORB	RPar	UF	8.45743	-105.21222	2634	50.14	2.75	16.19	9.71	0.15	5.48	8.88	3.83	1.34	0.62	48.55
4858_4	Sparky	EMORB	RPar	UF	8.47526	-105.21234	3055	50.03	2.87	15.81	9.9	0.17	5.36	9.07	3.87	1.36	0.65	47.43
4858_5	Sparky	EMORB	RPar	UF	8.47415	-105.21240	2967	49.92	2.89	15.86	9.95	0.15	5.45	9.08	3.83	1.35	0.64	46.72
4858_6	Sparky	EMORB	RPar	UF	8.47181	-105.21263	2900	50.04	2.88	15.97	9.7	0.16	5.47	8.99	3.85	1.38	0.64	47.82
4858_7	Sparky	EMORB	RPar	UF	8.47068	-105.21295	2887	49.66	2.78	16.36	9.54	0.15	5.72	8.95	3.92	1.37	0.62	49.50
OS6_A	Avery	EMORB	Seamount	USGS	8.35703	-105.28420	3306	48.86	2.38	15.94	9.94	0.18	6.52	9.78	3.36	0.71	0.41	29.81
OS6_B	Avery	EMORB	Seamount	USGS	8.35703	-105.28420	3306	49.27	2.38	16.07	9.96	0.18	6.56	9.72	3.4	0.73	0.4	30.59
OS6_C	Avery	EMORB	Seamount	USGS	8.35703	-105.28420	3306	49.05	2.39	16.06	9.99	0.17	6.5	9.72	3.43	0.73	0.4	30.62
OS6_D	Avery	EMORB	Seamount	USGS	8.35703	-105.28420	3306	49.01	2.38	15.94	10.08	0.18	6.74	9.7	3.35	0.69	0.4	29.09
OS6_E	Avery	EMORB	Seamount	USGS	8.35703	-105.28420	3306	49.05	2.4	16.02	10	0.17	6.42	9.77	3.4	0.73	0.4	30.42
OS6_F	Avery	EMORB	Seamount	USGS	8.35703	-105.28420	3306	49.18	1.9	16.82	9.11	0.16	7.51	10.77	3.08	0.6	0.32	31.49
OS6_G	Avery	EMORB	Seamount	USGS	8.35703	-105.28420	3306	49	2.39	16.08	9.96	0.18	6.54	9.7	3.38	0.72	0.4	30.21
OS5_A	Avery	EMORB	Seamount	UF	8.41303	-105.28486	2674	49.52	1.9	16.38	8.98	0.16	7.48	10.76	3.17	0.63	0.31	33.28
OS5_B	Avery	EMORB	Seamount	UF	8.41303	-105.28486	2674	49.51	1.94	16.36	9.04	0.18	7.5	10.77	3.17	0.63	0.33	32.47
OS5_C	Avery	EMORB	Seamount	UF	8.41303	-105.28486	2674	49.52	1.94	16.36	9.02	0.16	7.53	10.81	3.1	0.63	0.31	32.47
OS5_D	Avery	EMORB	Seamount	UF	8.41303	-105.28486	2674	49.1	1.93	16.36	8.93	0.19	7.5	10.77	3.18	0.65	0.32	33.55
OS5_E	Avery	EMORB	Seamount	UF	8.41303	-105.28486	2674	49.7	1.92	16.39	9.03	0.17	7.54	10.75	3.15	0.63	0.31	32.90
OS5_F	Avery	EMORB	Seamount	UF	8.41303	-105.28486	2674	49.67	1.92	16.32	8.99	0.16	7.42	10.9	3.19	0.63	0.31	32.86
OS5_G	Avery	EMORB	Seamount	UF	8.41303	-105.28486	2674	49.35	1.94	16.35	9.07	0.16	7.48	10.87	3.01	0.64	0.32	32.99
OS5_H	Avery	EMORB	Seamount	UF	8.41303	-105.28486	2674	48.96	1.9	16.42	9.01	0.17	7.43	10.91	3.15	0.63	0.3	33.39
4851_14	Avery	EMORB	Seamount	UF	8.40638	-105.30295	2538	49.17	1.54	16.48	8.66	0.16	8.15	11.58	2.71	0.27	0.22	17.24
4851_13	Avery	EMORB	Seamount	UF	8.40574	-105.30449	2440	48.54	1.62	15.73	9.16	0.16	7.83	11.63	2.72	0.29	0.23	18.06
4851_11	Avery	EMORB	Seamount	UF	8.40823	-105.30540	2451	48.92	1.55	16.51	8.74	0.16	8.12	11.57	2.69	0.29	0.22	18.90
4851_9	Avery	NMORB	Seamount	UF	8.40952	-105.30959	2467	48.22	1.11	16.2	10.29	0.18	9.49	10.88	2.5	0.1	0.12	8.94
OS4_A	Avery	EMORB	Seamount	USGS	8.42052	-105.31067	2695	48.78	2.06	16.21	9.18	0.17	7.35	10.75	3.07	0.54	0.32	26.13
OS4_B	Avery	EMORB	Seamount	USGS	8.42052	-105.31067	2695	48.83	2.08	16.17	9.24	0.16	7.32	10.72	3.05	0.55	0.32	26.29
OS4_C	Avery	EMORB	Seamount	USGS	8.42052	-105.31067	2695	49.07	2.1	16.31	9.25	0.16	7.16	10.78	3.08	0.53	0.33	25.43
OS4_D	Avery	EMORB	Seamount	USGS	8.42052	-105.31067	2695	49.05	2.09	16.34	9.26	0.16	7.12	10.76	3.15	0.55	0.32	26.21
OS4_E	Avery	EMORB	Seamount	USGS	8.42052	-105.31067	2695	48.48	1.93	16.41	9.13	0.16	7.76	10.76	3.02	0.58	0.3	30.28
OS4_F	Avery	EMORB	Seamount	USGS	8.42052	-105.31067	2695	48.76	2.08	16.19	9.19	0.16	7.35	10.72	3.08	0.53	0.32	25.73
OS4_H	Avery	EMORB	Seamount	USGS	8.42052	-105.31067	2695	49.14	2.11	16.23	9.23	0.16	7.35	10.76	3.09	0.53	0.33	25.27
OS4_I	Avery	EMORB	Seamount	USGS	8.42052	-105.31067	2695	48.84	2.06	16.34	9.22	0.15	7.32	10.74	3.09	0.54	0.33	26.33
OS4_J	Avery	EMORB	Seamount	USGS	8.42052	-105.31067	2695	48.29	1.92	16.44	9.08	0.16	7.63	10.73	3.03	0.57	0.3	29.79
OS4_K	Avery	EMORB	Seamount	USGS	8.42052	-105.31067	2695	49.04	2.08	16.34	9.26	0.17	7.27	10.77	3.08	0.56	0.32	26.71
OS4_L	Avery	EMORB	Seamount	USGS	8.42052	-105.31067	2695	48.85	2.09	16.2	9.25	0.16	7.26	10.73	3.07	0.54	0.32	25.70
4851_7	Avery	EMORB	Seamount	UF	8.41106	-105.31219	2667	48.73	1.43	16.45	8.6	0.16	8.14	11.74	2.65	0.25	0.19	17.23
4851_4	Avery	NMORB	Seamount	UF	8.41099	-105.32148	2605	47.95	1.11	16.65	10.06	0.18	9.2	11	2.5	0.09	0.13	8.13
4851_3	Avery	NMORB	Seamount	UF	8.41091	-105.32518	2603	48.27	1.09	16.32	10.19	0.19	9.34	10.85	2.47	0.1	0.13	9.01
4851_1	Avery	NMORB	Seamount	UF	8.40797	-105.32578	2686	47.9	1.11	16.46	10.54	0.19	8.8	10.84	2.48	0.09	0.12	7.92
4850_11	Matthew	NMORB	RPerp	UF	8.41693	-105.36070	2475	49.22	1.12	16.05	11.79	0.2	7.88	10.46	2.71	0.1	0.09	9.01
4850_10	Matthew	NMORB	RPerp	UF	8.41668	-105.36106	2491	49.35	1.13	16.03	11.78	0.21	7.93	10.51	2.71	0.1	0.08	8.65
4850_1	Matthew	EMORB	RPerp	UF	8.40369	-105.36189	2699	50.95	1.34	15.81	8.48	0.16	8.27	11.85	2.8	0.23	0.16	17.52
4850_3	Matthew	EMORB	RPerp	UF	8.40752	-105.36222	2553	51.04	1.34	15.84	8.51	0.17	8.24	11.74	2.79	0.23	0.16	17.18
4850_5	Matthew	NMORB	RPerp	UF	8.41184	-105.36285	2590	49.16	1.06	15.91	12.34	0.2	8.31	10.21	2.68	0.09	0.07	8.59
4850_4	Matthew	NMORB	RPerp	UF	8.40928	-105.36297	2618	49.33	1.17	15.94	12.21	0.21	7.66	10.58	2.78	0.13	0.08	11.37
4850_7	Matthew	NMORB	RPerp	UF	8.41326	-105.36316	2528	49.24	1.17	15.85	12.21	0.21	7.59	10.62	2.79	0.13	0.09	10.88
4850_8	Matthew	EMORB	RPerp	UF	8.41641	-105.36551	2532	48.66	1.43	16.34	11.56	0.21	8.13	10.14	2.84	0.44	0.17	30.73

Sample	Seamount	Lava Type	Morphology	Lab	Latitude	Longitude	Depth	SiO_2	TiO_2	Al_2O_3	FeO	MnO	MgO	CaO	Na_2O	K_2O	P_2O_5	K_2O/TiO_2
4849_3	Wayne	EMORB	Seamount	USGS	8.41599	-105.51108	2863	49.09	1.5	16.84	8.71	0.16	8.22	11.1	2.88	0.31	0.19	20.46
4849_4	Wayne	EMORB	Seamount	USGS	8.41587	-105.51116	2861	49.3	1.54	16.71	8.9	0.17	7.99	11.06	2.92	0.32	0.2	20.70
4849_2	Wayne	EMORB	Seamount	USGS	8.41634	-105.51116	2881	48.87	1.5	16.78	8.76	0.16	8.19	11.11	2.95	0.31	0.21	20.60
4849_6	Wayne	EMORB	Seamount	USGS	8.41651	-105.51588	2941	50.48	1.87	15.28	9.16	0.16	6.91	11.05	3.05	0.46	0.27	24.74
4849_8	Wayne	EMORB	Seamount	USGS	8.41492	-105.51654	2873	50.34	1.84	15.4	9.05	0.16	7	11.04	3.03	0.45	0.26	24.60
4849_9	Wayne	NMORB	Seamount	USGS	8.41154	-105.51746	2922	50.29	1.54	15.34	9.03	0.16	7.54	11.32	2.99	0.25	0.19	16.40
4849_11	Wayne	NMORB	Seamount	USGS	8.40949	-105.51863	2910	50.48	1.53	15.38	9	0.17	7.61	11.37	3	0.25	0.19	16.36
4849_20	Wayne	EMORB	Seamount	UF	8.40283	-105.51881	2718	48.43	1.76	16.19	8.9	0.15	8.07	10.92	3.09	0.54	0.28	30.68
4849_18	Wayne	EMORB	Seamount	USGS	8.40354	-105.51934	2775	48.53	1.74	16.49	8.9	0.15	8.43	10.48	2.93	0.52	0.25	29.73
4849_13	Wayne	EMORB	Seamount	USGS	8.40730	-105.51938	2894	48.54	1.77	16.8	8.9	0.16	7.73	10.72	2.95	0.52	0.25	29.48
4849_12	Wayne	EMORB	Seamount	USGS	8.40739	-105.51939	2908	48.63	1.73	16.67	8.94	0.16	8.35	10.6	2.92	0.51	0.26	29.50
4849_14	Wayne	EMORB	Seamount	UF	8.40649	-105.52027	2878	48.52	1.82	16.56	8.87	0.16	7.31	11.07	3.18	0.56	0.3	30.44
OS3_A	Wayne	NMORB	Seamount	USGS	8.42830	-105.52031	3041	49.88	1.58	15.51	9.18	NaN	7.55	11.4	2.98	0.24	0.19	15.36
4849_15	Wayne	EMORB	Seamount	USGS	8.40512	-105.52062	2822	48.59	1.72	16.61	8.88	0.15	8.24	10.63	2.94	0.5	0.25	28.92
4847_1	Max	DMORB	Cone	USGS	8.38207	-105.62746	3209	48.23	1.39	17.43	7.99	NaN	8.44	11.17	3.23	0.08	0.17	6.06
4847_2	Max	DMORB	Cone	USGS	8.38232	-105.62776	3171	48.67	1.37	17.55	7.87	NaN	8.53	11.22	3.29	0.08	0.16	5.92
4847_7	Max	DMORB	Seamount	USGS	8.38434	-105.63426	3051	49.03	1.43	17.47	7.84	NaN	8.46	11.22	3.29	0.08	0.19	5.36
4847_8	Max	DMORB	Seamount	USGS	8.38434	-105.63473	3007	48.33	1.35	17.41	7.88	NaN	8.86	11.17	3.24	0.08	0.16	6.25
4847_9	Max	NMORB	Seamount	USGS	8.38445	-105.63607	2933	49.98	1.32	15.01	9.28	NaN	7.9	11.97	2.46	0.18	0.15	13.32
4847_10	Max	NMORB	Seamount	USGS	8.38464	-105.63714	2851	50.65	1.57	14.61	10.3	NaN	6.87	11.25	2.72	0.23	0.17	14.55
4847_11	Max	NMORB	Seamount	USGS	8.38483	-105.63963	2787	50.81	1.74	14.35	10.88	NaN	6.65	10.84	2.89	0.26	0.2	14.86
4847_13	Max	NMORB	Seamount	USGS	8.38752	-105.64300	2714	50.06	1.53	14.52	10.23	NaN	7.12	11.22	2.72	0.23	0.18	14.79
4847_14	Max	NMORB	Seamount	USGS	8.38925	-105.64504	2676	50.33	1.5	14.64	10.2	NaN	7.22	11.2	2.73	0.22	0.17	14.40
4847_15	Max	NMORB	Seamount	USGS	8.38730	-105.64770	2658	49.9	1.32	16.03	8.53	NaN	8.22	11.83	2.7	0.22	0.16	16.44
4847_16	Max	NMORB	Seamount	USGS	8.38629	-105.64927	2575	49.78	1.31	16.06	8.5	NaN	8.24	11.84	2.69	0.2	0.16	15.56
4848_19	Ivy	EMORB	Seamount	UF	8.37695	-105.73430	2180	50.86	2.38	14	10.53	0.19	5.53	10.04	3.49	0.6	0.34	25.34
4848_15	Ivy	EMORB	Seamount	UF	8.37430	-105.73678	2193	50.69	2.51	13.59	12.02	0.21	5.34	9.56	3.3	0.47	0.32	18.90
4848_14	Ivy	EMORB	Seamount	UF	8.37375	-105.73693	2251	50.43	2.48	13.58	11.94	0.21	5.29	9.57	3.73	0.48	0.32	19.31
4848_10	Ivy	EMORB	Seamount	UF	8.36929	-105.73775	2300	49.72	1.95	15.95	8.38	0.14	7.38	10.7	2.79	0.6	0.31	30.59
4848_11	Ivy	EMORB	Seamount	UF	8.36929	-105.73775	2300	49.83	1.95	16.1	8.35	0.15	7.33	10.65	2.8	0.61	0.3	31.14
4848_8	Ivy	EMORB	Seamount	UF	8.36773	-105.74132	2312	49.83	1.93	15.92	8.52	0.15	7.24	10.81	2.86	0.6	0.31	31.26
4848_7	Ivy	EMORB	Seamount	USGS	8.36760	-105.74143	2339	49.54	1.91	16.06	8.39	0.14	7.51	10.77	2.84	0.58	0.3	30.36
4848_6	Ivy	EMORB	Seamount	USGS	8.36868	-105.74319	2350	49.95	2.18	15.3	8.94	0.16	6.72	10.77	2.87	0.65	0.33	29.69
4848_5	Ivy	EMORB	Seamount	USGS	8.36842	-105.74362	2332	49.69	1.89	16	8.23	0.14	7.5	10.75	2.82	0.57	0.29	30.26
4848_1	Ivy	EMORB	Seamount	UF	8.37327	-105.74756	2168	49.86	2.06	15.87	8.46	0.15	6.92	10.62	2.8	0.66	0.33	31.91
OS2_A	Liona	EMORB	Cone	USGS	8.56545	-106.10751	2988	49.09	2.13	16.23	9.22	0.15	7.23	10.01	3.09	0.89	0.36	41.53
OS2_C	Liona	EMORB	Cone	USGS	8.56545	-106.10751	2988	49.34	2.12	16.25	9.18	0.16	7.26	10.02	3.13	0.86	0.36	40.70
OS2_F	Liona	EMORB	Cone	USGS	8.56545	-106.10751	2988	49.08	2.14	16.17	9.08	0.17	7.16	10.1	3.08	0.88	0.36	41.13
OS2_G	Liona	EMORB	Cone	USGS	8.56545	-106.10751	2988	49.05	2.16	16.3	9.05	0.16	7.35	9.88	3.19	0.93	0.37	43.30
OS2_I	Liona	NMORB	Cone	USGS	8.56545	-106.10751	2988	50.54	1.5	15.05	9.44	0.18	7.62	11.82	2.73	0.22	0.18	14.68
OS2_K	Liona	EMORB	Cone	USGS	8.56545	-106.10751	2988	48.65	2.13	16.09	9.16	0.16	7.23	10.05	3.12	0.88	0.36	41.29
OS2_L	Liona	EMORB	Cone	USGS	8.56545	-106.10751	2988	49.15	2.11	16.15	9.17	0.16	7.19	10.06	3.17	0.87	0.36	41.32
OS2_M	Liona	EMORB	Cone	USGS	8.56545	-106.10751	2988	49.06	2.28	16.72	8.35	0.16	6.93	9.67	3.37	1.21	0.46	52.95
OS2_N	Liona	EMORB	Cone	USGS	8.56545	-106.10751	2988	49.14	2.17	16.41	9.07	0.16	6.78	10.1	3.19	0.89	0.37	40.82
OS1_D	Liona	EMORB	Seamount	USGS	8.57512	-106.18844	2676	49.21	1.82	16.69	8.08	0.14	7.48	10.96	3.05	0.83	0.32	45.77
OS1_F	Liona	EMORB	Seamount	UF	8.57512	-106.18844	2676	49.04	2.49	15.68	8.5	0.15	5.95	9.93	3.48	1.26	0.48	50.40
OS1_J	Liona	NMORB	Seamount	USGS	8.57512	-106.18844	2676	50.22	1.36	14.92	9.49	0.17	7.92	11.96	2.75	0.12	0.12	8.98
OS1_K	Liona	NMORB	Seamount	USGS	8.57512	-106.18844	2676	49.88	1.38	15.02	9.51	0.18	7.9	12.02	2.76	0.11	0.12	8.20
OS1_M	Liona	NMORB	Seamount	USGS	8.57512	-106.18844	2676	50.19	1.36	14.96	9.51	0.17	7.9	12.01	2.78	0.12	0.12	8.82
OS1_N	Liona	NMORB	Seamount	USGS	8.57512	-106.18844	2676	50.27	1.37	14.92	9.48	0.17	7.94	11.94	2.76	0.12	0.12	8.68
OS1_O	Liona	NMORB	Seamount	USGS	8.57512	-106.18844	2676	50.06	1.36	14.97	9.49	0.17	7.89	12.05	2.75	0.13	0.12	9.17
OS1_P	Liona	NMORB	Seamount	USGS	8.57512	-106.18844	2676	50.04	1.38	14.93	9.46	0.18	7.94	12	2.76	0.12	0.13	8.49
OS1_Q	Liona	NMORB	Seamount	UF	8.57512	-106.18844	2676	49.62	1.37	14.84	9.43	0.18	7.72	12.18	2.69	0.13	0.13	9.31
OS1_R	Liona	NMORB	Seamount	USGS	8.57512	-106.18844	2676	50.08	1.37	14.99	9.48	0.18	7.86	12.03	2.78	0.12	0.12	8.69
OS1_S	Liona	NMORB	Seamount	UF	8.57512	-106.18844	2676	49.55	1.34	14.9	9.4	0.19	7.66	12.28	2.68	0.13	0.12	9.98
OS1_T	Liona	NMORB	Seamount	USGS	8.57512	-106.18844	2676	49.96	1.36	15.05	9.51	0.17	7.87	12.03	2.81	0.11	0.13	8.42

Table A.2 Trace Element Concentrations of the 8˚20’ N seamount lavas measured on the LA-ICP-MS at Boise State University. Trace element concentrations are in ppm.

Sample	Seamount	Latitude	Longitude	Depth	Li	Sc	V	Cr	Co	Ni	Cu	Zn	Ga	Rb	Sr	Y	Zr	Nb	Cs	Ba	La	Ce	Pr	Nd	Sm	Eu	Tb	Gd	Dy	Ho	Er	Tm	Yb	Lu	Hf	Ta	Pb	Th	U
OS11_B	NEPR	8.44457	-104.28612	2947	4.39	33.1	167	253	42.6	159	72.7	61.1	12.7	1.11	162	21.6	72	2.4	0.02	13.3	3.0	8.6	1.44	7.5	2.50	0.96	0.58	3.19	3.71	0.82	2.31	0.35	2.26	0.35	1.64	0.16	0.36	0.16	0.06
OS11_C	NEPR	8.44457	-104.28612	2947	4.44	31.9	168	255	43.2	162	73.1	63.3	12.9	1.20	162	20.2	68	2.4	0.01	13.7	2.9	8.6	1.43	7.3	2.37	0.95	0.55	3.10	3.39	0.76	2.09	0.31	2.10	0.32	1.54	0.15	0.35	0.16	0.05
OS11_D	NEPR	8.44457	-104.28612	2947	4.71	31.9	179	285	42.5	139	73.3	64.2	13.2	1.62	167	19.3	69	3.2	0.02	18.8	3.4	9.8	1.60	7.8	2.44	0.99	0.53	2.98	3.41	0.72	2.07	0.29	2.03	0.28	1.52	0.19	0.38	0.20	0.07
4854_13	NEPR	8.40394	-104.39374	2319	4.01	32.0	153	213	48.2	143	89.3	68.0	13.0	0.56	151	20.0	55	1.2	0.01	7.7	1.8	5.6	1.00	5.4	1.78	0.88	0.52	2.92	3.47	0.76	2.25	0.34	2.18	0.33	1.30	0.08	0.29	0.09	0.03
4854_11	NEPR	8.40406	-104.39519	2418	3.74	29.2	146	205	46.6	141	86.4	66.2	12.4	0.59	145	17.8	48	1.2	0.01	7.1	1.6	5.4	0.92	5.0	1.76	0.82	0.46	2.54	3.01	0.66	1.87	0.31	1.94	0.30	1.18	0.08	0.27	0.08	0.04
4854_9	NEPR	8.40452	-104.39838	2535	4.35	40.9	168	221	46.2	100	96.5	71.7	13.1	0.64	151	27.2	72	1.4	0.02	8.2	2.1	6.4	1.20	6.6	2.56	1.03	0.67	3.81	4.46	1.02	2.80	0.47	3.00	0.42	1.86	0.11	0.29	0.11	0.04
4854_8	NEPR	8.40502	-104.40617	2469	5.06	42.4	263	138	40.0	41	75.5	76.7	13.9	2.35	188	28.9	117	5.6	0.03	27.1	5.8	15.5	2.48	12.6	3.66	1.44	0.81	4.68	5.04	1.12	3.00	0.43	2.97	0.40	2.66	0.35	0.59	0.31	0.14
4854_7	NEPR	8.40854	-104.40762	2436	5.00	40.9	261	145	40.0	44	74.3	76.2	13.8	2.28	187	26.8	110	5.4	0.02	26.6	5.6	15.1	2.41	11.9	3.45	1.31	0.79	4.52	4.74	1.03	2.97	0.40	2.76	0.39	2.46	0.31	0.58	0.33	0.13
4854_6	NEPR	8.41381	-104.40842	2430	4.30	32.4	162	269	47.6	147	81.4	72.3	13.9	0.43	195	23.1	63	1.1	0.02	6.8	1.7	5.6	1.03	6.2	2.12	0.96	0.62	3.50	3.85	0.85	2.60	0.37	2.53	0.38	1.51	0.09	0.38	0.10	0.04
4854_5	NEPR	8.41049	-104.41119	2434	5.57	30.8	237	190	34.1	59	62.0	86.1	20.1	17.70	348	26.7	199	28.5	0.20	199.2	19.5	42.9	5.59	23.8	5.24	1.96	0.88	5.59	5.16	1.01	2.87	0.38	2.48	0.36	4.10	1.66	1.57	1.92	0.61
4854_4	NEPR	8.40945	-104.41191	2388	5.59	30.9	236	189	34.2	61	59.1	83.7	19.8	17.71	353	26.7	198	28.6	0.18	201.4	19.6	43.1	5.74	23.7	5.36	1.90	0.88	5.67	5.15	0.99	2.79	0.38	2.52	0.35	3.93	1.62	1.52	1.84	0.61
4854_3	NEPR	8.40924	-104.41232	2440	5.87	30.0	242	193	35.1	62	63.4	87.2	20.7	18.39	352	25.6	191	28.8	0.20	204.7	19.2	44.0	5.68	23.2	5.15	1.90	0.82	5.27	4.63	0.91	2.63	0.40	2.34	0.35	3.76	1.60	1.65	1.84	0.59
4854_2	NEPR	8.40922	-104.41234	2444	6.41	32.3	255	207	37.4	67	71.3	87.7	21.6	19.34	354	29.1	212	29.3	0.21	205.7	20.4	44.6	5.72	24.3	5.47	1.93	0.91	5.90	5.28	1.13	3.09	0.40	2.77	0.41	4.40	1.70	1.60	2.00	0.63
4854_1	NEPR	8.40810	-104.41376	2478	3.78	30.1	163	210	48.0	153	101.5	61.6	12.4	0.50	136	18.5	54	1.1	0.00	4.7	1.9	6.3	1.09	5.8	1.86	0.92	0.47	2.62	3.11	0.68	2.00	0.32	2.16	0.28	1.23	0.06	0.31	0.10	0.04
OS12_B	Hook Ridge	8.44354	-104.42000	2961	5.20	40.2	210	373	51.5	186	74.9	78.2	15.1	1.70	172	26.3	83	3.5	0.01	20.3	3.9	10.6	1.74	9.0	2.96	1.17	0.71	3.94	4.59	0.99	2.77	0.42	2.80	0.41	1.92	0.21	0.46	0.23	0.07
OS12_F	Hook Ridge	8.44354	-104.42000	2961	4.68	33.5	182	330	45.9	177	66.5	68.0	12.9	1.48	146	21.6	70	2.9	0.01	17.4	3.3	9.1	1.50	7.4	2.53	0.98	0.58	3.23	3.57	0.83	2.30	0.35	2.34	0.33	1.64	0.18	0.40	0.19	0.07
4855_2	Hook Ridge	8.35626	-104.48912	2883	6.84	31.6	258	220	42.3	107	54.9	93.3	24.1	13.90	385	29.2	242	27.0	0.14	177.6	19.3	42.0	5.63	24.9	6.20	1.99	1.10	6.69	6.53	1.32	3.57	0.54	3.15	0.52	5.14	1.81	1.63	1.75	0.55
4855_3	Hook Ridge	8.35736	-104.48959	2825	6.92	29.5	259	239	34.9	59	52.4	89.1	25.6	17.55	390	28.4	251	32.6	0.19	217.0	22.1	48.5	6.29	26.6	6.39	2.06	1.07	6.68	6.28	1.29	3.47	0.52	3.13	0.50	5.08	2.03	1.81	2.04	0.67
4855_1	Hook Ridge	8.35280	-104.49137	2940	6.99	30.0	261	212	41.2	95	55.4	96.2	24.5	13.86	382	25.7	217	27.1	0.14	179.7	18.4	42.1	5.60	23.6	5.64	1.93	0.98	6.00	5.73	1.14	3.03	0.47	2.90	0.43	4.46	1.66	1.61	1.58	0.56
OS13_C	Midway Ridge	8.41004	-104.58592	2500	4.58	43.5	215	291	53.5	158	91.4	68.4	11.8	0.36	178	27.4	83	1.1	0.01	7.5	2.5	8.8	1.52	8.1	2.70	1.07	0.77	4.08	5.18	1.19	3.57	0.58	3.84	0.62	1.89	0.08	0.47	0.07	0.03
OS13_D	Midway Ridge	8.41004	-104.58592	2500	4.54	42.8	210	295	57.0	204	88.6	68.9	11.5	0.35	176	26.6	82	1.1	0.01	7.3	2.5	8.7	1.51	7.7	2.61	1.05	0.72	3.99	5.05	1.19	3.59	0.57	3.86	0.62	1.85	0.09	0.43	0.07	0.03
OS13_E	Midway Ridge	8.41004	-104.58592	2500	4.32	43.8	203	277	51.2	155	85.3	66.2	11.1	0.33	177	28.1	86	1.1	0.00	7.5	2.5	8.5	1.50	8.0	2.84	1.07	0.75	4.19	5.28	1.23	3.70	0.60	3.88	0.64	1.88	0.09	0.42	0.07	0.03
OS13_H	Midway Ridge	8.41004	-104.58592	2500	4.65	42.3	216	294	54.0	160	89.9	71.9	11.9	0.36	179	26.4	82	1.1	0.00	7.6	2.5	9.0	1.54	7.8	2.69	1.08	0.71	3.97	5.01	1.18	3.52	0.57	3.68	0.62	1.81	0.09	0.47	0.07	0.03
OS9_A	Beryl	8.41618	-104.64545	2800	4.47	32.1	200	233	39.8	122	68.7	72.2	13.3	3.93	219	23.4	99	5.4	0.06	40.6	5.4	14.4	2.14	10.1	2.87	1.11	0.61	3.70	3.88	0.83	2.26	0.34	2.33	0.34	2.04	0.33	0.63	0.41	0.14
OS9_B	Beryl	8.41618	-104.64545	2800	4.35	34.4	200	246	40.6	134	67.3	72.3	13.1	3.86	217	26.9	110	5.5	0.07	40.0	5.5	14.4	2.19	10.2	3.08	1.12	0.69	4.13	4.47	0.94	2.64	0.40	2.39	0.38	2.24	0.33	0.61	0.46	0.14
OS9_C	Beryl	8.41618	-104.64545	2800	4.39	31.3	201	256	41.1	138	69.2	74.3	13.5	3.63	213	23.4	97	5.4	0.05	37.2	5.2	14.4	2.12	9.6	2.93	1.14	0.60	3.77	3.75	0.80	2.22	0.34	2.34	0.32	1.91	0.31	0.60	0.39	0.13
4860_1	Beryl	8.32989	-104.64724	2987	7.14	19.8	202	121	33.7	76	31.9	94.3	24.4	23.69	497	29.2	235	36.9	0.20	285.5	23.6	54.2	6.79	27.5	6.41	2.12	0.93	5.82	5.22	1.04	2.85	0.41	2.49	0.37	4.60	2.14	1.97	2.23	0.76
OS18_A	Beryl	8.36108	-104.64903	2976	4.75	31.5	198	252	44.6	139	62.9	68.8	15.1	1.47	210	26.6	108	3.4	0.02	16.6	4.4	12.5	1.97	9.8	3.09	1.20	0.66	3.95	4.21	0.91	2.68	0.41	2.42	0.40	2.23	0.23	0.50	0.21	0.08
OS18_D	Beryl	8.36108	-104.64903	2976	5.00	30.2	213	251	46.7	133	67.8	78.1	16.2	1.62	212	24.0	99	3.5	0.02	17.4	4.3	12.9	2.02	9.7	3.03	1.16	0.65	3.73	3.97	0.87	2.40	0.37	2.31	0.34	2.03	0.23	0.57	0.20	0.08
OS18_G	Beryl	8.36108	-104.64903	2976	4.67	30.7	198	251	44.8	136	62.5	72.7	15.3	1.47	213	25.4	104	3.4	0.01	16.5	4.3	12.4	1.99	9.6	3.05	1.14	0.66	3.78	4.06	0.94	2.64	0.39	2.36	0.38	2.14	0.23	0.52	0.21	0.08
4853_2	Beryl	8.37874	-104.65410	2850	4.49	37.7	201	242	52.7	165	103.0	83.8	13.4	0.72	124	26.9	73	2.1	0.01	8.2	2.3	7.6	1.24	6.8	2.49	1.00	0.64	3.56	4.25	0.99	2.75	0.43	2.96	0.42	1.72	0.14	0.30	0.11	0.05
4853_3	Beryl	8.38015	-104.65417	2867	4.39	38.0	195	232	50.7	154	99.3	84.1	12.8	0.69	126	27.9	74	2.1	0.01	7.9	2.3	7.5	1.27	6.9	2.49	1.02	0.70	3.76	4.40	1.01	2.75	0.46	2.93	0.45	1.77	0.13	0.29	0.12	0.05
4860_4	Beryl	8.33361	-104.65425	2918	7.22	19.5	201	120	33.8	77	31.3	94.8	24.3	23.26	487	28.7	229	36.4	0.20	281.0	23.1	53.4	6.69	27.3	6.19	2.06	0.89	5.82	5.08	1.03	2.76	0.39	2.38	0.38	4.50	2.11	2.00	2.17	0.75
4853_1	Beryl	8.37812	-104.65480	NaN	4.88	41.0	198	234	50.3	141	98.8	82.1	12.8	0.70	128	30.2	82	2.2	0.01	8.1	2.5	7.7	1.36	7.2	2.76	1.07	0.72	3.97	4.77	1.09	3.07	0.49	3.22	0.48	1.91	0.15	0.27	0.13	0.05
4860_6	Beryl	8.33418	-104.65665	2866	7.30	21.5	204	90	29.7	47	31.2	87.7	26.8	31.76	534	31.3	295	46.9	0.27	367.4	30.2	64.1	7.94	32.2	7.13	2.28	0.99	6.47	5.57	1.12	2.96	0.43	2.59	0.40	5.74	2.84	2.44	3.01	0.98
4860_7	Beryl	8.33406	-104.65743	2827	7.69	23.6	227	162	26.3	23	34.7	97.7	27.1	35.28	465	34.8	331	52.8	0.31	395.0	33.9	71.8	8.96	36.2	7.94	2.45	1.10	7.43	6.30	1.26	3.28	0.49	2.85	0.44	6.42	3.21	2.79	3.51	1.10
4860_12	Beryl	8.34198	-104.66093	2713	7.15	19.3	205	91	30.4	52	31.4	93.5	26.5	31.78	518	26.8	257	46.0	0.28	364.6	28.0	63.6	7.60	29.7	6.43	2.20	0.88	5.68	4.89	0.96	2.55	0.38	2.32	0.35	4.81	2.58	2.55	2.73	1.00
4853_7	Beryl	8.38627	-104.66113	2724	6.89	25.1	222	119	34.9	73	40.0	101.4	26.3	21.51	460	28.3	231	37.8	0.22	278.4	22.8	51.5	6.41	26.6	6.03	2.07	0.90	6.05	5.17	1.03	2.65	0.41	2.45	0.38	4.70	2.15	2.03	2.25	0.75
4853_9	Beryl	8.38824	-104.66456	2662	7.12	24.9	232	122	35.3	72	40.7	104.9	26.9	22.70	460	27.5	228	38.5	0.22	287.3	23.0	53.7	6.56	26.4	5.94	2.04	0.89	5.84	5.00	1.00	2.56	0.39	2.43	0.36	4.59	2.17	1.99	2.24	0.78
4853_11	Beryl	8.39055	-104.66775	2454	7.30	24.5	209	82	28.4	44	36.5	87.5	29.4	30.89	482	31.1	304	51.9	0.31	373.8	31.0	67.3	8.20	32.6	7.17	2.29	1.02	6.62	5.64	1.13	2.91	0.43	2.72	0.40	6.05	2.96	2.47	3.36	1.06
4853_12	Beryl	8.39083	-104.67015	2390	6.80	25.4	219	118	35.2	83	37.3	97.7	25.8	21.56	466	28.4	233	38.2	0.22	284.4	23.3	52.3	6.60	27.0	6.31	2.08	0.93	6.07	5.21	1.06	2.72	0.39	2.50	0.35	4.76	2.15	1.88	2.33	0.75
4853_14	Beryl	8.39218	-104.67704	2261	7.17	23.4	211	89	29.2	46	34.2	93.9	29.3	29.37	496	29.1	278	50.1	0.31	365.2	29.2	65.3	7.83	31.6	6.89	2.26	0.96	6.27	5.35	1.06	2.69	0.40	2.55	0.36	5.55	2.81	2.44	3.05	1.02
4853_15	Beryl	8.39246	-104.67900	NaN	7.62	24.4	224	92	29.1	38	35.8	94.9	29.9	30.84	481	30.6	294	53.1	0.32	379.5	30.8	69.1	8.30	32.9	7.44	2.34	1.01	6.63	5.65	1.14	2.74	0.42	2.62	0.39	5.83	2.98	2.51	3.25	1.09
OS19_A	Beryl	8.35568	-104.76002	3127	5.18	29.7	209	200	45.4	110	61.4	83.7	17.2	4.02	241	25.1	105	6.2	0.04	43.9	5.9	16.0	2.32	10.6	3.19	1.19	0.67	3.84	4.00	0.89	2.50	0.39	2.43	0.37	2.11	0.38	0.73	0.43	0.14
OS19_F	Beryl	8.35568	-104.76002	3127	5.12	29.7	206	210	45.9	118	60.4	83.7	17.3	4.00	243	25.9	107	6.1	0.04	42.8	5.9	15.7	2.28	10.8	3.25	1.21	0.65	3.85	4.24	0.93	2.61	0.40	2.49	0.37	2.20	0.38	0.70	0.42	0.14
OS19_J	Beryl	8.35568	-104.76002	3127	4.45	28.9	187	247	46.4	152	73.2	68.9	15.2	1.34	167	21.4	73	2.6	0.01	15.1	3.0	9.1	1.49	7.4	2.46	0.96	0.54	3.08	3.41	0.76	2.18	0.34	2.12	0.33	1.58	0.17	0.40	0.16	0.06
4856_12	Rocky Ridge	8.39234	-104.82328	2358	6.30	31.4	229	188	31.1	88	48.9	78.7	18.9	16.80	324	34.0	216	21.9	0.20	163.5	17.4	38.4	5.15	21.9	5.37	1.78	0.96	5.76	5.63	1.21	3.31	0.50	3.16	0.47	4.01	1.28	1.53	1.80	0.51
4856_6	Rocky Ridge	8.40298	-104.82863	2741	4.89	35.5	190	241	42.8	115	78.0	76.7	14.2	2.05	186	27.3	92	3.4	0.03	21.7	4.1	11.3	1.82	8.9	2.85	1.08	0.64	3.70	4.34	0.95	2.73	0.44	2.82	0.43	1.90	0.20	0.49	0.26	0.08
4856_3	Rocky Ridge	8.40746	-104.83776	2807	5.42	30.1	216	259	37.6	134	50.4	79.7	16.9	10.52	263	27.1	129	12.0	0.17	106.3	10.1	23.2	3.11	13.9	3.74	1.36	0.72	4.43	4.50	0.94	2.66	0.40	2.47	0.37	2.62	0.68	1.05	1.06	0.31
4856_4	Rocky Ridge	8.40688	-104.83776	2787	5.45	30.4	217	260	37.6	135	50.1	81.2	17.1	10.61	267	27.2	130	12.3	0.16	107.4	10.2	23.4	3.22	14.1	3.85	1.41	0.72	4.49	4.50	0.93	2.61	0.40	2.53	0.36	2.64	0.69	1.07	1.09	0.32
4856_1	Rocky Ridge	8.41148	-104.83915	2736	5.16	29.9	219	309	37.6	134	50.9	80.6	16.2	8.14	257	24.2	122	11.4	0.11	82.4	9.0	21.7	2.97	13.3	3.57	1.31	0.67	4.05	4.14	0.86	2.39	0.37	2.26	0.32	2.41	0.64	0.85	0.82	0.27
4852_2	Coral1	8.42316	-104.93982	2549	5.53	37.3	268	266	39.7	107	59.2	81.3	17.3	10.95	255	30.2	151	12.9	0.13	95.6	11.3	26.3	3.64	15.7	4.20	1.48	0.85	5.29	5.29	1.09	3.17	0.43	2.88	0.44	3.49	0.73	1.08	1.08	0.33
4852_1	Coral1	8.42317	-104.93983	2551	5.71	33.4	269	269	40.2	109	60.0	84.0	17.6	10.50	257	24.7	127	13.0	0.18	97.6	10.6	26.8	3.57	15.3	3.97	1.37	0.71	4.29	4.28	0.90	2.55	0.36	2.31	0.33	2.72	0.74	1.01	0.92	0.32
4852_3	Coral1	8.42317	-104.93995	2499	5.19	35.6	253	244	37.2	94	55.4	77.7	16.4	10.19	262	27.6	140	13.3	0.13	98.3	11.2	26.2	3.66	15.8	4.34	1.46	0.75	4.73	4.98	1.01	2.69	0.41	2.54	0.38	3.09	0.78	0.99	1.00	0.30
4852_4	Coral1	8.42297	-104.94033	2498	5.24	35.0	254	247	37.7	97	55.7	77.6	16.7	10.19	258	26.3	135	13.2	0.13	97.4	11.2	26.1	3.60	16.2	4.26	1.46	0.76	4.72	4.80	0.97	2.80	0.39	2.53	0.38	3.02	0.76	0.99	1.02	0.31
4852_5	Coral1	8.42199	-104.94199	2529	5.35	33.8	259	246	38.1	103	54.7	77.7	17.4	12.53	271	25.2	131	13.9	0.17	117.4	11.9	27.8	3.72	15.8	4.10	1.39	0.75	4.39	4.46	0.95	2.61	0.39	2.28	0.34	2.88	0.77	1.10	1.15	0.36
4852_6	Coral1	8.42065	-104.94347	2455	5.46	36.4	269	259	40.2	113	56.8	79.0	18.2	13.24	271	29.4	150	14.2	0.21	118.8	12.6	28.4	3.80	16.2	4.40	1.45	0.83	5.18	5.14	1.09	3.04	0.42	2.73	0.41	3.33	0.87	1.19	1.26	0.38
4852_7	Coral1	8.42440	-104.95079	2512	4.95	38.2	207	217	44.4	89	93.2	75.4	13.8	0.91	175	25.2	84	2.1	0.00	10.5	3.4	10.5	1.75	8.7	2.76	1.10	0.63	3.56	4.34	0.90	2.68	0.39	2.70	0.41	1.85	0.13	0.46	0.12	0.06
4852_8	Coral1	8.42543	-104.95387	2277	4.68	36.9	192	205	45.8	108	85.7	72.9	14.1	0.65	180	24.9	82	1.8	0.00	8.8	3.1	9.7	1.59	8.2	2.78	1.03	0.61	3.60	4.25	0.89	2.78	0.40	2.70	0.40	1.86	0.11	0.43	0.11	0.05
4852_9	Coral1	8.42562	-104.95413	2240	4.65	35.8	190	204	46.2	116	84.7	72.9	13.5	0.70	180	24.0	80	1.7	0.01	8.5	3.0	9.4	1.55	8.1	2.72	1.00	0.58	3.61	4.03	0.94	2.57	0.39	2.65	0.37	1.78	0.13	0.41	0.12	0.05
4852_10	Coral1	8.42551	-104.95480	2186	4.95	37.0	190	202	45.5	109	84.8	73.7	13.8	0.63	180	24.6	81	1.7	0.01	8.5	3.0	9.5	1.60	8.2	2.56	1.11	0.63	3.70	4.17	0.88	2.65	0.40	2.58	0.41	1.76	0.12	0.44	0.11	0.06
4852_11	Coral1	8.42542	-104.95726	2108	4.73	37.1	193	208	47.6	122	88.7	73.3	14.1	0.70	184	25.4	82	1.8	0.00	8.8	3.1	9.6	1.62	8.2	2.75	1.08	0.62	3.52	4.14	0.95	2.65	0.37	2.68	0.41	1.84	0.11	0.47	0.12	0.06
4852_12	Coral1	8.42485	-104.95871	2088	4.61	39.7	187	201	46.0	118	85.2	69.5	13.6	0.70	181	28.4	90	1.6	0.01	7.9	3.2	9.3	1.66	8.6	2.81	1.03	0.68	3.95	4.67	1.01	2.99	0.46	2.87	0.43	2.30	0.12	0.42	0.11	0.05
4852_13	Coral1	8.42415	-104.95950	2104	4.66	36.2	188	201	45.9	117	85.3	73.0	13.6	0.70	183	24.6	81	1.7	-0.01	8.5	3.0	9.6	1.60	8.1	2.62	1.04	0.63	3.64	4.13	0.86	2.68	0.42	2.65	0.39	1.87	0.11	0.44	0.12	0.05
4852_14	Coral1	8.42347	-104.96069	2113	4.82	38.7	195	206	46.7	112	87.3	74.1	13.7	0.71	187	26.9	88	1.8	0.02	8.6	3.3	9.8	1.64	8.2	2.78	1.06	0.66	3.92	4.57	1.01	2.89	0.41	2.74	0.43	1.96	0.12	0.45	0.10	0.05
4852_15	Coral1	8.42315	-104.96196	2068	4.81	41.1	193	202	46.2	107	88.0	75.0	13.7	0.67	186	28.9	93	1.8	0.00	8.4	3.3	9.8	1.72	8.9	2.98	1.09	0.73	4.01	4.76	1.06	3.11	0.44	2.99	0.47	2.17	0.12	0.44	0.12	0.05
4852_16	Coral1	8.42242	-104.96254	2039	4.58	37.8	184	194	45.3	114	83.3	69.2	13.6	0.65	180	25.8	84	1.7	0.00	8.5	3.1	9.3	1.58	8.2	2.61	1.03	0.63	3.63	4.19	0.93	2.72	0.40	2.85	0.45	1.88	0.11	0.38	0.12	0.05

Sample	Seamount	Latitude	Longitude	Depth	Li	Sc	V	Cr	Co	Ni	Cu	Zn	Ga	Rb	Sr	Y	Zr	Nb	Cs	Ba	La	Ce	Pr	Nd	Sm	Eu	Tb	Gd	Dy	Ho	Er	Tm	Yb	Lu	Hf	Ta	Pb	Th	U
4859_16	Coral2	8.42146	-105.01521	2654	5.58	34.0	254	259	43.1	97	54.5	85.0	14.2	10.90	278	28.4	138	12.6	0.15	99.8	9.8	25.2	3.32	14.8	4.11	1.45	0.79	4.81	4.64	0.97	2.62	0.39	2.52	0.38	2.78	0.66	1.00	0.91	0.30
4859_13	Coral2	8.42127	-105.02011	2801	4.99	39.2	256	264	40.3	77	60.8	74.4	11.9	6.79	236	28.4	128	10.7	0.09	70.5	8.2	20.4	2.90	13.6	3.78	1.38	0.75	4.65	4.64	0.92	2.64	0.41	2.47	0.40	2.59	0.59	0.71	0.71	0.24
4859_12	Coral2	8.42079	-105.02145	2703	5.07	40.8	263	268	40.1	68	63.6	75.1	12.2	7.11	232	30.2	136	11.1	0.09	72.0	8.7	20.8	3.04	14.0	4.02	1.41	0.82	4.95	4.98	0.99	2.84	0.44	2.77	0.42	2.77	0.62	0.71	0.75	0.23
OS17_C	Coral2	8.42976	-105.02181	3021	4.84	33.3	208	361	41.8	135	77.8	71.5	13.6	2.49	160	21.8	74	4.9	0.02	28.8	4.1	10.4	1.64	8.3	2.61	0.98	0.61	3.57	3.83	0.79	2.14	0.33	2.09	0.30	1.70	0.30	0.39	0.31	0.12
OS17_E	Coral2	8.42976	-105.02181	3021	4.52	34.1	196	336	39.0	130	71.4	65.4	12.7	2.25	158	22.8	77	4.7	0.02	27.1	4.0	9.9	1.58	8.1	2.61	1.01	0.62	3.65	3.94	0.85	2.28	0.33	2.23	0.32	1.85	0.30	0.36	0.31	0.11
OS17_F	Coral2	8.42976	-105.02181	3021	4.58	32.3	200	356	41.7	156	76.5	68.8	13.2	2.34	155	21.0	70	4.7	0.02	27.3	3.8	9.9	1.53	7.8	2.45	1.00	0.61	3.38	3.66	0.76	2.04	0.29	2.09	0.29	1.61	0.28	0.37	0.28	0.10
OS7_B	Coral2	8.38070	-105.02490	3134	5.55	33.9	248	263	33.8	98	50.5	82.0	15.5	10.23	232	33.1	146	10.7	0.16	94.8	10.2	23.1	3.29	14.8	4.15	1.45	0.86	5.20	5.44	1.19	3.19	0.48	3.03	0.45	3.06	0.63	1.04	1.10	0.29
OS7_G	Coral2	8.38070	-105.02490	3134	5.51	31.7	255	272	35.1	107	51.7	88.2	16.0	10.58	228	30.0	134	10.6	0.16	96.6	9.8	23.4	3.22	14.3	4.05	1.39	0.79	4.75	5.09	1.06	2.98	0.43	2.83	0.40	2.78	0.62	1.08	1.00	0.30
4859_10	Coral2	8.42022	-105.02577	2774	5.61	36.3	263	259	41.3	75	57.6	81.6	13.7	10.62	252	31.2	147	12.6	0.14	94.5	9.9	24.6	3.33	15.4	4.10	1.45	0.86	5.16	5.25	1.05	3.03	0.46	2.76	0.42	3.00	0.66	0.95	0.95	0.29
4859_8	Coral2	8.42073	-105.02934	2926	4.69	31.0	179	289	53.7	203	67.7	73.0	10.1	1.65	199	22.5	77	2.8	0.01	19.3	3.0	9.5	1.55	8.1	2.67	1.07	0.59	3.38	3.70	0.76	2.18	0.34	2.02	0.31	1.72	0.16	0.38	0.17	0.06
4859_6	Coral2	8.42119	-105.03156	2960	4.97	41.9	224	248	54.6	160	69.1	78.1	11.4	3.72	219	32.9	105	5.8	0.04	37.0	5.3	13.9	2.06	10.1	3.06	1.17	0.78	4.36	5.10	1.09	3.30	0.49	3.18	0.53	2.09	0.33	0.52	0.39	0.13
4859_5	Coral2	8.42144	-105.03297	2931	4.66	39.4	209	237	51.6	152	64.2	73.0	10.6	3.49	209	29.9	96	5.6	0.04	35.6	5.0	13.1	1.95	9.3	2.73	1.11	0.71	3.96	4.57	0.99	2.97	0.48	2.83	0.47	1.91	0.32	0.47	0.35	0.12
4859_4	Coral2	8.42215	-105.03639	2869	5.19	37.5	257	283	43.6	90	62.2	80.4	12.5	6.14	256	25.7	118	10.0	0.06	62.4	7.6	20.0	2.83	12.7	3.63	1.33	0.70	4.24	4.32	0.87	2.38	0.38	2.23	0.36	2.34	0.53	0.71	0.59	0.21
4859_3	Coral2	8.42105	-105.03780	2920	5.13	39.1	252	278	42.5	89	60.5	76.6	12.1	5.93	258	27.4	126	10.2	0.06	62.1	7.8	19.7	2.83	13.1	3.70	1.41	0.73	4.53	4.48	0.93	2.57	0.41	2.43	0.36	2.53	0.54	0.66	0.62	0.21
4859_2	Coral2	8.41969	-105.03938	2993	4.73	43.0	216	199	49.4	129	64.9	71.5	11.1	3.69	227	33.5	112	6.1	0.04	37.9	5.6	13.9	2.13	10.5	3.27	1.18	0.78	4.60	5.27	1.16	3.26	0.53	3.26	0.52	2.32	0.37	0.48	0.40	0.12
4859_1	Coral2	8.41788	-105.04138	2882	6.33	35.1	253	237	49.0	125	54.9	107.4	13.5	6.56	215	28.9	104	7.5	0.08	60.0	6.3	16.8	2.36	11.1	3.53	1.28	0.74	4.45	4.76	0.97	2.75	0.42	2.63	0.40	2.17	0.41	0.67	0.57	0.18
OS16_B	Coral2	8.45955	-105.04702	3070	6.97	31.9	231	220	33.4	95	48.1	92.9	18.1	9.22	248	38.2	202	13.0	0.12	80.2	11.8	28.8	4.13	19.1	5.26	1.76	1.03	6.34	6.31	1.34	3.74	0.56	3.43	0.52	4.03	0.78	1.12	0.97	0.29
OS16_F	Coral2	8.45955	-105.04702	3070	7.24	32.5	240	230	34.8	98	50.7	94.4	18.7	9.63	250	39.3	206	13.2	0.11	81.6	12.0	29.8	4.17	19.2	5.35	1.80	1.03	6.48	6.51	1.38	3.78	0.58	3.48	0.53	4.09	0.77	1.13	1.01	0.32
4857_18	Otto Ridge	8.45384	-105.10629	2265	4.97	34.1	187	198	43.8	132	69.5	72.4	13.3	1.08	225	25.7	104	2.3	0.01	13.6	4.1	12.4	1.97	9.7	2.94	1.19	0.66	3.97	4.31	0.92	2.62	0.40	2.68	0.39	2.05	0.16	0.55	0.16	0.06
4857_15	Otto Ridge	8.45258	-105.11015	2432	5.68	38.5	223	215	43.9	86	76.3	83.8	14.9	1.35	231	28.5	116	2.9	0.01	16.4	4.6	14.6	2.27	10.8	3.29	1.29	0.76	4.31	4.87	1.03	2.89	0.44	2.98	0.43	2.38	0.17	0.64	0.19	0.07
OS14_A	Otto Ridge	8.47033	-105.11047	3127	7.30	32.2	260	212	35.0	93	52.4	87.7	22.8	16.33	337	37.5	274	25.9	0.20	178.0	20.5	46.6	6.25	26.5	6.66	2.13	1.27	7.58	7.88	1.69	4.53	0.71	4.50	0.70	5.40	1.63	1.87	1.85	0.59
OS14_B	Otto Ridge	8.47033	-105.11047	3127	7.23	32.8	261	216	35.7	99	53.0	86.6	22.6	16.38	336	39.0	285	25.8	0.21	175.4	20.9	46.7	6.23	26.7	6.94	2.13	1.32	8.04	8.26	1.76	4.83	0.73	4.52	0.74	5.73	1.66	1.89	1.94	0.59
OS14_D	Otto Ridge	8.47033	-105.11047	3127	7.60	31.3	272	223	36.6	100	54.5	88.4	22.7	17.01	333	35.9	264	25.9	0.23	180.9	20.4	48.2	6.21	26.3	6.61	2.06	1.25	7.48	7.54	1.59	4.38	0.70	4.27	0.66	5.20	1.56	1.89	1.85	0.63
4857_12	Otto Ridge	8.45142	-105.11197	2546	5.10	35.5	197	200	44.1	123	69.9	72.7	13.6	1.24	220	27.6	110	2.5	0.01	15.3	4.2	12.6	2.06	9.8	2.99	1.21	0.74	4.35	4.58	1.00	2.80	0.43	2.83	0.41	2.27	0.16	0.57	0.18	0.07
4857_9	Otto Ridge	8.45080	-105.11301	2636	5.01	35.1	198	198	42.8	116	78.3	74.6	13.4	1.26	217	26.4	107	2.6	0.01	15.4	4.1	12.8	2.03	10.0	3.05	1.16	0.68	4.09	4.38	0.93	2.69	0.40	2.75	0.38	2.24	0.17	0.60	0.17	0.07
4857_7	Otto Ridge	8.45073	-105.12000	2476	5.30	43.3	227	217	48.9	165	87.9	71.3	13.8	0.60	177	34.4	108	1.4	0.01	8.1	3.2	10.8	1.87	9.6	3.05	1.24	0.83	4.62	5.43	1.24	3.59	0.57	3.59	0.55	2.27	0.09	0.53	0.11	0.04
4857_8	Otto Ridge	8.45073	-105.12000	2476	5.05	41.3	198	217	46.6	153	83.8	69.8	13.0	0.58	176	30.7	99	1.4	0.01	8.1	3.0	10.4	1.77	9.3	2.87	1.21	0.74	4.01	4.96	1.13	3.19	0.48	3.36	0.50	2.05	0.10	0.50	0.10	0.04
4857_4	Otto Ridge	8.45013	-105.12316	2480	5.91	32.0	250	221	37.4	112	45.8	82.0	18.6	11.39	262	29.1	159	13.1	0.16	106.1	11.5	29.0	3.82	16.6	4.10	1.52	0.84	4.89	5.06	1.08	2.91	0.42	2.89	0.40	3.08	0.73	1.21	1.06	0.36
4857_5	Otto Ridge	8.45014	-105.12317	2480	5.98	32.9	255	227	38.7	119	50.5	84.4	18.9	11.55	267	30.6	166	13.2	0.16	107.2	11.8	29.2	3.86	16.9	4.27	1.56	0.89	5.35	5.26	1.14	3.06	0.45	2.95	0.42	3.24	0.73	1.27	1.11	0.37
4857_2	Otto Ridge	8.45191	-105.12983	2440	5.34	37.2	257	259	39.1	116	50.9	79.2	18.5	13.06	292	31.2	159	14.3	0.19	124.7	12.6	28.2	3.77	16.6	4.21	1.44	0.86	5.16	5.25	1.14	3.11	0.46	2.94	0.44	3.33	0.87	1.21	1.36	0.38
4857_1	Otto Ridge	8.45190	-105.13016	2456	5.69	35.4	274	321	42.0	126	52.4	87.3	19.5	13.76	295	27.7	145	14.7	0.18	128.2	12.1	29.4	3.81	16.2	3.94	1.42	0.78	4.69	4.74	1.02	2.68	0.41	2.70	0.38	2.79	0.84	1.26	1.21	0.41
4858_9	Sparky	8.46514	-105.21138	2756	6.98	26.2	210	106	32.6	66	29.9	92.2	22.8	25.71	507	34.7	271	40.1	0.22	315.9	27.4	57.7	7.43	31.8	7.32	2.38	1.14	7.41	6.65	1.30	3.45	0.48	3.06	0.46	5.69	2.42	2.02	2.78	0.86
4858_3	Sparky	8.47623	-105.21215	3062	6.56	27.5	225	173	34.9	102	34.9	79.0	19.5	20.69	414	30.5	202	29.4	0.22	225.4	20.4	46.1	5.90	24.7	5.84	1.97	0.93	5.77	5.59	1.13	3.04	0.43	2.87	0.41	4.10	1.62	1.59	1.98	0.64
4858_1	Sparky	8.48148	-105.21217	3066	6.83	27.4	218	151	32.9	88	32.9	75.4	19.3	21.27	430	31.4	209	30.7	0.23	235.5	21.7	47.8	6.15	25.9	6.06	1.99	0.97	6.15	5.73	1.18	3.14	0.48	3.00	0.44	4.17	1.75	1.63	2.14	0.65
4858_5	Sparky	8.47415	-105.21240	2967	7.16	28.2	226	99	31.5	51	31.9	97.1	23.3	26.27	484	36.7	285	41.0	0.24	322.7	28.7	59.8	7.84	33.8	7.91	2.48	1.22	7.85	7.00	1.39	3.62	0.53	3.20	0.46	6.04	2.49	2.05	2.93	0.89
4858_7	Sparky	8.47068	-105.21295	2887	6.82	24.9	210	105	31.7	61	29.5	92.0	22.2	25.20	502	31.9	253	40.2	0.22	317.2	26.6	57.3	7.37	31.0	7.24	2.31	1.07	6.81	6.03	1.21	3.10	0.45	2.85	0.42	5.14	2.32	1.96	2.65	0.86
OS6_C	Avery	8.35703	-105.28420	3306	7.49	31.2	285	180	35.1	85	48.6	107.9	21.0	18.50	267	41.6	225	19.4	0.29	153.9	16.2	40.8	5.46	23.0	5.97	2.00	1.21	7.21	7.15	1.51	4.09	0.61	4.03	0.60	4.50	1.12	1.65	1.74	0.48
OS6_D	Avery	8.35703	-105.28420	3306	7.26	31.6	272	178	34.2	89	46.6	102.0	19.5	16.48	263	43.6	230	18.6	0.23	141.7	16.1	38.8	5.21	22.7	6.13	1.99	1.22	7.10	6.89	1.53	4.20	0.65	3.85	0.59	4.56	1.06	1.48	1.62	0.48
OS6_F	Avery	8.35703	-105.28420	3306	5.61	33.0	238	211	35.4	92	47.3	83.0	17.5	13.41	324	33.1	181	15.4	0.22	127.9	13.3	31.9	4.35	18.5	4.96	1.63	0.90	5.63	5.49	1.15	3.17	0.47	2.94	0.49	3.51	0.89	1.25	1.40	0.40
OS5_C	Avery	8.41303	-105.28486	2674	5.90	31.2	238	217	33.5	86	45.7	80.7	18.4	13.04	312	31.3	172	15.1	0.20	125.0	12.9	31.0	4.21	18.3	4.85	1.62	0.86	5.22	5.32	1.08	3.03	0.44	2.84	0.41	3.39	0.84	1.24	1.29	0.39
OS5_D	Avery	8.41303	-105.28486	2674	5.78	31.1	235	213	32.8	84	42.9	81.0	18.3	12.96	305	31.1	170	15.0	0.19	124.1	12.8	30.7	4.09	18.0	4.63	1.59	0.83	5.15	5.23	1.07	2.98	0.44	2.85	0.42	3.32	0.86	1.25	1.27	0.39
OS5_H	Avery	8.41303	-105.28486	2674	5.83	30.9	238	217	33.3	87	44.3	79.6	18.7	13.18	299	31.0	168	14.8	0.20	123.7	12.5	30.6	4.01	17.5	4.55	1.56	0.82	5.11	5.21	1.07	2.86	0.44	2.77	0.41	3.29	0.85	1.31	1.28	0.39
4851_13	Avery	8.40574	-105.30449	2440	5.60	33.9	225	296	34.9	89	71.8	81.8	15.1	4.00	185	28.2	113	6.8	0.04	38.4	6.3	15.9	2.47	12.0	3.65	1.35	0.75	4.43	4.68	1.01	2.75	0.40	2.56	0.38	2.46	0.41	0.61	0.45	0.15
4851_11	Avery	8.40823	-105.30540	2451	5.33	31.2	210	277	35.3	115	64.0	77.6	14.9	4.02	189	26.5	110	6.9	0.04	38.7	6.2	15.5	2.41	11.2	3.49	1.27	0.70	4.15	4.43	0.93	2.49	0.37	2.41	0.36	2.29	0.42	0.59	0.42	0.15
4851_9	Avery	8.40952	-105.30959	2467	3.85	24.8	156	210	26.2	85	49.4	55.3	11.0	2.83	137	22.0	88	4.8	0.03	26.8	4.4	11.2	1.73	8.7	2.66	0.95	0.58	3.40	3.68	0.78	2.16	0.32	2.02	0.30	1.96	0.31	0.41	0.33	0.11
OS4_C	Avery	8.42052	-105.31067	2695	5.93	33.8	246	232	32.6	85	47.9	83.9	17.8	10.46	281	37.4	196	14.5	0.13	98.6	12.6	29.4	4.13	18.7	5.05	1.72	1.02	6.13	6.24	1.33	3.61	0.54	3.41	0.52	3.84	0.88	1.15	1.17	0.35
OS4_E	Avery	8.42052	-105.31067	2695	5.68	30.6	235	277	34.3	97	45.8	83.5	17.5	12.36	306	29.1	159	14.6	0.18	119.4	12.4	29.0	3.85	17.0	4.48	1.53	0.80	4.96	4.93	1.01	2.85	0.43	2.70	0.40	3.10	0.83	1.24	1.25	0.35
4851_3	Avery	8.41091	-105.32518	2603	4.77	35.1	183	382	44.8	195	76.7	75.5	13.4	1.00	136	27.5	79	2.2	0.01	11.8	2.8	8.1	1.38	7.1	2.51	0.97	0.65	3.71	4.44	0.96	2.85	0.42	2.80	0.41	1.78	0.15	0.34	0.15	0.05
4851_1	Avery	8.40797	-105.32578	2686	4.99	32.3	189	344	45.0	169	81.7	84.7	14.0	0.90	129	24.1	68	2.0	0.01	10.5	2.4	7.7	1.27	6.6	2.29	0.93	0.57	3.25	3.87	0.84	2.39	0.35	2.35	0.34	1.45	0.13	0.31	0.13	0.05

Sample	Seamount	Latitude	Longitude	Depth	Li	Sc	V	Cr	Co	Ni	Cu	Zn	Ga	Rb	Sr	Y	Zr	Nb	Cs	Ba	La	Ce	Pr	Nd	Sm	Eu	Tb	Gd	Dy	Ho	Er	Tm	Yb	Lu	Hf	Ta	Pb	Th	U
4850_1	Matthew	8.40369	-105.36189	2699	4.83	37.7	217	339	35.7	78	71.7	65.5	14.6	2.57	196	27.4	112	5.1	0.03	28.0	5.3	13.5	2.07	10.6	3.23	1.18	0.66	4.13	4.50	0.96	2.54	0.39	2.39	0.36	2.45	0.34	0.53	0.36	0.11
4850_5	Matthew	8.41184	-105.36285	2590	5.47	31.1	206	288	42.5	133	71.9	102.0	15.4	1.29	91	24.1	47	1.8	0.02	12.7	1.7	5.0	0.84	4.7	1.90	0.79	0.55	3.03	4.00	0.82	2.37	0.36	2.34	0.37	1.20	0.09	0.18	0.14	0.05
4850_4	Matthew	8.40928	-105.36297	2618	5.81	32.5	220	265	40.4	101	73.2	104.0	16.3	1.88	109	24.2	53	2.4	0.03	17.8	2.3	6.2	1.02	5.4	2.16	0.89	0.58	3.18	4.02	0.86	2.40	0.36	2.30	0.35	1.30	0.13	0.26	0.19	0.06
4850_7	Matthew	8.41326	-105.36316	2528	5.89	32.0	224	268	40.9	100	74.4	105.1	16.3	1.86	104	23.8	53	2.3	0.03	18.2	2.3	6.3	0.99	5.2	2.02	0.84	0.56	3.13	3.85	0.84	2.31	0.35	2.39	0.35	1.23	0.13	0.24	0.19	0.06
4850_8	Matthew	8.41641	-105.36551	2532	5.73	30.5	234	239	41.1	128	57.8	101.4	18.4	12.02	203	25.9	89	9.9	0.21	117.6	8.9	19.4	2.46	10.8	3.01	1.11	0.64	3.73	4.08	0.89	2.49	0.38	2.41	0.36	1.92	0.53	1.06	1.19	0.30
4849_3	Wayne	8.41599	-105.51108	2863	5.13	30.0	213	227	39.7	85	59.3	74.4	16.0	5.52	214	26.4	114	7.2	0.06	52.1	6.7	16.8	2.50	11.8	3.46	1.27	0.71	4.16	4.29	0.95	2.71	0.41	2.37	0.38	2.43	0.43	0.70	0.54	0.17
4849_6	Wayne	8.41651	-105.51588	2941	5.79	34.0	260	257	37.3	50	59.9	86.9	17.5	8.12	240	27.8	142	11.0	0.09	74.3	9.3	23.1	3.28	14.7	4.08	1.46	0.77	4.63	4.67	1.02	2.79	0.41	2.54	0.39	2.92	0.67	0.98	0.78	0.26
4849_11	Wayne	8.40949	-105.51863	2910	5.62	39.0	254	225	40.6	54	63.5	79.2	16.4	2.97	194	31.2	129	5.8	0.03	32.7	5.8	15.4	2.40	12.0	3.71	1.31	0.84	4.93	5.12	1.11	3.16	0.47	2.79	0.45	2.95	0.41	0.63	0.41	0.14
4849_20	Wayne	8.40283	-105.51881	2718	5.15	31.3	214	278	36.1	118	51.0	76.6	17.5	10.61	300	27.6	153	12.7	0.15	102.4	11.2	25.4	3.52	15.4	4.24	1.47	0.76	4.78	4.80	0.97	2.73	0.39	2.42	0.36	2.95	0.76	1.07	1.09	0.30
4849_18	Wayne	8.40354	-105.51934	2775	5.67	31.5	210	276	35.8	122	50.3	78.3	17.3	10.43	298	28.0	153	12.5	0.15	100.3	11.0	24.9	3.46	15.6	4.18	1.43	0.77	4.69	4.78	0.98	2.67	0.41	2.53	0.37	3.01	0.74	1.05	1.09	0.29
4849_14	Wayne	8.40649	-105.52027	2878	5.45	30.5	222	294	33.8	87	51.8	83.6	18.2	11.11	308	26.3	146	13.1	0.17	107.1	11.1	26.5	3.56	15.7	4.15	1.45	0.72	4.60	4.63	0.92	2.53	0.36	2.30	0.35	2.80	0.76	1.14	1.04	0.32
OS3_A	Wayne	8.42830	-105.52031	3041	5.00	35.8	242	245	36.7	57	64.4	74.4	14.1	2.37	182	27.0	110	5.5	0.02	26.4	5.3	14.6	2.35	11.4	3.47	1.31	0.74	4.17	4.61	0.94	2.66	0.40	2.52	0.37	2.42	0.33	0.59	0.34	0.13
4847_2	Max	8.38232	-105.62776	3171	4.71	29.6	180	281	36.5	122	65.6	58.8	12.6	0.68	191	25.8	109	1.6	0.03	7.0	3.0	10.7	1.94	10.2	3.24	1.19	0.69	4.18	4.37	0.92	2.48	0.37	2.28	0.35	2.43	0.12	0.47	0.10	0.04
4847_8	Max	8.38434	-105.63473	3007	4.73	26.7	183	305	37.9	137	64.0	63.6	13.0	0.67	186	21.1	91	1.7	0.01	7.3	2.8	10.7	1.87	9.4	2.95	1.16	0.59	3.53	3.62	0.75	2.08	0.29	1.93	0.28	1.93	0.10	0.46	0.09	0.04
4847_11	Max	8.38483	-105.63963	2787	6.36	36.8	300	55	39.6	31	66.4	97.7	14.9	2.94	138	32.2	115	6.0	0.03	24.9	5.7	15.5	2.37	11.8	3.67	1.35	0.82	4.83	5.39	1.15	3.17	0.48	3.11	0.46	2.55	0.35	0.62	0.38	0.14
4847_14	Max	8.38925	-105.64504	2676	5.52	39.0	274	82	38.6	32	65.8	81.5	13.8	2.32	135	31.4	107	4.9	0.02	19.4	5.0	13.1	2.06	10.3	3.29	1.18	0.77	4.43	5.16	1.10	3.19	0.46	2.98	0.46	2.47	0.32	0.52	0.33	0.12
4847_15	Max	8.38730	-105.64770	2658	4.33	35.4	217	340	36.0	76	70.9	67.5	12.8	1.84	175	23.4	95	4.6	0.02	18.9	4.5	12.4	1.94	9.4	2.82	1.09	0.61	3.58	3.87	0.82	2.31	0.34	2.18	0.33	2.01	0.28	0.49	0.28	0.10
4848_19	Ivy	8.37695	-105.73430	2180	7.46	38.4	302	28	37.0	22	65.5	100.4	18.8	10.43	216	45.3	210	15.5	0.14	90.5	12.7	29.6	4.31	20.3	5.85	1.94	1.21	7.47	7.68	1.59	4.37	0.63	4.00	0.61	4.60	0.94	1.15	1.21	0.38
4848_14	Ivy	8.37375	-105.73693	2251	8.41	36.0	324	21	40.0	17	58.7	118.9	18.5	7.57	171	46.4	189	11.9	0.09	63.2	9.8	25.2	3.83	19.1	5.93	2.05	1.24	7.35	7.79	1.65	4.54	0.68	4.17	0.64	4.30	0.71	0.99	0.86	0.28
4848_7	Ivy	8.36760	-105.74143	2339	5.35	28.6	213	244	34.9	97	63.6	78.4	16.8	10.39	250	26.9	146	14.3	0.14	93.7	10.8	25.3	3.39	15.1	4.15	1.45	0.76	4.75	4.71	0.95	2.64	0.38	2.43	0.34	2.95	0.82	0.96	1.02	0.33
4848_6	Ivy	8.36868	-105.74319	2350	6.06	33.2	247	271	34.7	65	70.6	85.1	18.2	12.01	256	31.6	171	16.2	0.15	103.6	12.3	28.8	3.90	17.3	4.86	1.65	0.89	5.52	5.54	1.12	3.03	0.45	2.81	0.41	3.54	0.92	1.13	1.18	0.38
4848_5	Ivy	8.36842	-105.74362	2332	5.08	41.0	194	252	32.5	101	60.0	53.7	16.8	9.44	273	46.9	226	13.4	0.13	89.2	13.1	23.4	3.55	18.7	5.29	1.65	1.18	7.62	7.78	1.63	4.57	0.65	3.84	0.61	4.93	0.96	1.07	1.34	0.28
4848_1	Ivy	8.37327	-105.74756	2168	5.84	32.1	233	249	35.4	85	69.2	80.9	18.6	12.66	263	33.4	180	16.7	0.16	109.0	12.9	29.1	3.96	17.9	4.95	1.66	0.95	5.76	5.75	1.17	3.25	0.49	2.91	0.45	3.75	0.99	1.13	1.33	0.41
OS2_F	Liona	8.56545	-106.10751	2988	6.14	28.4	259	169	34.8	80	35.5	84.7	19.8	19.68	277	33.1	179	20.3	0.27	177.2	15.7	34.2	4.51	19.6	5.03	1.68	0.94	5.54	5.59	1.20	3.30	0.50	2.97	0.47	3.87	1.28	1.62	1.91	0.55
OS2_I	Liona	8.56545	-106.10751	2988	5.34	36.1	278	212	41.6	59	69.0	82.7	15.9	3.36	145	27.9	101	5.5	0.04	30.5	5.2	14.1	2.19	10.6	3.38	1.21	0.73	4.17	4.53	1.00	2.80	0.42	2.73	0.41	2.28	0.34	0.58	0.38	0.13
OS2_K	Liona	8.56545	-106.10751	2988	6.00	26.5	259	170	35.1	81	35.4	87.4	19.8	19.72	271	29.7	163	20.2	0.27	177.6	15.0	34.1	4.37	18.4	4.74	1.62	0.86	5.12	5.04	1.09	3.03	0.43	2.73	0.41	3.42	1.21	1.65	1.76	0.55
OS1_D	Liona	8.57512	-106.18844	2676	4.98	27.4	228	232	35.5	89	72.6	73.6	18.7	17.81	248	23.3	136	21.1	0.32	161.3	13.9	33.0	4.02	16.1	3.92	1.39	0.71	4.40	4.23	0.83	2.39	0.33	2.31	0.32	2.94	1.21	1.43	1.70	0.52
OS1_F	Liona	8.57512	-106.18844	2676	6.07	33.9	252	142	29.8	47	51.5	75.2	23.3	27.02	321	40.5	255	31.3	0.56	243.5	23.0	47.1	6.01	25.8	6.58	2.05	1.17	7.45	7.18	1.51	4.14	0.58	3.71	0.58	5.66	2.10	2.18	3.18	0.78
OS1_M	Liona	8.57512	-106.18844	2676	5.01	39.4	288	357	44.5	73	106.3	85.2	13.4	1.77	125	31.7	95	3.0	0.02	13.9	3.7	11.2	1.73	9.6	3.30	1.19	0.79	4.72	5.46	1.16	3.31	0.51	3.09	0.51	2.42	0.21	0.46	0.21	0.09
OS1_N	Liona	8.57512	-106.18844	2676	4.66	37.5	259	321	39.8	66	92.8	80.6	12.0	1.60	128	28.9	89	3.0	0.04	13.9	3.6	11.0	1.80	9.6	3.11	1.20	0.74	4.38	4.97	1.10	3.01	0.46	2.90	0.45	2.21	0.21	0.44	0.21	0.08
OS1_R	Liona	8.57512	-106.18844	2676	4.41	37.8	249	308	37.9	63	86.7	78.7	11.6	1.62	126	29.2	90	3.0	0.03	13.3	3.6	10.6	1.74	9.4	3.22	1.20	0.73	4.40	4.92	1.08	3.03	0.45	2.95	0.46	2.31	0.21	0.41	0.19	0.08
OS1_T	Liona	8.57512	-106.18844	2676	4.50	38.5	252	311	38.6	65	95.2	77.5	11.7	1.57	126	30.7	93	3.0	0.03	13.6	3.7	10.7	1.79	9.4	3.28	1.23	0.79	4.58	5.25	1.14	3.28	0.49	2.91	0.47	2.24	0.21	0.45	0.23	0.08

Table A.3 Radiogenic Isotope Ratios of the 8˚20' N seamount lavas measured on the MC-ICP-MS at University of Florida. Errors are provided for each ratio in the table.

Sample	Seamount	Lava Type	Latitude	Longitude	Depth	End	143/144	143/144err	87/86	87/86err	208/204	208/204err	207/204	207/204err	206/204	206/204err	208/206	208/206err	207/206	207/206err
4854_13	NEPR	NMORB	8.40394	-104.39374	2319	8.29	0.513063	0.000008	0.702647	0.000013	37.867	0.009	15.535	0.00317	18.425	0.00331	2.055	0.00016	0.8431	0.00004
4854_4	NEPR	EMORB	8.40945	-104.41191	2388	7.28	0.513011	0.00001	0.702897	0.000019	37.894	0.00921	15.497	0.003	18.555	0.00262	2.042	0.00023	0.8352	0.00005
OS12_F	Hook Ridge	NMORB	8.44354	-104.42000	2961	9.38	0.513119	0.00001	0.702669	0.000021	37.675	0.00648	15.492	0.00233	18.173	0.00215	2.073	0.00021	0.8525	0.00004
4855_2	Hook Ridge	EMORB	8.35626	-104.48912	2883	6.96	0.512995	0.000006	0.702841	0.000013	37.917	0.0211	15.499	0.00655	18.628	0.00513	2.036	0.00056	0.8322	0.00012
OS13_E	Midway Ridge	DMORB	8.41004	-104.58592	2500	8.19	0.513058	0.000006	0.702593	0.000021	37.879	0.00677	15.516	0.00268	18.290	0.00305	2.071	0.00005	0.8483	0.00003
OS9_A	Beryl	EMORB	8.41618	-104.64545	2800	8.43	0.51307	0.000006	0.702818	0.000017	37.985	0.00646	15.510	0.00201	18.568	0.00175	2.046	0.00018	0.8353	0.00004
Redo_OS9_A	Beryl	EMORB	8.41618	-104.64545	2800	9.09	0.5131035	0.000009	0.702818	0.000017	37.985	0.00646	15.510	0.00201	18.568	0.00175	2.046	0.00018	0.8353	0.00004
4860_1	Beryl	EMORB	8.32989	-104.64724	2987	6.61	0.512977	0.000005	0.702949	0.0000089	38.019	0.00226	15.543	0.00086	18.612	0.0009	2.043	0.00004	0.8351	0.00001
4853_1	Beryl	NMORB	8.37812	-104.65480	NaN	7.90	0.513043	0.000006	0.702743	0.000017	38.244	0.0111	15.501	0.00416	18.781	0.00455	2.036	0.00014	0.8253	0.00003
4860_12	Beryl	EMORB	8.34198	-104.66093	2713	6.26	0.512959	0.000004	0.702917	0.000015	37.976	0.00149	15.542	0.00048	18.577	0.00051	2.044	0.00004	0.8366	0.00001
4856_12	Rocky Ridge	EMORB	8.39234	-104.82328	2358	7.69	0.513032	0.000008	0.702922	0.000017	38.036	0.00964	15.512	0.00299	18.621	0.0025	2.043	0.00026	0.8330	0.00005
4859_10	Coral2	EMORB	8.42022	-105.02577	2774	8.49	0.513073	0.000009	0.702782	0.000012	38.098	0.0178	15.518	0.00541	18.622	0.00435	2.046	0.00057	0.8333	0.00012
4859_6X	Coral2	EMORB	8.42119	-105.03156	2960	8.00	0.513048	0.000008	0.702804	0.00001	38.038	0.00648	15.521	0.00214	18.536	0.00202	2.052	0.00017	0.8373	0.00004
4859_6	Coral2	EMORB	8.42119	-105.03156	2960	8.04	0.51305	0.000011	0.702693	0.000011	38.050	0.00382	15.530	0.00153	18.540	0.00193	2.052	0.00006	0.8376	0.00002
4857_8	Otto Ridge	DMORB	8.45073	-105.12000	2476	8.52	0.5130747	0.000005	0.702607	0.000018	38.045	0.0063	15.536	0.0027	18.536	0.0032	2.053	0.000071	0.8381	0.000022
Redo_4857_8	Otto Ridge	DMORB	8.45073	-105.12000	2476	NaN	NaN	NaN	0.702607	0.000018	38.045	0.0063	15.536	0.0027	18.536	0.0032	2.053	0.000071	0.8381	0.000022
4858_3	Sparky	EMORB	8.47623	-105.21215	3062	7.00	0.512997	0.000006	0.702984	0.0000084	38.091	0.0229	15.519	0.00705	18.714	0.00573	2.035	0.00061	0.8293	0.00012
OS5_D	Avery	EMORB	8.41303	-105.28486	2674	8.21	0.513059	0.000006	0.703065	0.000012	38.131	0.00279	15.524	0.00114	18.618	0.00139	2.048	0.00005	0.8338	0.00001
Redo_OS5_D	Avery	EMORB	8.41303	-105.28486	2674	8.39	0.5130675	0.000006	0.703198	0.000012	38.169	0.0036	15.538	0.0012	18.628	0.0013	2.049	0.000062	0.8341	0.000017
4850_1	Matthew	NMORB	8.40369	-105.36189	2699	9.03	0.513101	0.000008	0.70263	0.000014	37.975	0.00782	15.506	0.00238	18.546	0.00202	2.048	0.00023	0.8361	0.00005
4849_14	Wayne	EMORB	8.40649	-105.52027	2878	8.27	0.513062	0.000007	NaN	NaN	38.221	0.0039	15.553	0.00134	18.655	0.00129	2.049	0.00008	0.8337	0.00002
4847_8X	Max	DMORB	8.38434	-105.63473	3007	10.96	0.5132	0.000005	0.702486	0.00001	37.570	0.00783	15.469	0.00265	18.073	0.00231	2.079	0.00018	0.8559	0.00004
4847_8	Max	DMORB	8.38434	-105.63473	3007	11.18	0.513211	0.000006	0.702333	0.0000081	37.325	0.00878	15.435	0.00288	17.911	0.00238	2.084	0.00023	0.8618	0.00005
4848_5	Ivy	EMORB	8.36842	-105.74362	2332	8.02	0.513049	0.000009	0.702893	0.0000098	38.191	0.00648	15.530	0.0022	18.685	0.00196	2.044	0.00014	0.8312	0.00003

APPENDIX B

Supplementary Information

Datasets from PetDB

The data used for the regional comparison datasets were downloaded from PetDB Database (www.earthchem.org/petdb) on 20 October 2018. The following parameters were used for the on-axis data: "Latitude = 10 N, 8.3 S; Longitude = -104.34 W, -104.15 E; Analysis Type: Glass; Rock Type: Basalt; Tectonic Name: Spreading Center", and the following parameters for the Northern EPR data: "Latitude = 11 N, 8.2 S; Longitude = -105 W, -103 E; Analysis Type: Glass; Rock Type: Basalt" (Lehnert et al., 2012).

Distribution of Chemistry (Additional Figures)

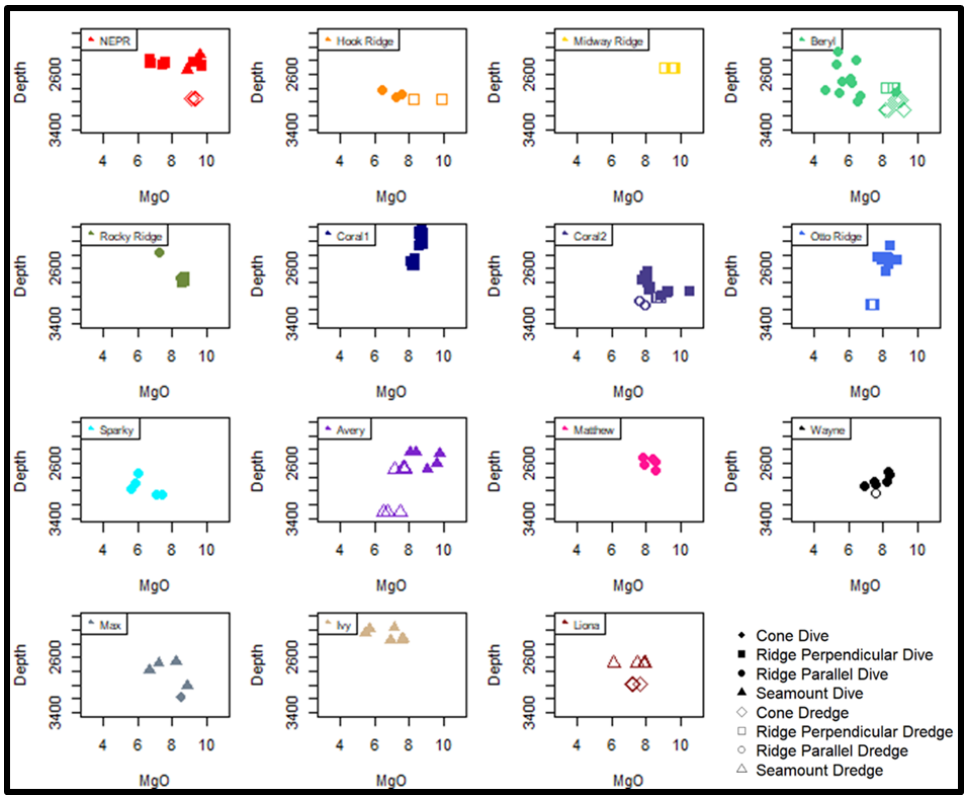

Supplementary Figure 1. MgO contents of the 8˚20' N lavas versus depth below sea level (m) for each seamount, starting from closest to axis (NEPR) through farthest from axis (Liona). Shapes indicate volcanic morphology types. Open symbols are from dredges and closed symbols are from Alvin dives. In general, there is no systematic difference in MORB-type with depth.

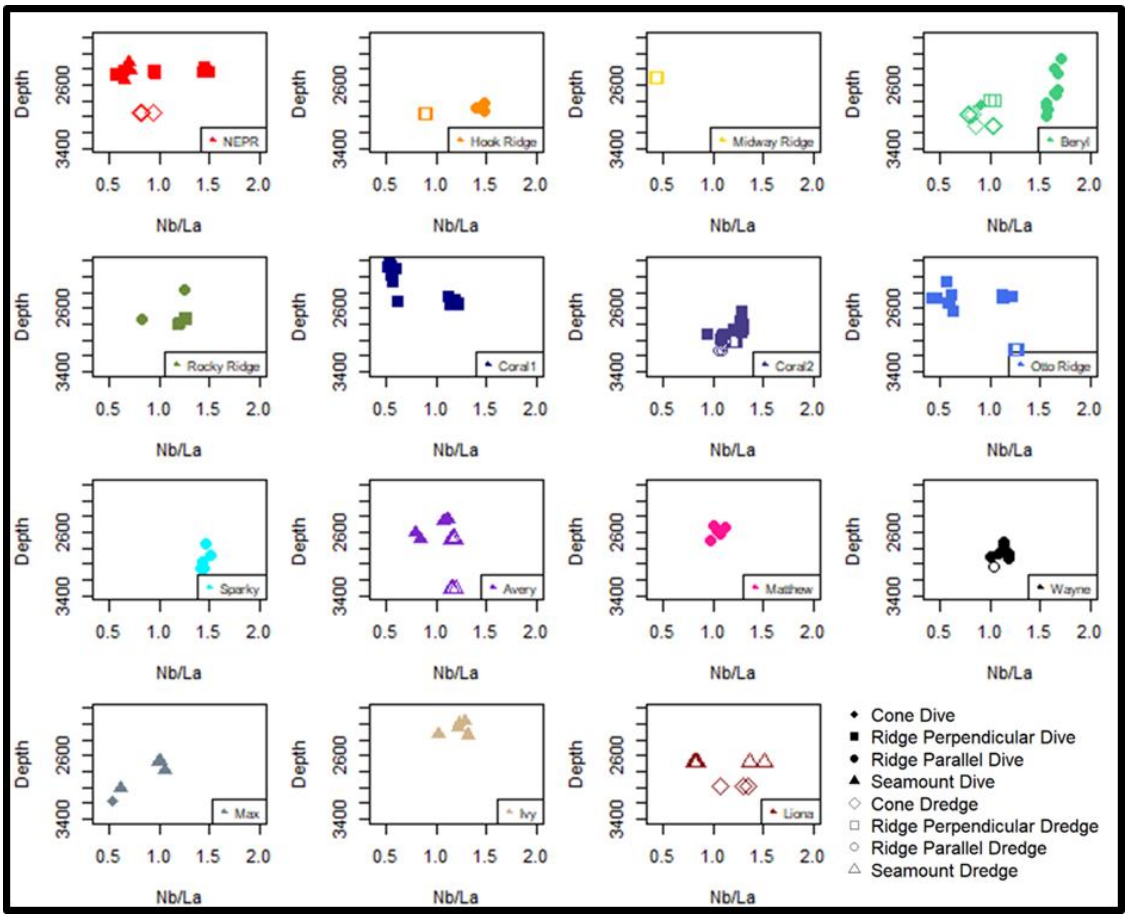

Supplementary Figure 2. Nb/La contents of the 8˚20' N lavas versus depth below sea level (m) for each seamount, starting from closest to axis (NEPR) through farthest from axis (Liona). Shapes indicate volcanic morphology types. Open symbols are from dredges and closed symbols are from Alvin dives. In general, there is no systematic difference in MORB-type with depth.

Measured Standards

Table A.4 Major Element Standards Measured at UF and USGS

	SiO2	TiO2	Al2O3	FeO	MnO	MgO	CaO	Na2O	K2O	P2O5
UF										
JDF avg	50.23	1.86	13.75	11.88	0.22	6.53	10.80	2.53	0.21	0.22
stdev	0.30	0.07	0.15	0.15	0.03	0.08	0.15	0.08	0.01	0.02
USGS										
A99	50.94	3.99	12.48	13.19	0.18	4.95	9.32	2.91	0.82	0.44
2392-9	49.78	1.32	15.40	9.28	0.17	8.37	12.32	2.78	0.09	0.11
USNM	51.39	1.28	15.20	9.04	0.16	7.93	11.45	2.78	0.08	0.12

Duplicate Major Element Analyses

Table A.5 Duplicate Major Element Analyses from UF for Interlaboratory Comparison. Major element contents are in wt. %

Sample	Seamount	Lab	SiO2	TiO2	Al2O3	FeO	MnO	MgO	CaO	Na2O	K2O	P2O5	Total
OS9_A	Beryl	UF	47.95	1.32	17.20	8.91	0.15	8.30	11.33	2.71	0.24	0.16	98.26
OS9_B	Beryl	UF	47.97	1.31	17.09	8.95	0.16	8.55	11.24	2.70	0.24	0.15	98.36
OS9_C	Beryl	UF	47.84	1.31	17.11	8.97	0.16	8.65	11.26	2.68	0.23	0.16	98.37
OS9_E	Beryl	UF	47.72	1.29	17.04	8.97	0.16	8.55	11.29	2.67	0.23	0.15	98.06
OS9_F	Beryl	UF	47.63	1.29	17.11	8.91	0.16	8.60	11.23	2.64	0.23	0.15	97.96
OS9_H	Beryl	UF	47.83	1.31	17.05	8.94	0.15	8.60	11.24	2.68	0.23	0.15	98.19
OS6_A	Avery	UF	48.68	2.40	15.69	9.92	0.17	6.43	10.03	3.41	0.74	0.44	97.90
OS6_B	Avery	UF	48.67	2.39	15.75	9.89	0.18	6.50	9.96	3.48	0.75	0.43	98.00
OS6_C	Avery	UF	48.72	2.43	15.75	9.83	0.19	6.41	10.02	3.48	0.74	0.43	97.99
OS6_D	Avery	UF	48.70	2.41	15.72	9.95	0.17	6.70	9.91	3.39	0.71	0.45	98.13
OS6_E	Avery	UF	48.92	2.39	15.76	9.86	0.17	6.42	9.91	3.46	0.75	0.44	98.07
OS6_F	Avery	UF	49.08	1.91	16.42	8.92	0.16	7.38	11.06	3.16	0.57	0.33	98.99
OS6_G	Avery	UF	48.82	2.39	15.79	9.95	0.17	6.47	9.87	3.44	0.74	0.44	98.08
OS1_D	Liona	UF	49.10	1.78	16.76	8.03	0.15	7.41	11.26	2.99	0.85	0.33	98.62
OS1_F1	Liona	UF	49.82	2.44	15.68	8.89	0.16	5.88	10.31	3.41	1.19	0.45	98.23
OS1_F2	Liona	UF	49.08	2.40	17.25	7.72	0.15	6.30	9.70	3.50	1.37	0.50	97.97
OS1_F3	Liona	UF	49.04	2.49	15.68	8.50	0.15	5.95	9.93	3.48	1.26	0.48	96.95
OS1_J	Liona	UF	49.80	1.40	14.75	9.55	0.19	7.73	12.27	2.64	0.13	0.12	98.59
OS1_M	Liona	UF	49.69	1.36	14.73	9.49	0.17	7.74	12.13	2.70	0.12	0.13	98.27
OS1_N	Liona	UF	50.04	1.35	14.89	9.46	0.17	7.73	12.33	2.67	0.14	0.14	98.90
OS1_O	Liona	UF	49.68	1.35	14.94	9.40	0.18	7.72	12.27	2.67	0.13	0.13	98.46
OS1_P	Liona	UF	49.55	1.35	14.87	9.35	0.17	7.69	12.23	2.70	0.13	0.13	98.16
OS1_Q	Liona	UF	49.62	1.37	14.84	9.43	0.18	7.72	12.18	2.69	0.13	0.13	98.28
OS1_R	Liona	UF	49.45	1.35	14.90	9.44	0.18	7.68	12.16	2.74	0.13	0.13	98.15
OS1_S	Liona	UF	49.55	1.34	14.90	9.40	0.19	7.66	12.28	2.68	0.13	0.12	98.24
OS1_T	Liona	UF	49.62	1.35	14.85	9.45	0.15	7.74	12.16	2.67	0.13	0.13	98.24
OS1_N	Liona	UF	49.98	1.40	14.75	9.55	0.18	7.74	12.30	2.66	0.13	0.13	98.84
OS1_M	Liona	UF	49.69	1.36	14.73	9.49	0.17	7.74	12.13	2.70	0.12	0.13	98.27

Adjusted Mantle Component Trace Element Contents

Table A.6 Compositions used as mantle component end-members. Trace element contents adjusted from DDMM of Workman and Hart (2005) and EMM of Donnelly et al. (2004)

Element	Adjusted EMM	Adjusted DDMM
SiO2	44.9	44.71
Al2O3	4.44	3.98
Fe2O3	0.116	0.191
FeO	7.926	8.008
MnO	0.13	0.13
MgO	37.71	38.73
CaO	3.54	3.17
Na2O	0.36	0.28
Cr2O3	0.38	0.57
TiO2	0.2	0.13
Ni	1965	1886
Cr	2600	3900
Mn	822	822
Cs	0.032	0.032
Tl	0.005	0.005
Rb	0.684	0.02
Ba	12	0.227
W	0.02	0.02
Th	0.086	0.004
U	0.023	0.0011
Nb	1.7	0.08
Ta	0.041	0.0056
K	250	49.8078
La	1	0.19
Ce	1.65	0.48
Pb	0.075	0.017
Pr	0.276	0.087
Mo	0.063	0.063
Sr	18.51	6.092
P	95	82.9274
Nd	1.1	0.52
F	26	26
Sm	0.26	0.25
Zr	11.2	4.269
Hf	0.288	0.127
Eu	0.149	0.086
Sn	0.17	0.17
Sb	0.005	0.005
Ti	1300	650
Gd	0.536	0.324
Tb	0.108	0.064
Dy	0.666	0.471
Li	1.6	1.6
Y	4.28	3.129
Ho	0.148	0.108
Er	0.437	0.329
Tm	0.074	0.074
Yb	0.441	0.348
Lu	0.068	0.056